University of Kerbala
College of Sciences
Department of Chemistry

Synthesis and Characterization of Heterogeneous solid acid catalysts derived From Rice Husks for Imidazole derivatives

A Thesis

Submitted to the College of Science / University of Kerbala in partial Fulfilment of The Requirement for The Degree of Master of Science in Chemistry

Written By

Noor Abbas Mohammed

B.SC. chemistry, college of science

Supervised By

Prof. Dr. Hayder Hamied Mihsen

and

Prof. Dr. Haitham Dalol Hanoon

2024 A.C 1446 A.H

بِسْمِ اللَّهِ الرَّحْمَٰنِ الرَّحِيمِ

﴿فَتَعَالَى اللَّهُ الْمَلِكُ الْحَقُّ وَلَا تَعْجَلْ بِالْقُرْآنِ مِنْ قَبْلِ أَنْ يُقْضَىٰ إِلَيْكَ
وَحْيُهُ وَقُلْ رَبِّ زِدْنِي عِلْمًا﴾

صَدَقَ اللهُ العَلِيُّ العَظِيمْ

سورة طة - الآية (114)

Examination Committee Certification

We certify that we have read this entitled " Synthesis and Characterization of Heterogeneous solid acid catalysts derived From Rice Husks for Imidazole derivatives" at the examining committee, examined the student " Noor Abbas Mohammed" on its contents, and that in our opinion, its adequate for the partial fulfillment of the requirements for the Degree of Master in science of chemistry

Signature:
Name: Dr. Zeid Hassan Abood
Title: Professor
Address: University of Kerbala, College of Science, Department of Chemistry.
Date: / /2024
(Chairman)

Signature:
Name: Saleh Hadi Kadhim
Title: Professor
Address: University of Babylon, College of Science, Department of Chemistry.
Date: / /2024
(Member)

Signature:
Name: Dr. Atheer Hasan Yas
Title: Lecturer Doctor
Address: University of Kerbala, College of Science, Department of Chemistry.
Date: 13/10/2024
(Member)

Signature:
Name: Dr. Hayder Hamied Mihsen
Title: Professor
Address: University of Kerbala, College of Science, Department of Chemistry.
Date: 14/10/2024
(Member & supervisor)

Signature:
Name: Dr. Haitham Dalol Hanoon
Title: Professor
Address: University of Kerbala, College of Science, Department of Chemistry.
Date: 14 / 10 / 2024
(Member & supervisor)

Approved by the council of the College of Science
Signature:
Name: Dr. Hassan Jameel Al-Fatlawy
Title: Professor
Address: Dean of College of Science, University of Kerbala.
Date: / / 2024

Report of the Head of the Chemistry Department

According to the recommendation presented by the Chairman of the Postgraduate Studies Committee, I forward this thesis " Synthesis and Characterization of Heterogeneous solid acid catalysts derived From Rice Husks for Imidazole derivatives" for examination.

Signature:

Assist. Prof. **Dr. Thaer Mahdi Madlool**

Head of Chemistry Department

Address: University of Kerbala, College of Science, Department of Chemistry

Date: 12/8/2024

Kerbala University

Science College

Asst. Prof. Dr. Thaer M. M. Al-Rammahi

Head of Chemistry Department

Acknowledgement

First, and foremost, praise is to our almighty God for giving me the power and persistence to accomplish this thesis.

I would like to express my sincere appreciation to the department of chemistry, College of Sciences, University of Kerbala, the Iraqi Ministry of Higher Education and Scientific Research, for giving me the opportunity and support for my study.

Words fail me to express my gratitude to my supervisors, **Dr. Hayder Hamied Mihsen** and **Dr. Haitham Dalol Hanoon**, for their invaluable advice, endless support, and continuous encouragement throughout. They have always been there for me, and are always ready with a solution to any problem.

Finally, I would like to thank **my family** members for their continuous support and encouragement. They have been incredibly supportive of me over the years, and I cannot thank them enough.

Dedication

To my dear father, to the light that illuminates my life, to the one who spent her life for us, nothing can do justice to you.

To my dear mother, to the tenderness that never leaves me in reality or in a dream.

To my dear husband, my support, the father of my children, my companion in hardship and study, and his endurance of all my troubles.

To my dear brothers and my strength in life.

To my children, the apple of my eye, and my companions in my studies, Ahmed, Zaid, and Ali.

To my supervisors, with special appreciation.

Noor

Abstract

Catalysts are very important in our daily life, as they are more efficient and speed up the reaction. Catalysts also have a key property called selectivity, by which they can direct a reaction to increase the amount of desired product and reduce the number of unwanted byproducts. In addition, they can be Reusability as in the catalysts we prepared RH-SiO_2PrANSA and RH-SiO_2PrOPDA-SO4H, which are solid acid catalysts. The preparation of these catalysts is considered green chemistry, which is the focus of researchers' attention, as it has the benefit of reducing pollution and getting rid of waste such as rice husks, which are usually disposed of by burning. However, in this research, we prepared catalysts from rice husks and from new components or compounds that researchers have never used before, in environmentally safe and inexpensive ways that do not take much time. Catalysts have been used in many applications such as environmentally friendly industries, medical industries, petroleum refining, etc. They were used in new chemical reactions, namely the preparation of imidazole derivatives. Several techniques have been used to characterize some of the prepared compounds, such as FT-IR Technique, where a appears peak (S=O) group at 1354 cm^{-1} for RH-SiO_2PrANSA and 1465 cm^{-1} for RH-SiO_2PrOPDA-SO_3H, also, the (C−Cl) group of RH-SiO2PrCl appears at 698 cm^{-1}, and the XRD diffraction pattern showed a strong and broad peak diffused at 22° (2θ) indicating the amorphous nature of RH-SiO_2PrANSA and RH-SiO_2PrOPDA-SO_3H, according to the FESEM images, the formed structures appear to be irregular and regular in shape, elemental analysis (CHNS) showed the presence of nitrogen and sulfur for RH-SiO_2PrANSA and RH-SiO_2PrOPDA-SO_3H, respectively, which can be regarded as further evidence of the effective incorporation of the organic molecules on the silica surface; as for nitrogen adsorption analysis showed that the specific surface area of RH-SiO_2PrANSA and RH-SiO_2PrOPDA-SO_3H was less than the specific surface area of RH-SiO_2PrCl, due to large molecules attached to the surfaces of the functional silica matrix and.

The results of the TGA for the two new catalysts showed two stages for each, the first stage was caused by the loss of water adsorbed on the surface of the sample and the second stage was due to the decomposition of components on the surface of the catalyst.

2,4,5-trisubstituted imidazole derivatives are organic compounds characterized by an imidazole ring containing three substituents at the 2, 4, and 5 positions. In general, 2,4,5-trisubstituted imidazole derivatives have a wide range of potential applications in various fields, making them an important class of compounds for research and development, including pharmaceuticals, polymers and corrosion inhibitors. All synthesized of 2,4,5-trisubstituted imidazole derivatives were characterized using FTIR, ^{1}HNMR and mass spectra. The method has several advantages, for example, these products can be easily monitored, Good production rates can be achieved, shorter reaction times of this reaction method with the reusability of catalyst, by easily filtering the catalyst from the mixture at the end of the reaction.

Table of Contents

List of Figures

List of Schemes

List of Tables

Abbreviations

symbol	Definition
BF4	1-Butyl Imidazolium Tetrafluoroborat
DNA	Deoxyribonucleic Acid
EDX	Energy Dispersive X-Ray Spectroscopy
IUPAC	International Union Of Pure And Applied Chemistry
PBH	Rice husks That Are Parboiled (PBH)
pKa	Acid Dissociation Constant
RH	Rice Husk
RHA	Rice Husk Ash
XRD	X-Ray Diffraction Analysis
CPTES	3-(chloropropyl)triethoxysilane
RH-NO_3	Rice husk-nitrate
ISRO	Indian Space Research Organization

Chapter One Bibliography

1.0 Porous Materials

Because of their numerous industrial uses as ion exchangers, adsorbents, and catalysts, porous materials are of tremendous interest [1]. Different porous materials have different degrees of crystallinity, pore size, geometry, and chemical content. Porous materials are divided into three classes per the IUPAC definition [2,3], Porous materials can be classified according to their size in nanometers, 0-2 nm called microporous, 2-50 nm called mesoporous and 50-1000 nm called macroporous as shown in Figure 1.1[4].

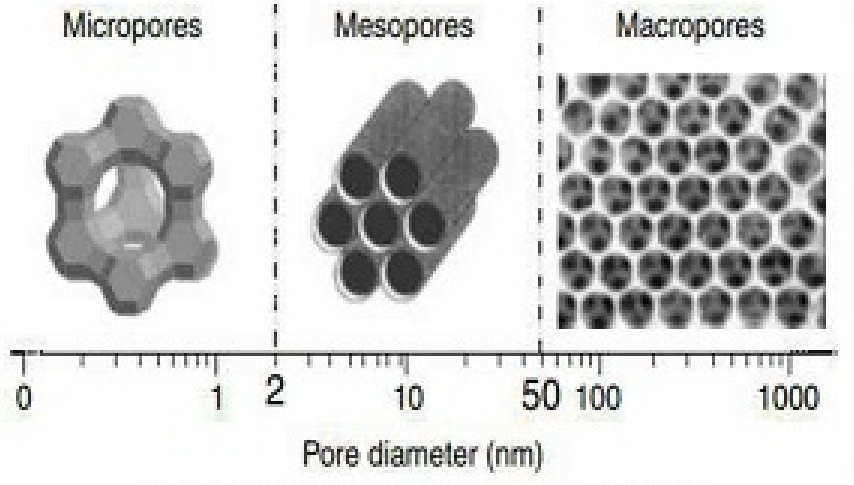

Fig.1.1: IUPAC classification of porous materials[4].

1.1 Rice and rice husks (RH)

Rice is the most important food crop in the Asia-Pacific region[5], with increasing demand for it from the population of these regions, and more than 90% of the world's rice is produced and consumed[6]. Moreover, these aforementioned regions constitute over 56% of the global populace. As a result of the increasing consumption of rice due to the increase in population density in these countries, these producing countries are developing a plan for self-sufficiency in rice. Also, not all countries are able to produce rice, as they import it in large quantities[7]. It is expected that the percentage of rice production will increase by 20% by 2025[8].

Rice husks are one of the most abundant plant residues in rice-producing countries[9]. The tough protective husks that cover rice grains, known as rice husks (see Figure 1.2), are removed from rice seed as a secondary produce of milling[10].

Fig 1.2: The rice grains covered in husk in plant spike.

Rice husk is a valuable raw material that is added for a variety of uses[11]. Rice husk biomass consists of the three polymers cellulose, hemicellulose and lignin[12]. Similar to other lignocellulosic biomass feedstock's, rice husk has been investigated as the most affordable feedstock for the synthesis of bio-ethanol[13].

It is virtually devoid of forest remnants and wastes from the agricultural industry, by using these wastes, the disposal issue might be resolved and waste treatment costs could be decreased[14]. Rice husk ash is what's left over when rice husks are burned. Parboiled rice husks (PRH) are utilized as a substrate or media in gardening, including some types of hydroponics[15]. Rice husks have been demonstrated to have no effect on the regulation of plant growth (see Figure 1.3). The husks of rice are filling for pillows, because they maintain the contour of the skull, the lightly stuffed pillows are said to be therapeutic [16].

Fig.1.3: Rice husks.

1.1.1 Components of rice husk

The chemical components of rice husks vary depending on the type of rice, soil type and climate[11]. Rice husk constitutes about 20% of the weight of rice, rice husks contain 28-30% inorganic compounds and 70-72% organic compounds[17]. Its composition consists mainly of: cellulose, lignin, silica, and moisture[18] as shown in Table 1.1.

Table. 1.1: chemical components of rice husks[18].

Components	Content (Wt. %)
Cellulose	50
lignin	25–30
silica	15–20
moisture	10–15

1.1.2 Rice Husk Applications

a) Due to the features of good scales, it is a good insulator, including high porosity, melting point, low density, and good thermal conductivity, because of these features scales are used in steel production[19].

b) Use in building materials: A substance called porcelan is extracted from the peel ash, which is a substance used in the manufacture of building materials or added to it, which is highly reactive and used in the production of concrete blocks[11].

c) Use as a source of inorganic materials: husks ash contains inorganic materials, including silica[20]. When extracting these materials, it is less time-consuming and cost-effective, and is used in the food industry as an antioxidant, as well as a strengthening ingredient in the rubber, cosmetic, and toothpaste sectors[21]. Fine amorphous silica is becoming more and more in demand for usage in nuclear power plants, bridges, maritime settings, and the manufacturing of high-performance cement and concrete[22]. Rice husk (RH)-prepared silica aerogels are used as dielectric materials, catalyst supports, and superthermal insulators. It might be a raw ingredient that makes silicate and silica manufacture economically feasible[23].

d) Additional uses: The Indian Space Research Organization has effectively created a method for extracting high-purity silica from RHA, which applies to the production of silicon wafers and to create high-efficiency phosphor[24]. Rice Husk (RH) is also used to reduce insect pests in food items that are stored. ISRO has found that RHA works well as an oil spill absorbent, fire retardant, water repellent and pesticide carrier[24].

1.2 Silica

Silica is a substance composed of silicon dioxide SiO_2, which is the main component of quartz and sand[25]. Silica has many remarkable properties such as controllable pore size, modifiable surface, strong mechanical properties, and a comparatively inert chemical composition, making it suitable for various applications[26]. It has been widely used in food and medical industries due to its safe and non-toxic nature[27]. Although there is a difference in their structure, all types of silica are composed of the same materials, as there are two main types of silica, crystalline and amorphous silica (see Figure 1.4). Quartz is the most common form of crystalline silica, and there are other types as well, which are less common [28]. The silicon and oxygen atoms in crystalline silica are arranged in a specific geometric shape, and there is no spatial arrangement of atoms in amorphous silica[29].

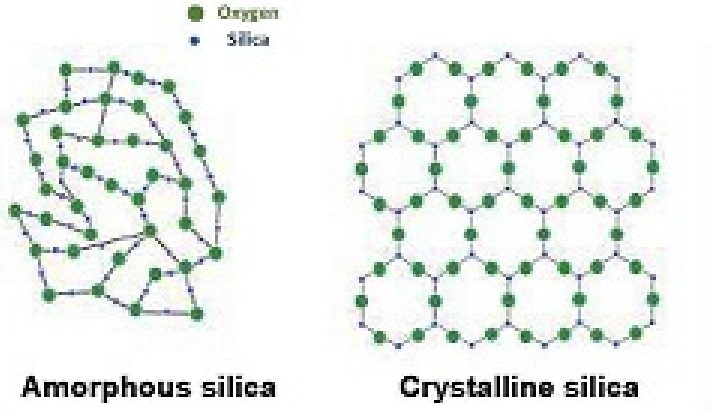

Fig.1.4: Crystalline and amorphous forms of silica.

All parts of the environment, including rocks, sand, clay, soil, air, and water, contain silica compounds[30]. Many commercial products, including talcum powder, cleaners, granite, bricks, glass and ceramics, plaster, and concrete, include silica[31]. Amorphous silica comes in various forms and is utilized in toothpaste, cosmetics, food wrappers, and additives[32]. An inorganic substance called amorphous silica (SiO2) is frequently utilized in semiconductor circuits to separate various conducting zones.

Amorphous silica has also emerged as a crucial component in chromatography and microelectronics because of its selectivity for chemical modification.[33] It has good immovability of mechanical and high dielectric strength, Molecular biologists use (SiO_2) in resins and optical beads to study bio macromolecules due to its unique qualities, making it essential for a wide range of applications[34]. Many applications involving macromolecules and silica have been possible in recent years, this is due to the great development in technology[35].

1.2.1 Surface of silica

There are two types of functional groups on the silica surface, which are silanol (Si-OH) groups, through which the first path on the silica surface is modified, and the second type is siloxane (Si–O–Si) [36].

There are two main methods by which silanol groups are formed on the surface[37]. These types of groups are produced during the production of silica by condensation[38]. Second, when handled with water or other aqueous solutions, surface groups may develop as a result of the rehydroxylation of dehydroxylated silica [39]. Three types of silanol groups can be distinguished on the surface of silica, as shown in Figure 1.5[37]:

1. Isolated groups, also known as free silanols, in which the bulk structure of the surface silicone atom consists of three bonds, with the fourth bond being joined to a single –OH group[40].

2. Vicinal silanols, also known as bridging silanols, are silanols with two isolated groups linked to separate silicon atoms that are sufficiently close to the hydrogen bond[41].

3- Germinal silanols are two hydroxyl groups attached to a single silicon atom and are too close to one another to create a hydrogen bond[42].

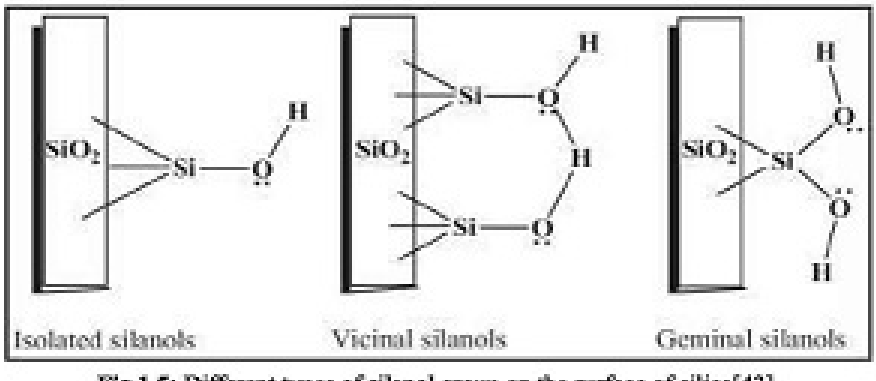

Fig.1.5: Different types of silanol group on the surface of silica[43].

1.3 Sol–gel process

This process involves constructing a 3D model through the formation of an inorganic suspension that forms a gelatinous substance in the liquid phase. Organometallic compounds with reactive functional groups encircling them make up the precursors used to create colloidal sols [44]. After being heated, sol-gels can take the shape of films, particles, fibers, aerogels, and dense structures at the micro- and nanoscale[45].

Since sol-gel products are originally amorphous, the right heat treatments can be used to convert them into crystalline forms[45]. Through this chemical process, a "sol" (a colloidal solution) is created, which then develops gradually into a gel-like diphasic system with a liquid phase and a solid phase with morphologies ranging from discrete particles to continuous polymer networks (Scheme 1.1). When it comes to the colloid, it's possible that the volume fraction of particles, or particle density, is so low that a sizable amount of fluid must be evacuated before the gel-like characteristics can be identified.

$$\equiv Si-OR + H_2O \Longrightarrow \equiv Si-OH + ROH \quad \textbf{(Hydrolysis) (1)}$$

$$\equiv Si-OH + RO-Si \Longrightarrow \equiv Si-O-Si + ROH \quad \textbf{(condensation with formation of alcohol) (2)}$$

$$\equiv Si-OH + OH-Si \Longrightarrow \equiv Si-O-Si \equiv + H_2O \quad \textbf{(condensation with formation of water) (3)}$$

Scheme. 1.1: Sol-gel formation equations.

There are numerous ways to achieve this. The easiest way is to let the sedimentation happen naturally and then drain the liquid that remains. Phase separation can also be expedited using centrifugation[46]. Metal oxides, particularly silicon and titanium oxides, are produced via the sol-gel process[47]. Inorganic salts or metal precursors are typically utilized as precursors[48]. The pH of the solution and the amount and rate of water addition are the two primary factors that define the final product's characteristics[49]. The sol-gel method, a gel substance, is one way to make sodium silicate from rice husks. Silica is extracted from the leftover ash to create sodium silicate[50], then Which is used in the production of heterogeneous solid catalysts [51].

1.4 Modification of the surface of silica by Silylating Agents

Surface modification of a substance is a change in the properties of that substance from a biological, physical, or chemical perspective, and these properties must differ from those present on the surface of the substance whose surface is to be modified [52]. A variety of techniques can be used to modify the surface in order to change a broad range of properties, including reactivity, roughness, hydrophilicity, surface charge, and surface energy [53].

In order to alter the surface and interface characteristics of powder, silica is frequently utilized as an agent[54]. In adsorption and ion exchange, the active silica surface with a large specific surface area is crucial[55]. Any procedure that results in alterations to the surface's chemical makeup is considered a modification of silica surfaces[56]. It is possible to modify the surface chemically, changing the silica surface's chemical properties, or physically, through thermal or hydrothermal treatment, which alters the concentration of silanol and siloxane on the surface[57].

There are two different ways to modify the surface of silica: inorganic functionalization, where the group anchored on the surface might be either a metallic oxide or an organometallic composite, and organic functionalization, where the modifying agent is an organic group[58]. Two different types of functional groups make up the silica surface: silanol groups (Si-OH) and siloxane groups (Single Bond O Single Bond Si). It has been discovered that the primary mechanism for modification happens when a certain molecule reacts with silanol groups that are present on the silica surface[59]. An essential first step in the creation of a variety of silica-based products is the organo chloro functionalization of amorphous silica. Other organic moieties can be anchored to the silica surface using organo-chloro-functionalized silica with a single-bonded C-Cl end group. Additionally, it can serve as a foundational ingredient in the manufacturing of heterogeneous catalysts[60].

The most common method for surface functionalization of silica with 3-(chloropropyl)triethoxysilane (CPTES) is a solid-liquid mixed phase reaction. As shown in (Scheme 1.2) [61][36]. the reaction needs reflux in toluene for 12 hours. Reflux in toluene can also cause silica to form for 24 hours. In order to achieve the same result, 3-(chloropropyl)trimethoxysilane (CPTMS) can be used to activate silica surfactant functionalization by refluxing CPTMS with silica for a whole day [62].

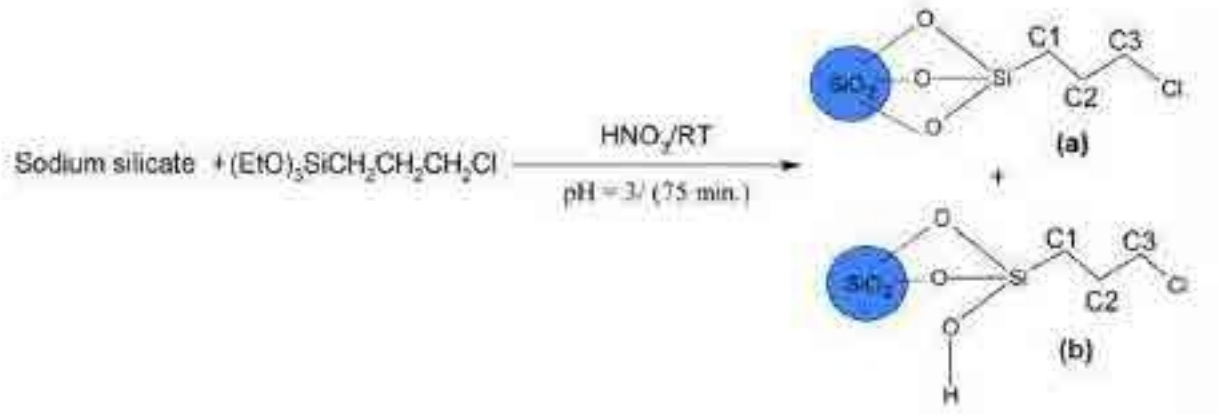

Scheme. 1.2: (a) T3 — three siloxane bonds to silica, (b) T2 — two siloxane bonds to silica.

In addition to functionalizing the silica surface with chemicals that had chloro groups, the resulting functionalized silica was employed in the creation of catalysts by reacting Brønsted acids (Scheme 1.3). Due to their special qualities, which include high efficiency because of their larger surface area, more thermal stability and reusability, low toxicity, greater selectivity, ease of handling, and high selectivity, Brønsted acid-supported silica, like polyphosphoric acid and sulfonic acid, have attracted a lot of interest in organic synthesis[63] [64][65].

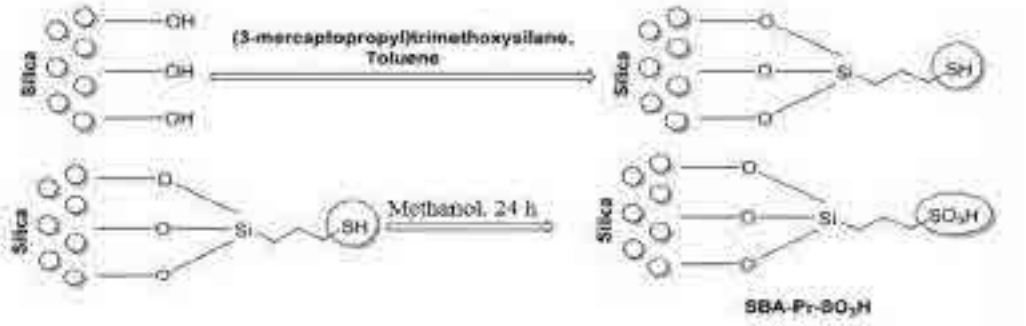

Scheme. 1.3: Synthesis and Structure of SBA-Pr-SO_3H.

Sulfonic acid has been documented to be used in a number of diverse organic reactions. There are two applications for silicate sulfuric acid catalyst: silicate sulfuric acid and sulfuric acid adsorbed on the silica surface (Scheme 1.4)[66]. Since sulfuric acid adsorbed on silica may be recovered and utilized again for multiple cycles without affecting the catalytic system's activity, it is a very straightforward and cost-effective method for large-scale synthesis[65]. It is a reusable, safe, and environmentally friendly stimulant, according to studies[66][67][68].

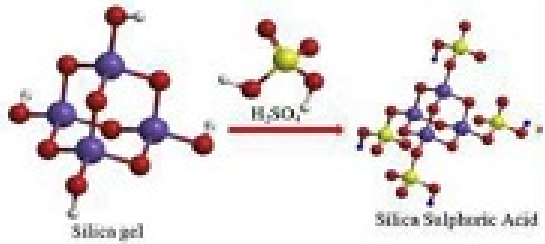

Scheme. 1.4: Synthesis of catalyst Silica sulfuric acid (SSA).

It is sometimes necessary to use sulfonic acid from various sources in order to stabilize it on the silica surface. In this case, the acid is stabilized on the functionalized silica surface by substituting 7-amino-1-naphthalene sulfonic acid for the chlorine group, resulting in heterogeneous solid acid catalysts, as shown in (Scheme 1.5)[69].

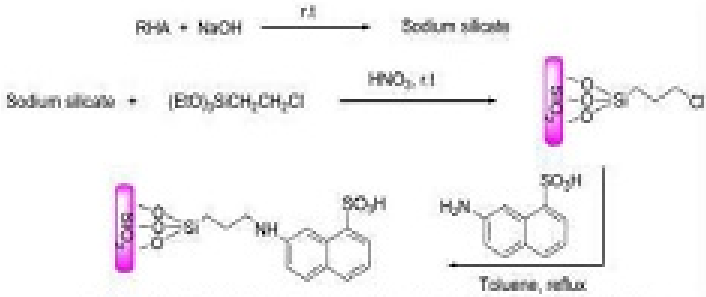

Scheme. 1.5: 7-Amino-1-naphthalene sulfonic acid immobilized silica.

1.5 Catalysts

This substance works to reduce the temperature of the reaction, accelerate it, or reduce the pressure necessary for the reaction, and this happens without consuming this substance [70]. The catalysis process occurs by adding a specific substance as a catalyst, and it occurs by breaking the molecules that make up the substance, which is breaking the bonds of the atoms and rebuilding and organizing them during the reaction, which leads to the formation of new molecules, as in Figure 1.6[71]. The role of the catalyst as a catalyst is to activate the reaction energy when a decrease in energy occurs[72].

This facilitates the breakdown of molecules and creates new molecules, and catalytic processes are carried out more efficiently and faster when used as a catalyst[73].

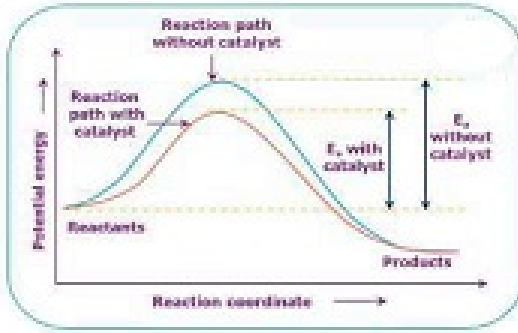

Fig.1.6: Diagram of a Catalyzed Reaction.

One of the characteristics of a good catalyst is selectivity, and this distinctive characteristic controls the reaction, reduces undesirable produced materials, and works to increase production according to demand [70].

About two centuries ago, in 1835, Swedish physicist Jöns Jakob Berzelius made the discovery of catalysis [74]. elucidated the findings of previous research conducted by a number of scientists, including Faraday and Döbereiner [75]. Berzelius found that the presence of a certain chemical, referred to as a catalyst, was necessary for a number of reactions to start [76]. Nonetheless, catalysis was employed for thousands of years prior to its discovery and rationalization, such as in the fermentation of yeast to create ethanol [77].

In accordance with IUPAC2, a catalyst is "A substance that increases the rate of a reaction without altering the overall standard Gibbs energy change in the reaction; the process is called catalysis [9-10]. " This is a more precise definition of what a catalyst and catalysis are. The current work focuses on heterogeneous catalysis, which is characterized by the formation of at least two phases by the catalyst, reactants, and products. Solid catalysts are used in the gas-phase processes that are the subject of this analysis [79].

1.5.1 Catalysis in chemical industry

Nearly 90% of the goods produced in the chemical industry are the result of catalytic processes, which are highly significant for sustainable development, energy production, environmental protection, and food production[80]. Due to its significant strategic and economic value, the topic of catalysis is one that is developing quickly[81]. Gaining a basic understanding of the structure and phenomena of catalytic surfaces as well as the connections between a catalyst's composition, synthesis method, characteristics, and industrial process performance is imperative in light of the major difficulties of the modern era[82]. To enhance current catalysts or create novel systems that may effectively and selectively produce a specific product through a particular reaction (Figure 1.7). The development of early industrial catalysts was primarily driven by quantitative factors. In order to achieve the criteria needed for contemporary catalytic processes, new catalysts must be developed. This development was seen in the World War II boat and automobile industries.

Fig.1.7: Different forms and shapes of catalysts[83].

The following are the general qualities that an industrial catalyst must possess [84]:

1) Activity: the quantity of product compared to the reactant utilized or the quantity of catalyst.

2) Selectivity is the quantity of desired product generated per reactant consumed, in a catalytic reaction,
3) Lifetime, or the amount of time the catalyst can be utilized without losing its ability to function.
4) The catalyst regeneration's ease of use.
5) Toxicity in the sense of being easy to use and causing less issues with toxic waste.
6) Price is the total of all the procedures that, when the catalyst is used in a process, result in extra expenses.

1.1.5 Types of catalysts

Catalysts are typically categorised based on their solubility or insolubility in the reaction medium [84]. Homogeneous and heterogeneous catalysts are the two broad categories of catalysts. While heterogeneous catalysts are typically not soluble in the reaction medium, homogeneous catalysts are soluble in the reaction medium. However, since soluble catalysts, for instance, may generate insoluble metal particles in situ, using solubility as the only criterion for catalyst classification is not truly adequate. Then, these metal particles can serve as catalysts that are heterogeneous[85]. The next subsection goes into detail on both forms of catalysis.

1.1.5.1 Homogeneous catalysts

The creation of organic catalysts provides the foundation for the majority of developments in industrial homogeneous catalysis. The last several decades have seen the discovery of thousands of organometallic complexes, or molecules containing metal–carbon bonds. The potential uses of transition metals as industrial catalysts has fueled the rapid advancement of their organic chemistry[86]. The reactivity of organic ligands attached to the metal centre is used to explain the chemistry of organo transition metal catalysis. Transition metal d orbitals enable the binding of ligands such alkenes, CO, and H (hydride) in a way that activates them for additional reactions[87].

Reactions involving ligands in the coordination sphere of the same metal centre are the most significant in catalytic cycles. The products must be easily released from the coordination sphere and the reactants must be loosely coordinated to the central atom for the chemical changes to occur.

Extremely labile metal complexes are necessary for both processes to proceed with the lowest feasible activation energy. These complexes contain one or more weakly bound ligands, or an empty coordination site. The ability of transition metals to exist in a variety of oxidation states and to display a range of coordination numbers accounts for their binding capability. The ligands of the coordination complexes can be categorised into two groups: ionic and neutral.[88].

and alkenes, phosphates, phosphines, arsine, H_2O, and amines are a few examples of neutral ligands. This distinction is helpful in characterizing the path of reactions as well as assigning oxidation states. It is important to note that this explanation is mostly formal and occasionally misses the mark on the actual bonding scenario. Therefore, while it is true that alkyl groups react as R^- and hydrogen ligands typically respond as H^-, it is also plausible that other groups, such methyl groups, react as CH_3 or CH^{+3}. This chapter aims to provide an overview of the most significant types of reactions, which is adequate to comprehend the reaction cycles of homogeneous transition metal catalysis, instead of delving into the principles of organometallic chemistry.

1.1.5.2 Heterogeneous catalysts

Solids catalyst reactions between molecules in a gas or solution in heterogeneous catalysis. Catalytic reactions take place at the surface of solids because, unless they are porous, they are often impermeable. Catalysts are typically nanoscale particles supported on an inert, porous structure to make economical use of the frequently costly materials (such as platinum) (see Figure 1.8). Heterogeneous catalysts are the workhorses of the chemical and petrochemical industry[89].

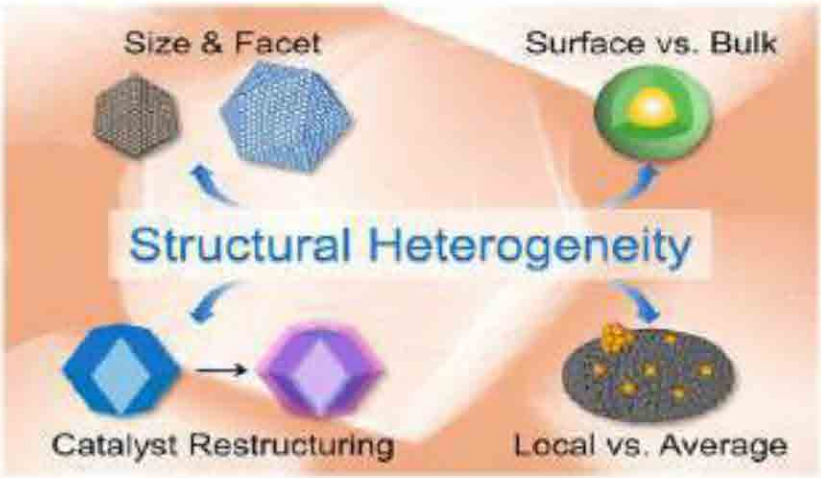

Fig.1.8: Types of structural heterogeneity in Nano catalysts.

In the field of catalysis, nanoparticles have been used commercially for nearly a century, if we define nanotechnology as the branch of materials science that aims to regulate material properties on the nanoscale scale[90]. To create small particles for heterogeneous catalysts and maintain their stability under the frequently harsh conditions of an industrial reactor, numerous synthetic approaches are available. Nanotechnology is at the forefront of modern catalysis[91]. Contact catalysis is a type of heterogeneous catalysis. This type describes catalytic processes or reactions that involve solid materials, materials in the liquid phase, or materials in the gas phase [92].

The main advantage of using a heterogeneous catalyst is that it can be readily isolated from the product stream and reused multiple times, making the chemical processes more profitable and continuous. Furthermore, heterogeneous catalysts usually withstand harsh working conditions better than their homogeneous counterparts[75].

1.6 Imidazole

German scientist Heinrich Debus originally reported imidazole in 1858, however several of its compounds were found as early as the 1840s [93]. It has been demonstrated that imidazole, or glyoxalin as it was initially termed, is formed when glyoxal, formaldehyde, and ammonia condense [94]. This preparation process yields a modest amount of the molecule; however, imidazole derivatives are nevertheless made using it. Imidazole can be produced using a variety of techniques in addition to the Debus process that is described below.

By modifying the functional groups on the reactants, many of these production techniques can also be used to create imidazole derivatives[95]. The amount of components that react determines how these techniques are typically categorised. Because hydrogen can establish a connection with any one of the two nitrogen atoms, it exists in two equivalent forms. Because the imidazole has a planar ring with six π electrons, it is categorised as aromatic [96]. Alkaloids in particular are rich in chemical molecules containing the imidazole ring. Several essential biologically developing substances, like as histidine and the related hormone histamine, include this ring shape. An imidazole ring is present in a number of drugs, such as nitro imidazole-containing antibiotics, antifungals, and the sedative midazolam[97].

1.6.1 Chemistry of Imidazole

Imidazole is an organic compound with the formula $C_3H_4N_2$ and its Molecular weight is 68.077 g/mol, it has a resonance value of 14.2 kcal/mol, which is approximately half that of pyrazole. It is an aromatic heterocycle with non-adjacent nitrogen molecules in met substitution that is classed as a di-azole in chemistry. Because it can attach hydrogen to either or both nitrogen atoms, imidazole is a planar, five-membered ring with two parallel tautomeric types. With a dipole moment of 3.67 D, imidazole is a strongly polar molecule that dissolves readily in water.

The substance is classified as aromatic due to the presence of a planar ring with six π electrons. Imidazole resonance structures are as follows:

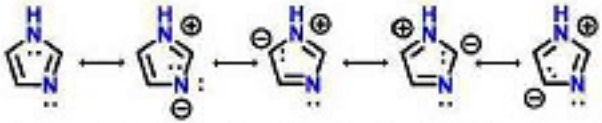

Because imidazole is amphiprotic, it can function as both a base and an acid simultaneously. With a pKa of 14.5, imidazole is somewhat more acidic than alcohols but slightly less acidic than carboxylic acids and phenols.

The acidic proton is the one that has a connection to nitrogen. The symmetrical imidazolide anion is produced by deprotonation [98]. Because the conjugate acid has a pKa of about 7 (also known as pKBH+ to prevent confusion), imidazole is approximately sixty times more basic than pyridine. The basic site is the nitrogen with the lone pair. The symmetrical imidazolium cation is produced by protonation[99]. Furthermore, Imidazoles typically undergo electrophilic substitution, while their nuclei undergo nucleophilic substitution when an electron-withdrawing group is present [100].

1.6.2 Physical properties

Imidazole is a highly polar substance that dissolves readily in water. It is a colourless or white material that evaporates in water to produce a combination that is somewhat basic. As an amphoteric molecule, imidazole has the ability to function as both a base and an acid. It is slightly more acidic than alcohols, but less acidic than phenols, imides, and carboxylic acids. Generally speaking, pyridine is sixty times less basic than imidazole[101].

With a melting point of 90°C, imidazole is a tautomeric material with a weak base since positions 4 and 5 are equal.

In dioxane, imidazole exhibits a significant dipole moment of 4.8 D. Compared to pyrazole and pyridine, imidazole has a pKa of 7.2 and exhibits amphoteric properties [100].

1.6.3 Synthesis

1.6.3.1 Synthesis of imidazole in general

Many techniques can be used to synthesise imidazole. By changing the reactant's functional group, many of these syntheses can also be applied to various substituted imidazoles. Imidazole derivatives can be synthesised using a variety of methods, including Wallach synthesis from aminonitrile and aldehyde, Marckwald synthesis, Debus synthesis, Radiszewski synthesis, and dehydrogenation of imidazolines[100]. The synthetic processes' specifics are listed below.

1) Debus Synthesis: Using formaldehyde and glyoxal in ammonia, Debus synthesised imidazole. C-substituted imidazoles are still made using this process, despite its very low yields [102].

2) Radiszewski Synthesis: In the presence of ammonia, Radiszewski showed how to condense benzil and α-ketoaldehyde, benzaldehyde, or α-diketones, yielding 2, 4, 5-triphenylimidazole [103].

3) Dehydrogenation of Imidazoline: In the presence of Sulphur, Knapp et al. have reported using barium manganate, a gentler reagent, to convert imidazolines to imidazoles. 2-substituted imidazoles are produced when imidazolines made from alkyl nitriles and 1,2-ethanediamine react with $BaMnO_4NH$[104].

4) Wallach Synthesis: Wallach observed that *N,N*-dimethyloxamide treated with phosphorus pentachloride yields a molecule containing chlorine, which subsequently reduces to *N*-methyl imidazole when reduced with hydroiodic acid. *N,N*-diethyloxamide is transformed under the same circumstances into a chlorine molecule, which upon reduction yields 1-ethyl-2-methyl imidazole[105].

5) By the production of one bond: An imidate and an α-aminoacetal or aminoaldehyde can react to generate the (1,5) or (3,4) link, which causes an imidine to cycle into an imidazole.

6) Markwald Synthesis: A typical technique for the synthesis of imidazoles is the creation of 2-mercaptoimidazoles from a-amino ketones or aldehyde and potassium thiocyanate or alkylisothiocyanates. The necessary imidazoles can be easily obtained by removing the Sulphur using a variety of oxidative methods. The primary obstacle to the Markwald synthesis is likely the unavailability of the starting chemicals, α-aminoaldehyde or ketone[104].

1.6.3.2 Synthesis of 2,4,5-trisubstituted imidazole

The literature has documented a variety of techniques for the one-pot synthesis of imidazole derivatives of benzil, aromatic aldehyde, and ammonium acetate. Heterogeneous catalysts for the effective synthesis of substituted imidazoles include Lewis acids[106], ionic liquids (ILs) [107]. On the other hand, ILs are costly and difficult to recycle [108]. There have also been reports of the synthesis of imidazoles using organic solvents such glycerol, acetic acid, glyoxylic acid, and natural acids. Multiple aided syntheses of 2,4,5-trisubstituted imidazole have been reported. A conventional approach for obtaining 2,4,5-triphenyl imidazoles was independently reported by Sharma & Lakshmi [109]. It involved condensing 1,2-dicarbonyl compounds with various aldehydes and ammonia in an acidic medium (Scheme 1.6).

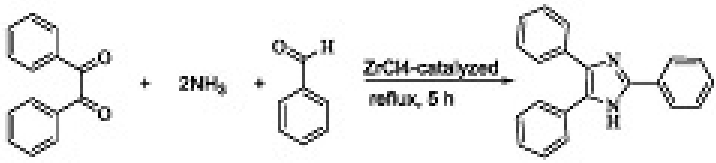

Scheme. 1.6: Syntheses of 2,4,5-trisubstituted imidazoles using $ZrCl_4$-catalyzed.

Teimouri et al. [110] reported on a straightforward, incredibly adaptable, and effective method for creating 2,4,5-trisubstituted imidazoles. The method involves utilizing clays, zeolite, and nano-crystalline sulfated zirconia (SZ) as catalyst in ethanol at a moderate temperature to achieve three-component cyclo-condensation of 1,2-dicarbonyl compounds, aldehydes, and NH_4OAc as an ammonia source.

This process yields 2,4,5-trisubstituted imidazoles with high yields, milder conditions, short reaction times, easy work-up, and purification of the products using non-chromatographic methods. Without significantly losing any of their efficiency, the catalysts can be retrieved and employed again for the next processes (Scheme 1.7).

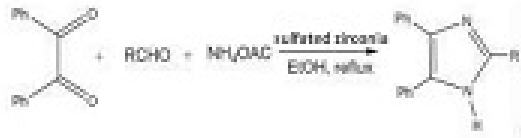

Scheme. 1.7: Syntheses of 2,4,5-trisubstituted imidazoles using Acid-catalyzed.

Lewis acid-catalyzed synthesis of tri-substituted imidazole derivatives was reported by Kerru, N. et al.[111] using combinations of phenanthroquinone and benzaldehyde derivatives in the presence of ammonium acetate. Polar solvents were employed in each reaction, and reflux conditions were maintained throughout. The IR and ^{1}HNMR were used to confirm the structures of all substances. This technique showed a number of benefits, such as good yields, ease of separation, and simplicity of use. The outcomes demonstrated that low reaction times and large yields of products were generated. Additionally, the Lewis acid catalyst's metal atom lengthened the reaction time and raised the substrate's reactivity (Scheme 1.8).

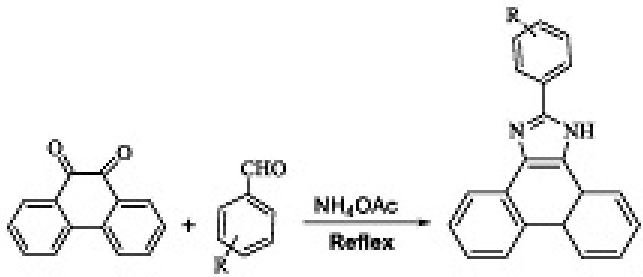

Scheme. 1.8: One-pot three component synthesis of substituted imidazoles in the presence of ammonium acetate under reflux conditions.

According to Das et al. [112] , benzil was treated with aldehydes and ammonium acetate in water under reflux while *p*-dodecylbenzenesulfonic acid was present as a catalyst to create 2,4,5-trisubstituted imidazoles. One more amine is added to the same procedure to produce 1,2,4,5-tetrasubstituted imidazoles. Under environmentally friendly conditions, the products develop in high yields in 4 hours (Scheme 1.9).

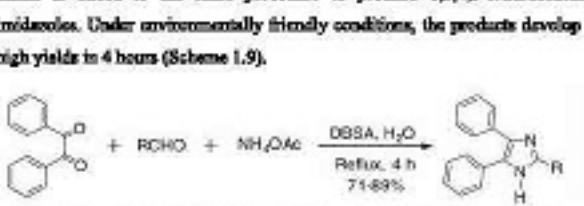

Scheme 1.9: Synthesis of 2,4,5-trisubstituted imidazole derivatives under reflux conditions[112].

1.6.4 Applications

In drug development, the imidazole nucleus is a crucial synthesis approach. As pharmaceutical drugs, several imidazoles have been created, including clotrimazole, zoraolidine, ergothioeine, miconazole, and cloxidine.

The use of imidazole derivatives as a treatment for denture stomatitis is one of their most significant uses. Imidazole is now a crucial component in numerous medications. Numerous fungicides, antifungal, antiprotozoal, and antihypertensive drugs contain synthetic imidazoles.

Theophylline, a chemical included in coffee beans and tea leaves that activates the central nervous system, includes imidazole. Because it interferes with DNA activity, mercaptopurine, an anticancer drug, contains it. It is used to treat leukaemia. In the industrial sector, imidazole is also used to prevent the corrosion of some transition metals, including copper. Corrosion causes the copper's conductivity to drop.

Imidazole derivatives are present in several substances of significant industrial and technological value. As a fire retardant, the thermostable polybenzimidazole imidazole fused to a benzene ring. Additionally, imidazole is included in a number of chemicals used in electronics and photography[113].

The purification of his tagged proteins using immobilised metal affinity chromatography (IMAC) is one use for imidazole. In the chromatography column, imidazole is utilised to elute tagged proteins bound to Ni ions that are bonded to the surface of beads. When too much imidazole is run through the column, the His-tagged proteins are released from nickel coordination and are dislocated.

Room temperature buffers with a pH range of 6.2–7.8 can be made with imidazole. It is advised to include it in a buffer for the horseradish peroxide assay. Additionally, it functions as a chelator to help various divalent cations connect to one another[114].

Imidazole used orally has been shown to be effective for psoriasis and seborrhoeic dermatitis. The first improvement in psoriasis appears one and a half to three months later. Patients with seborrhea dermatitis start to experience decreased redness, itching, and scaling after four to six weeks[115].

1.7 Aims of the study

1) Preparation of Sodium silicate from rice husk.
2) Preparation of precursor material of silica RH-SiO_2PrCl.
3) The use of RH-SiO_2PrCl for synthesis of heterogeneous catalysts which are RH-$SiO_2PrANSA$ and RH-$SiO_2PrOPDA$-SO_4H.
4) Characterization of these catalysts using various spectroscopic and microscopic techniques; such as CHNS analysis, TGA, powder X–ray, nitrogen adsorption/desorption analysis, FT-IR, AFM, FESEM/EDS and TEM.
5) Synthesis and production of imidazole derivatives using solid catalysts, as these products can be easily monitored, give good production rates and shorter reaction times.
6) Characterization of these imidazole derivatives revealed by FTIR, ^{1}HNMR, and mass spectroscopy.

Chapter Two

Experimental Work

2.1 Chemicals and Techniques

2.1.1 Chemicals

All chemicals were used directly without further purification. Rice husks were collected from a factory for rice production in Najaf Governorate-Abbasiya city. Table 2.1 shows the chemicals used in this work.

Table 2.1: Chemicals used in this work and their providers.

Chemicals	Formula	Purity (%)	Provider
Acetone	C_3H_6O	98	BDH, British
Ethanol	C_2H_5OH	99	Sigma-Aldrich, Germany
Methanol	CH_3OH	99	BDH, England
Toluene	C_7H_8	99	Merk, KGaA, Germany
Benzil	$C_6H_5CO_2$	99	BDH, England
Ammonium acetate	NH_4OAcCO_2	97	BDH, England
4-Hydroxybenzaldehyde	$C_7H_6O_2$	98	BDH, England
4-Nitrobenzaldehyde	$C_7H_5NO_3$	98	BDH, England
4-Chlorobenzaldehyde	C_7H_5ClO	98	BDH, England
Sodium hydroxide	NaOH	98	BDH, England
Nitric acid	HNO_3	70	CDH, India
THF	C_4H_8O	99	BDH, England
m-Hydroxybenzaldehyde	HOC_6H_4CHO	99	Sigma-Aldrich, Germany
Benzaldehyde	C_6H_5CHO	99	Sigma-Aldrich, Germany
4-(Dimethylamino)benzaldehyde	$(CH_3)_2NC_6H_4CHO$	99	Sigma-Aldrich, Germany
Dichloromethane	CH_2Cl_2	98	Sigma-Aldrich, Germany
Sulfuric acid	H_2SO_4	98	Merk, KGaA, Germany
Benzoyl nitrate	$C_6H_5NO_3$	99	Sigma-Aldrich, Germany
(3-Chlorophenyl)(2-hydroxyphenyl)methanone	$C_{13}H_9ClO_2$	95	Sigma-Aldrich, Germany
1-(4-nitro-3-vinylphenyl)-4-sulfonic acid	$C_8H_7NO_5S$	99	Sigma-Aldrich, Germany
o-Phenylenediamine	$C_6H_8N_2$ (solid)	99	Fluka
Hydrochloric acid	HCl	98	Scharlau, Spain.

2.1.2 Techniques

Table. 2.2: List of instruments, supplier companies and place of measurement

Instrument	Manufacturer	Place of measurement
FTIR	Shimadzu 8400s	University of Karbala / College of science – Iraq
FESEM-EDX	FESEM MIRA II (TESCAN)	Pars Particle Size Measurement Lab/Iran
TGA/ DSC	SDT Q600 V20.9 Build 20	Pars Particle Size Measurement Lab/Iran
CHNS	Eager 300 for EA1112	Pars Particle Size Measurement Lab/Iran
AFM	Model AA3000/ Angstrom Advanced Inc. USA	Pars Particle Size Measurement Lab/Iran
Nitrogen adsorption/desorption	nova 2000, quantachrome, USA	Pars Particle Size Measurement Lab/Iran
TEM	Philips CM12 instrument	Beam Gostar Tabas Lab/Iran
XRD	Shimadzu X-ray Diffractometer	Beam Gostar Tabas Lab/Iran
NMR	Bruker 400 MHz Germany	Pars Particle Size Measurement Lab/Iran
MASS	Agilent 5173	Pars Particle Size Measurement Lab/Iran
pH meter	WTW (model 720)	University of Karbala / College of science – Iraq
Centrifuge	Model EBA-720	University of Karbala / College of science – Iraq
Oven	Model un 110 plus	University of Karbala / College of science – Iraq
Balance	BL 210 S, Sartorius	University of Karbala / College of science – Iraq

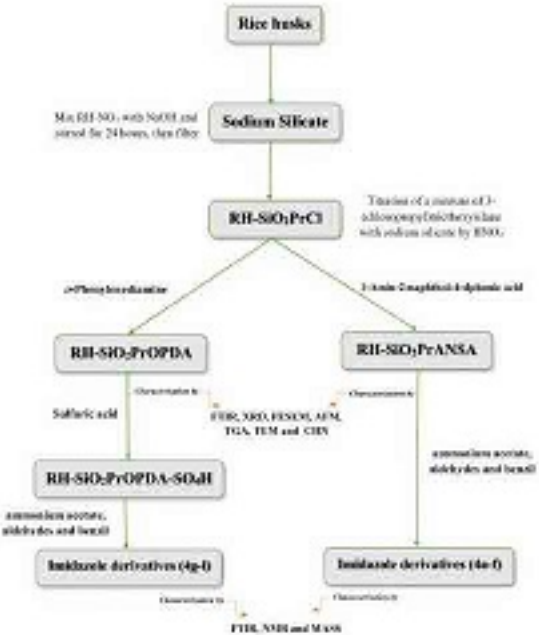

Fig. 3.1: Schematic of the preparation of catalysts and imidazole derivatives.

2.2 Preparation methods

2.2.1 Preparation Process of Rice Husks

Rice husk (RH) was collected from the quarry rice of Najaf and was washed three times with distilled water and dried at room temperature for 2 days. 50 g of cleaned rice husk was stirred with 500 mL of 1M nitric acid at room temperature for 24 hrs and washed many times very well and with distilled water until reached pH 6-7 and dried in an oven at 110 °C overnight to obtain RH-NO_3.

2.2.2 Preparation of Sodium Silicate Solution from Rice Husks

The preparation process of the non-crystalline sodium silicate from RH was performed using a recently reported method[116], briefly, 30 g of RH-NO_3 were mixed with 200 mL of 1M sodium hydroxide in a plastic container and stirred for 24 hrs. The mixture was filtered to remove the cellulose, and then was dried. The filtered part represented sodium silicate, was used as a precursor to the synthesis catalyst as shown in Scheme 2.1.

2.2.3 Preparation of Rice Husk Silica-3-(Chloropropyl)triethoxysilane (RH-SiO_2PrCl)

About 6 mL of 3-(chloropropyl)triethoxysilane (CPTES) was added to 50 mL of the prepared sodium silicate solution. The mixture titrated with 3M HNO_3 until the pH value reached 3. The formed gel was separated by centrifuge at 4000 r/min for 5 min. The mixture was washed with distilled water five times, and finally washed with acetone, then dried up to 24 h at 110°C in the oven. The prepared sample was labeled as RH-SiO_2PrCl, as shown in Scheme 1. The weight of the product was 6.4 g.

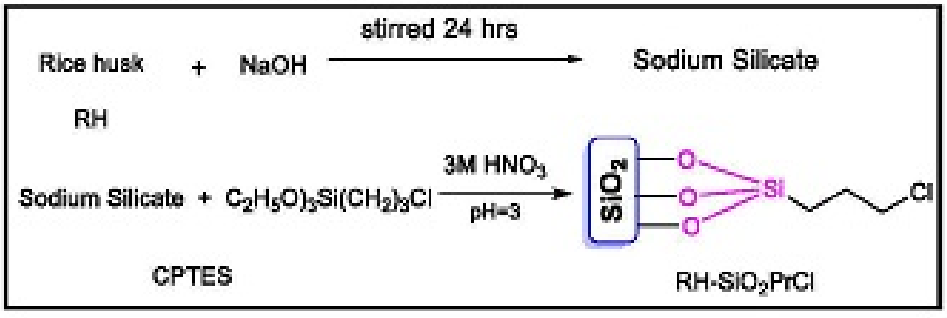

Scheme. 2.1: Preparation process of RH-SiO_2PrCl.

2.2.4 Preparation of acid catalyst (RH-SiO_2PrANSA)

(1g, mmol) RH-SiO_2PrCl was added to (2 g, 8.3 mmol) of 1-Amino-2-naphthol-4-slphonic acid, the mixture was refluxed for 24 hrs at 115°C in a mixture of 30 mL of toluene and (1.16 mL, 8.3 mmol) triethylamine (Et_3N) (Scheme 2.2). The resulting solution containing the yellow solid was filtered and washed with ethanol, acetone, and DMSO. Then dried for 24 hrs at 110°C. Finally, 0.7 g of the powder was collected as RH-SiO_2PrANSA.

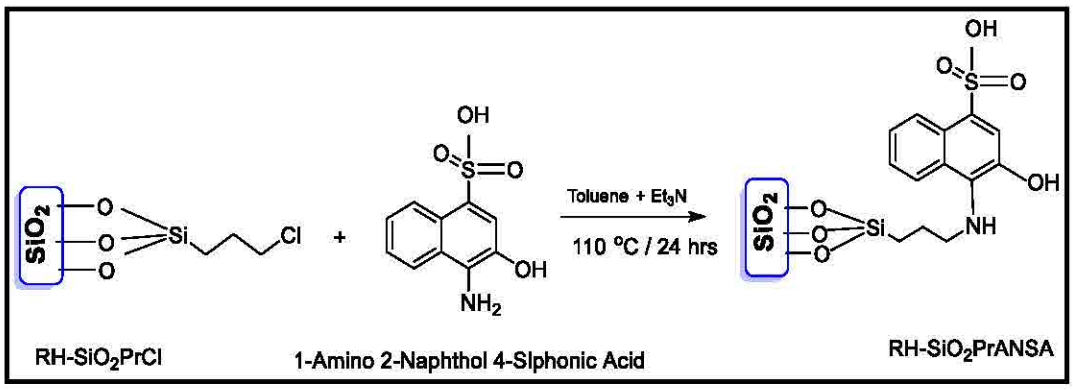

Scheme.2.2: Preparation process of RH-SiO_2PrANSA

2.2.5 Synthesis of imidazole derivatives (4a-f) using RH-SiO_2PrANSA as a catalyst

A mixture of (5 mmol) ammonium acetate, (1 mmol) aldehydes and (1 mmol) benzil were dissolved in 5 mL of ethanol, and then 0.08 g of RH-SiO_2PrANSA was added as a catalyst. The mixture was heated under reflux with stirring for 2.5 hrs. After the reaction was finished, the crude product was poured on dichloromethane (10 mL) with stirring for 15 minutes, and the solid Brønsted acid catalyst was removed by simple filtration. The catalyst was recovered in three successive cycles under the same conditions (Figure 3.13). The filtrate was poured into cold water (10 mL) and stirred for 10 min, a precipitated solid was filtered, washed with distilled water, and then dried. The product was purified by recrystallizing in ethanol:water mixture to afford imidazole derivatives as shown in Scheme 2.4. All the products were confirmed by melting points, FTIR, ^{1}H NMR and mass spectra.

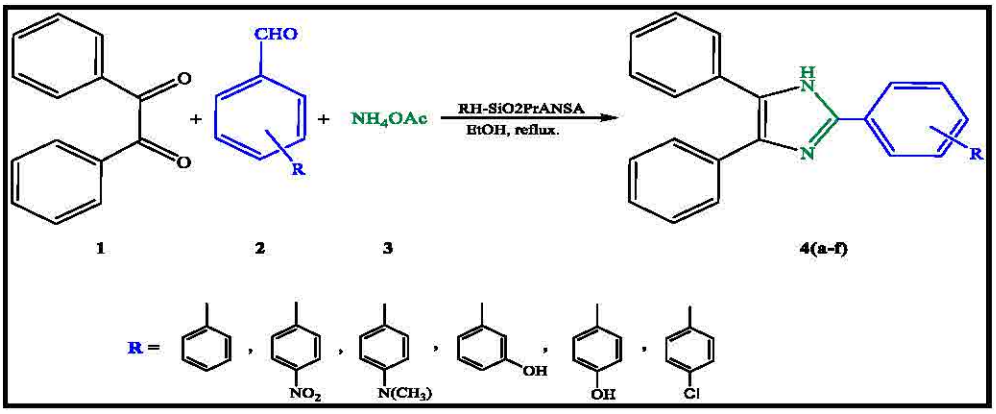

Scheme.2.3: Synthesis of some useful imidazole derivatives using RH-SiO_2PrANSA as a catalyst.

Table.2.3: Some physical properties and other characteristics of imidazole derivatives using RH-SiO_2PrANSA as a catalyst

Comp. No.	Name	Color	Molecular formula	M. Wt. (g/mol)	Yield (%)	m.p. (°C)		Ref.
						Found	Lit.	
4a	*2,4,5-triphenylimidazole*	beige	$C_{21}H_{16}N_2$	296.37	95	271-273	271-273	[117]
4b	*2-(4-nitrophenyl)-4,5-diphenylimidazole*	yellow	$C_{21}H_{15}N_3O_2$	341.36	83	194-196	199–201	[118]
4c	*4-(4,5-diphenylimidazol-2-yl)-N,N-dimethylaniline*	gray	$C_{23}H_{21}N_3$	339.34	71	259-261	256–258	[119]
4d	*3-(4,5-diphenylimidazol-2-yl)phenol*	gray	$C_{21}H_{16}N_2O$	312.36	97	255–258	254–257	[119]
4e	*4-(4,5-diphenylimidazol-2-yl)phenol*	beige	$C_{21}H_{16}N_2O$	312.36	80	236-238	233–236	[119]
4f	*2-(4-chlorophenyl)-4,5-diphenylimidazole*	white	$C_{21}H_{15}ClN_2$	330.81	95	263-265	260–262	[119]

2.2.6 Preparation of RH-SiO_2PrOPDA

An amount of (1 g) RH-SiO_2PrCl was added to (2 g ,8.3 mmol) of *o*-Phenylenediamine and the mixture was refluxed for 24 hrs at 115°C in 30 mL of toluene and triethylamine (Et_3N) (1.3 mL, 0.0148 mmol). The resulting solution containing the yellow solid was filtered and washed with ethanol, acetone, and DMSO. Then, 24 hrs. of drying at 110°C. Finally, 0.7 g of the powder was collected as RH-SiO_2PrOPDA. Then, 40 mL of 0.5 M sulfuric acid was stirred with (1.3 g) of the product at room temperature for 24 hrs, and the solid was filtered, washed with three times of distilled water, and dried in an oven at 110 °C for 24 hrs. Finally, brown powder (0.9 g) was obtained, and the product compound was designated as RH-SiO_2PrOPDA-SO_4H. As shown in Scheme 2.3.

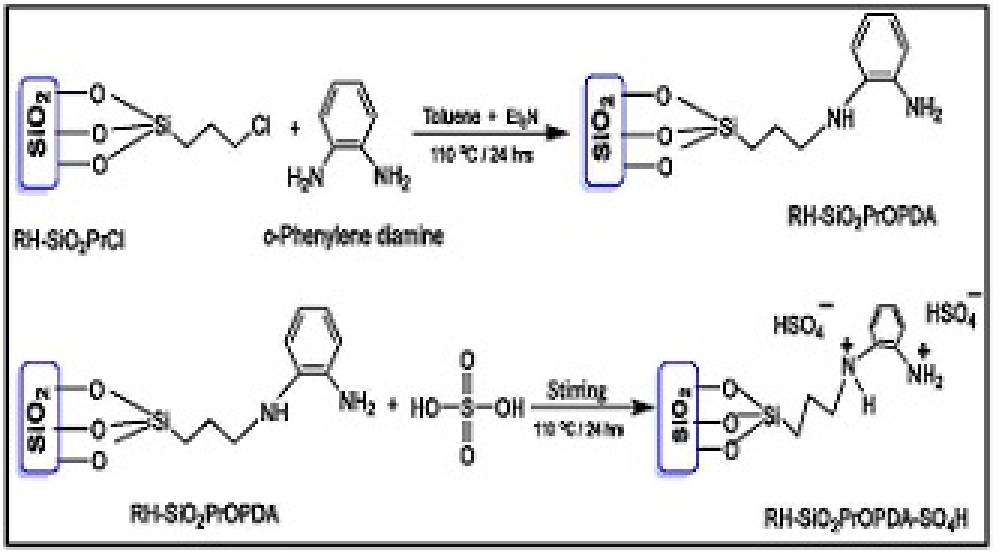

Scheme.2.4: Preparation process of RH-SiO_2PrOPDA-SO_4H

2.2.7 Synthesis of imidazole derivatives (4g-l) using RH-SiO_2PrOPDA-SO_4H as a catalyst

A mixture of (5 mmol) ammonium acetate, (1 mmol) aldehydes and (1 mmol) benzil were dissolved in 5 mL of ethanol, and then 0.04 g of RH-SiO_2PrOPDA-SO_4H was added as a catalyst. The mixture was heated under reflux with stirring for 4 hrs. After the reaction was finished, the crude product was poured on dichloromethane (10 mL) with stirring for 15 min, and the solid Brønsted acid catalyst was removed by simple filtration. The catalyst was recovered in three successive cycles under the same conditions (Figure 3.36). The filtrate was poured into cold water (10 mL) and stirred for 10 min, a precipitated solid was filtered, washed with distilled water, and then dried. The product was purified by recrystallizing in ethanol:water mixture to afford imidazole derivatives as shown in Scheme 2.5. All the products were confirmed by melting points, FTIR, ^{1}H NMR and mass spectra.

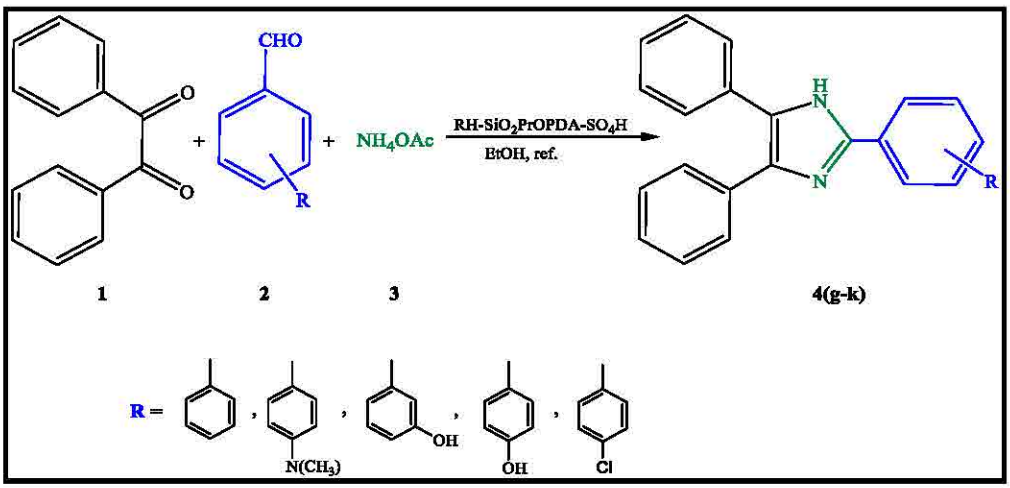

Scheme.2.5: Synthesis of some useful imidazole derivatives using RH-SiO_2PrOPDA-SO_4H as a catalyst.

Table. 2.4: Some physical properties and other characteristics of imidazole derivatives using RH-SiO_2PrOPDA-SO_4H as catalyst

Comp. No.	Name	Color	Molecular formula	M. Wt. (g/mol)	Yield (%)	m.p. (°C)		Ref.
						Found	Lit.	
4g	*2,4,5-triphenyl-1H-imidazole*	white	$C_{21}H_{16}N_2$	296.37	99	267-269	267-269	[120]
4h	*4-(4,5-diphenyl-1H-imidazol-2-yl)-N,N-dimethylaniline*	beige	$C_{23}H_{21}N_3$	339.34	74	224-226	220-222	[121]
4i	*3-(4,5-diphenyl-1H-imidazol-2-yl)phenol*	gray	$C_{21}H_{16}N_2O$	312.36	71	256-259	258-260	[122]
4j	*4-(4,5-diphenyl-1H-imidazol-2-yl)phenol*	beige	$C_{21}H_{16}N_2O$	312.36	84	232-235	233–236	[119]
4k	*2-(4-chlorophenyl)-4,5-diphenyl-1H-imidazole*	white	$C_{21}H_{15}ClN_2$	330.81	44	258-261	262–264	[123]

Chapter Three
Results and discussions

Characterization of RH-SiO_2PrCl and its derivatives RH-SiO_2PrANSA, RH-SiO_2PrOPDA and RH-SiO_2PrOPDA-SO_4H

3.1 Introduction

Rice husks were treated with nitric acid and sodium hydroxide to prepare sodium silicate. 3-(chloropropyl)triethoxysilane was added to the prepared sodium silicate to form RH-SiO_2PrCl.The chloro group present in RH-SiO_2PrCl was replaced with a 1-Amino-2-naphthol-4-sulfonic acid group to prepare the new catalyst RH-SiO_2PrANSA. The chloro group was also replaced with *o*-phenylenediamine in the functionalized silica to form the second new catalyst RH-SiO_2PrOPDA.After that, sulfuric acid was added to the second catalyst to form a catalyst supported with sulfuric acid, RH-SiO_2PrOPDA-SO_4H.

3.2 Characterization of RH-SiO_2PrCl and RH-SiO2PrANSA

Sodium silicate was treated with 3-(chloropropyl)triethoxysilane (CPTES) and titrated with 3.0 M nitric acid until the pH value reached 3, and the resulting gel was separated by centrifugation to produce RH-SiO_2PrCl. Scheme 3.1 shows the preparation of RH-SiO_2PrCl.

The stabilization of 1-Amino-2-naphthol-4-Sulphonic acid in functionalized silica was performed by replacing the chloro group with the 1-Amino-2-naphthol-4-Sulphonic acid group by using triethylamine as a scavenger for HCl molecule. As it appears in Scheme 3.1. To get the required samples, the combination was refluxed at 110 °C for 24 hours in toluene.

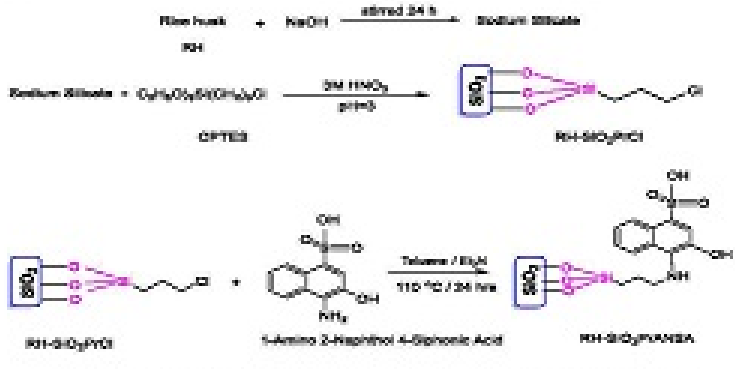

Scheme. 3.1: Synthesis of RH-SiO_2PrCl and RH-SiO_2PrANSA.

3.2.1 FT-IR of RH-SiO_2PrCl and RH-SiO_2PrANSA

In this technique, it is possible to obtain the emission spectrum of gaseous, solid or liquid materials, or the absorption spectrum of these materials. At the same time, on a wide plate, the spectrometer of this technique collects data on that material with high accuracy [124].

It was observed that the peaks in the FTIR spectrum of the RH-SiO_2PrCl complex were weak and not well defined, but when the first catalyst was prepared and 1-Amino-2-naphthol-4-sulphonic acid was added, the peaks appeared better.

In Figure 3.1, FT-IR images of the compound formed from RH-SiO_2PrCl show the presence of extended peaks ranging from 3600-3300 for the (Si-OH) group, and these are caused by water absorbed on the surface of the sample. The peak at 2958 cm^{-1} due to stretching vibration modes of (C–H)[125]. The band at 1647 cm^{-1} could be due to the bending vibration of absorbed water. The FT-IR spectrum of the RH-SiO_2PrCl showed the band at 802 cm^{-1}, which are assigned to siloxane (Si–O–Si) vibration modes[126]. A band at 698 cm^{-1} can be assigned to the C-Cl end in the RH-SiO_2PrCl bond. These results indicate that CPTES is successfully incorporated into sodium silicate.

While, the FT-IR spectrum of the new catalyst RH-SiO_2PrANSA in Figure 3.1 showed the presence of a band 3240 cm^{-1}, which is the stretching vibration of the hydroxyl group and adsorbed water on the surface of silica [127][128], the presence of a band at 2908 cm^{-1} due to the C-H group stretching vibration[125]. The bands at 1354 cm^{-1} and 1168 cm^{-1} were attributed to the vibration of the extension of the S=O group due to the presence of sulfonic acid [129]. The band of 1219 cm^{-1} indicates the group of stretching vibrations (C–N). Furthermore, the bands observed at 1658 cm^{-1} are usually assigned to the vibration of adsorbed water, 1087 cm^{-1} is assigned to Si–O–Si vibration and 655 cm^{-1} due to S–O group [130]. All these absorption bands inducted to the successful laded of functionalized silica RH-SiO_2PrCl with 1-Amino-2-naphthol-4-sulfonic acid.

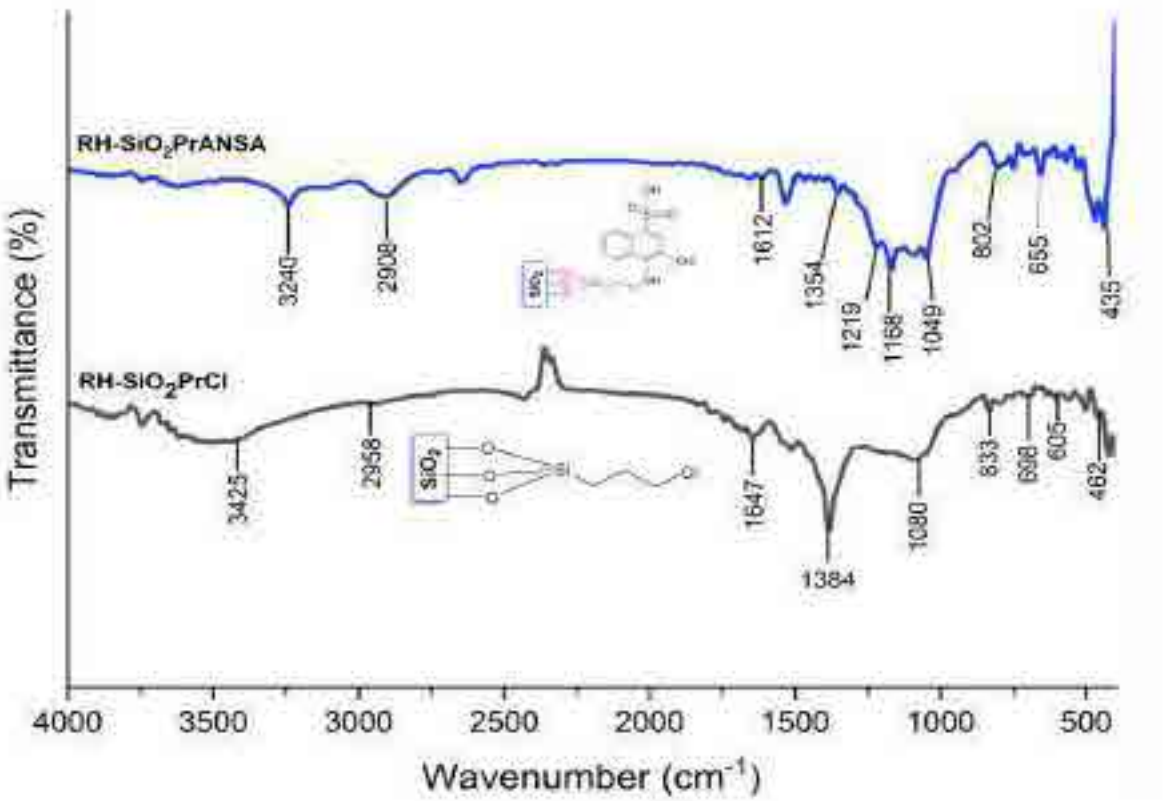

Fig.3.1: FT-IR of RH-SiO_2PrCl and RH-SiO_2PrANSA.

3.2.2 X-ray diffraction of RH-SiO_2PrCl and RH-SiO_2PrANSA

Figure 3.2 shows that the resulting silica has a broad peak at 2θ = 22°,which is an indicator of the amorphous nature of RH-SiO_2PrCl [131]. However, no absorption of any crystalline structure can be seen through the absence of sharp peaks after immobilization of 3-(chloropropyl)triethoxysilane (CPTES) on silica[36].

Figure 3.2 shows the XRD pattern of the RH-SiO_2PrANSA catalyst, it was noted that no sharp peak appeared in crystalline form. This indicates that catalyst RH-SiO_2PrANSA is amorphous and gives two broad peaks at 2θ =21° and 23° [132, 133]. However, no change in the catalyst phase after the 1-Amino-2-naphthol-4-sulfonic acid immobilized onto RH-SiO_2-PrCl.

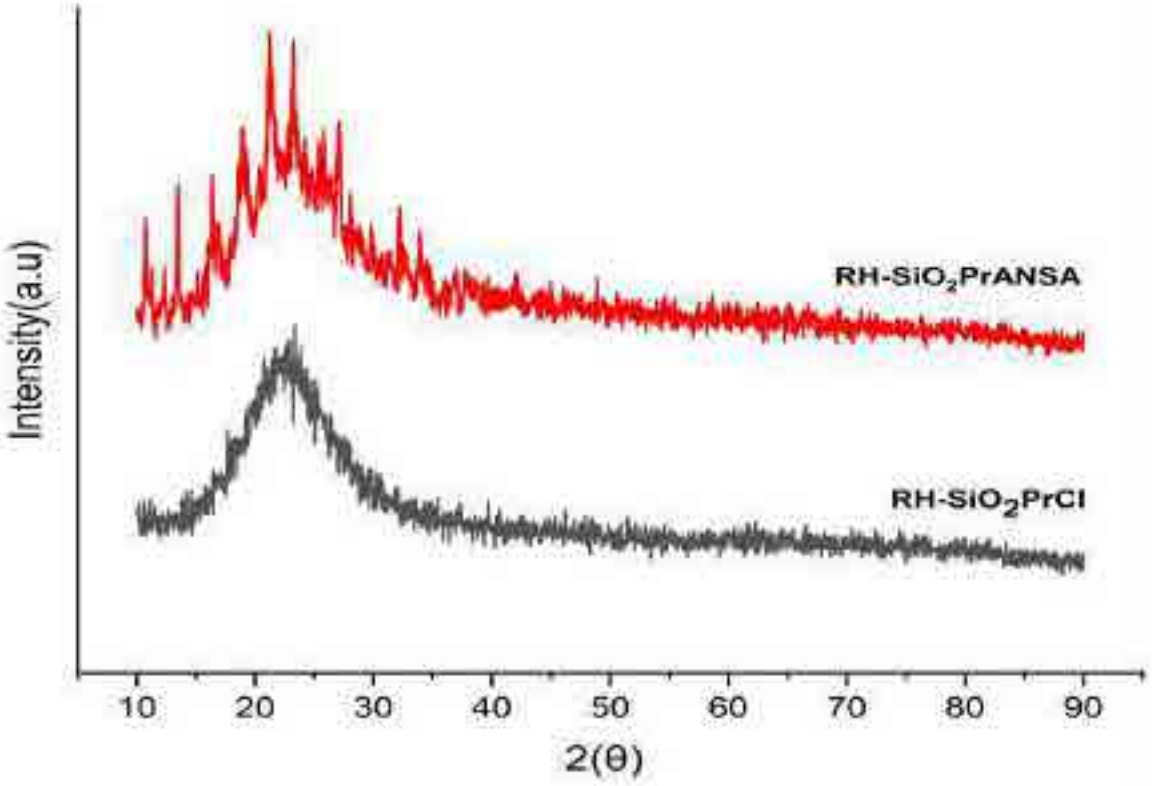

Fig. 3.2: X-ray diffraction of RH-SiO_2PrCl and SiO_2PrANSA.

3.2.3 Thermal analysis TGA/DSC of RH-SiO_2PrCl and SiO_2PrANSA

Thermogravimetric analysis (TGA) was used to ascertain the thermal stability of RH-SiO_2PrCl. The TGA thermogram of RH-SiO_2PrCl (Figure 3.3) shows two distinct phases in the first phase, at a temperature ranging from 50 to 200 °C, attributed to loss of water adsorbed on the compound sample surface (about 10%). In the second stage, at a temperature from 308 to 850 °C, the weight loss increased by 37% due to the decomposition of the chloropropyl groups anchored onto silica and the condensation of silanol groups to form the stable Si-O-Si siloxane bonds [134]. An exothermic reaction caused by crystallization was indicated by the exothermic peak that was seen in the DSC histogram at about 102 °C. A "decomposition" endothermic reaction is indicated by the endothermic peak that was seen at about 425°C.

While, TGA thermogram Figure 3.4 of the catalyst RH-SiO2PrANSA, shows two distinct phases in the first phase, at a temperature ranging from 50 to 200 °C, attributed to the loss of water adsorbed on the compound sample surface (about 18%).

Decomposition of the 1-Amino-2-naphthol-4-sulfonic acid bonded to the silica accounts (about 60%) for the second mass loss at a temperature from 200 to 650 °C, at high-temperature silanol groups were aggregated, as seen between 650 and 900 °C (about 20%) [10,11].

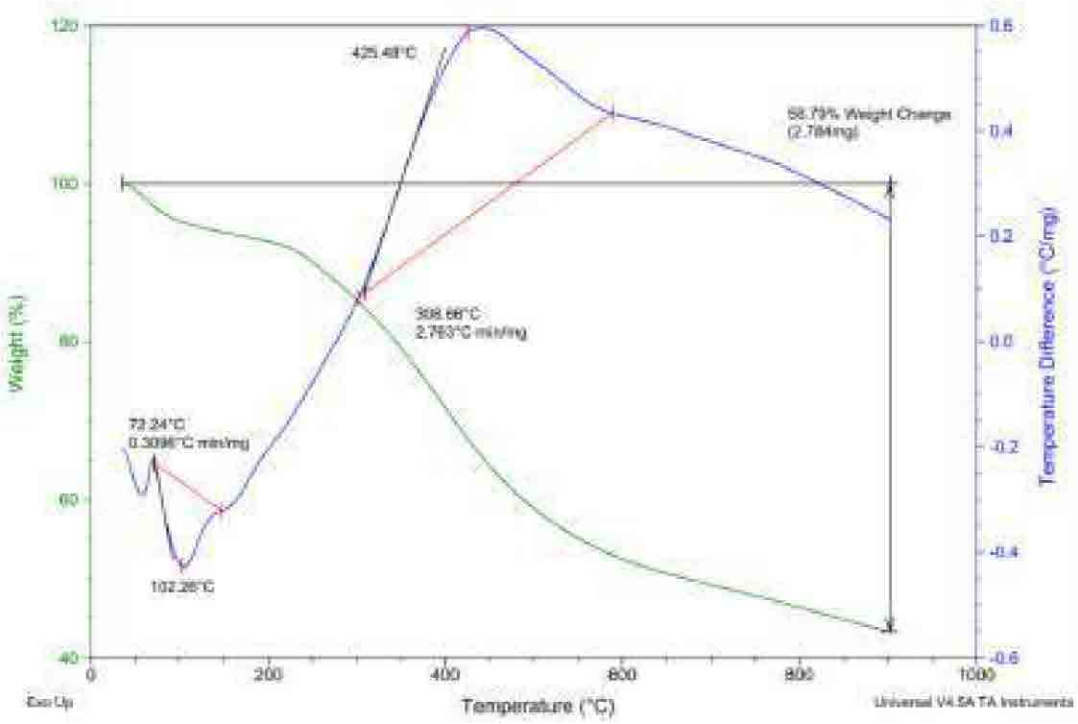

Fig. 3.3: Thermal analysis (TGA/DSC) of RH-SiO_2PrCl

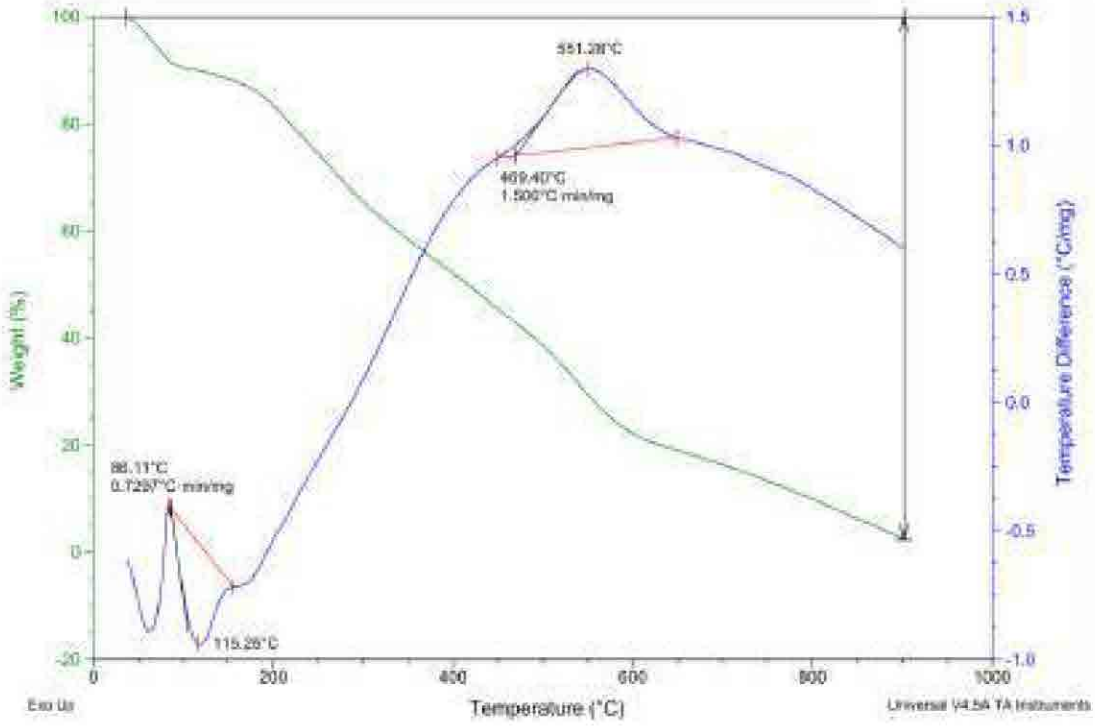

Fig. 3.4: TAG analysis of RH-SiO_2PrANSA

3.2.4 Nitrogen adsorption/desorption Analysis

In Figure 3.5, the results for nitrogen adsorption/desorption are shown, where the pore diameter of the compound formed RH-SiO_2PrCl was 3.97 nm, as well as the surface area of the same compound was 205.42 $m^2 . g^{-1}$, and these results are within the IUPAC classification. The hysteresis loops of the formed compound are of the H2 type, and the nitrogen isotherm of the sample appears to be of the (IV) type [137]. Hence, it can be assumed that the higher specific surface area of RH-SiO_2PrCl is due to CPTES, which acts as a template-directing agent. The pore size distribution was shown in the inset of Figure 3.4, the RH-SiO_2PrCl showed distribution of pores width ranging from 2–20 nm and was within the mesoporous materials.

In Figure 3.6, the results for nitrogen adsorption/desorption are shown, where the pore diameter of the catalyst formed SiO_2PrANSA was 5.14 nm, as well as the surface area of the same compound was 61.739 $m^2 . g^{-1}$, and these results are within the IUPAC classification. The hysteresis loops of the formed compound are of the H2 type, and the nitrogen isotherm of the sample appears to be of the (IV) type [28]. It was observed that the decrease in the value of the specific surface area of the catalyst RH-SiO_2PrANSA could be due to the replacement of 1-amino-2-naphthol-4-sulfonic acid with a chloro which leads to cracking of the surface, which is crowded with the ligand network on the surface and thus clogs pores.

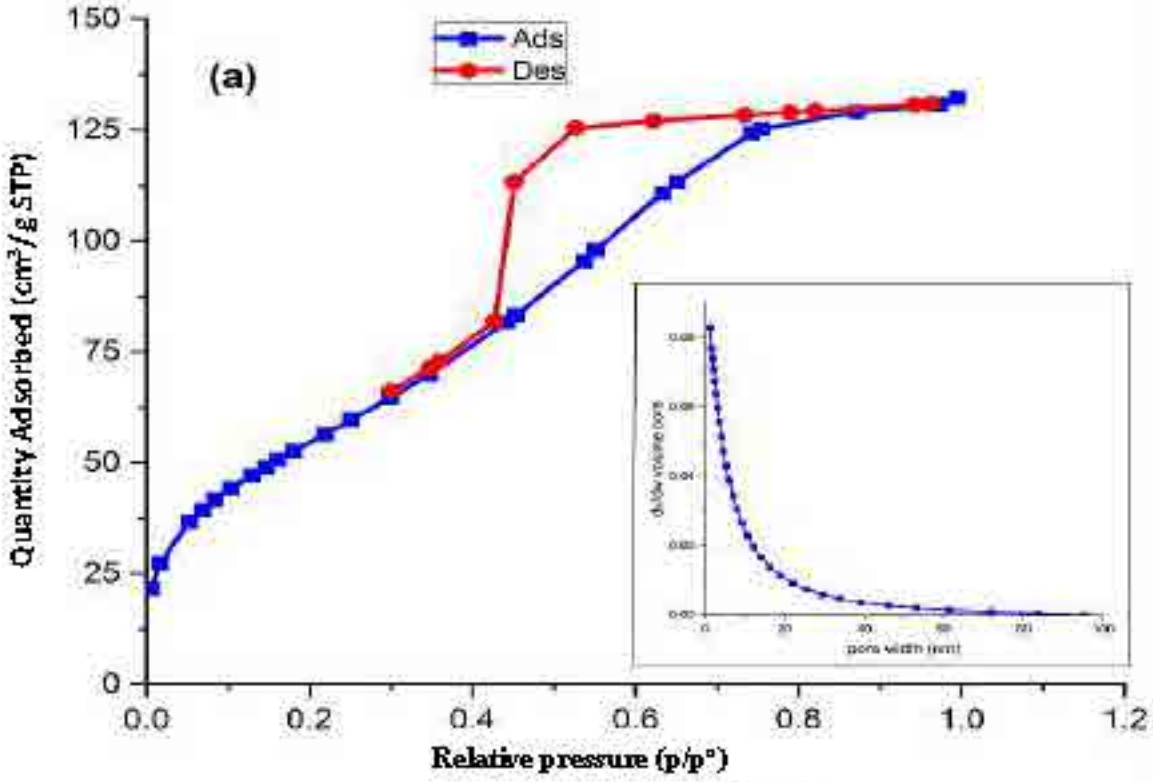

Fig. 3.5: Nitrogen adsorption/desorption analysis for RH-SiO₂PrCl.

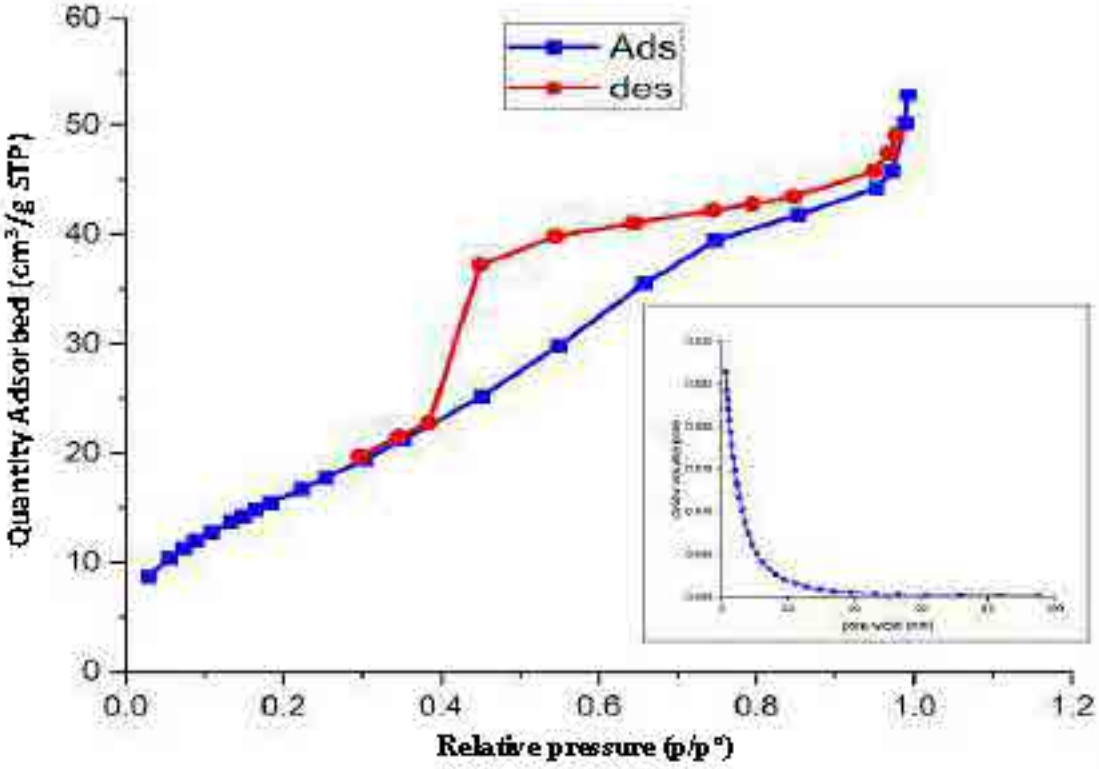

Fig. 3.6: Nitrogen adsorption/desorption analysis of RH-SiO₂PrANSA.

3.2.5 FESEM/EDS of RH-SiO_2PrCl and RH-SiO_2PrANSA

Field emission scanning electron microscopy (FESEM) of RH-SiO_2PrCl are shown in Figure 3.7. The images indicates a heterogeneous porous structure where a large number of particles aggregate loosely on the surface of the sample to form many agglomerates as a result of the functionalized silica by silylating agent [138] with an average diameter of ca. 50.6 nm. The EDX spectrum of RH-SiO_2PrCl is shown in Figure 3.7. The spectrum analysis revealed that the compounds contained carbon, chloride, in addition to oxygen and silicon elements in compound.

Shows images of field emission scanning electron microscopy (FESEM) of RH-SiO_2PrANSA catalyst in Figure 3.8, where a large gathering of particles appears on the surfaces of the catalyst to form gaps similar to channels and grooves. These gaps facilitate the diffusion of the formed particles on the sample's surface, with an average diameter of 61.8 nm. Figure 3.8 shows the EDX of RH-SiO_2PrANSA. EDX spectrum showed a peak silica density at 27.83%, carbon at 25.80%, sulfur at 23.32%, Oxygen at 16.33 % and Nitrogen at 6.72. The manufactured components of this catalyst indicate the presence of sulfur and nitrogen and are not found in the previous compound [139] due to the treatment of this catalyst with 1-Amino-2-naphthol-4-Sulphonic acid.

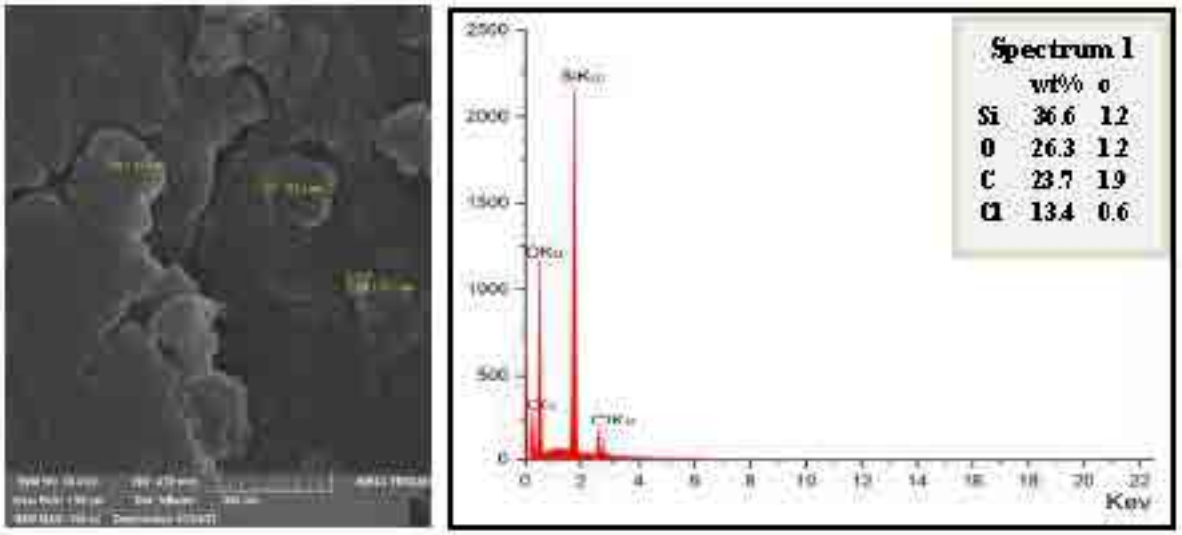

Fig. 3.7: FESEM and EDS of RH-SiO_2-PrCl.

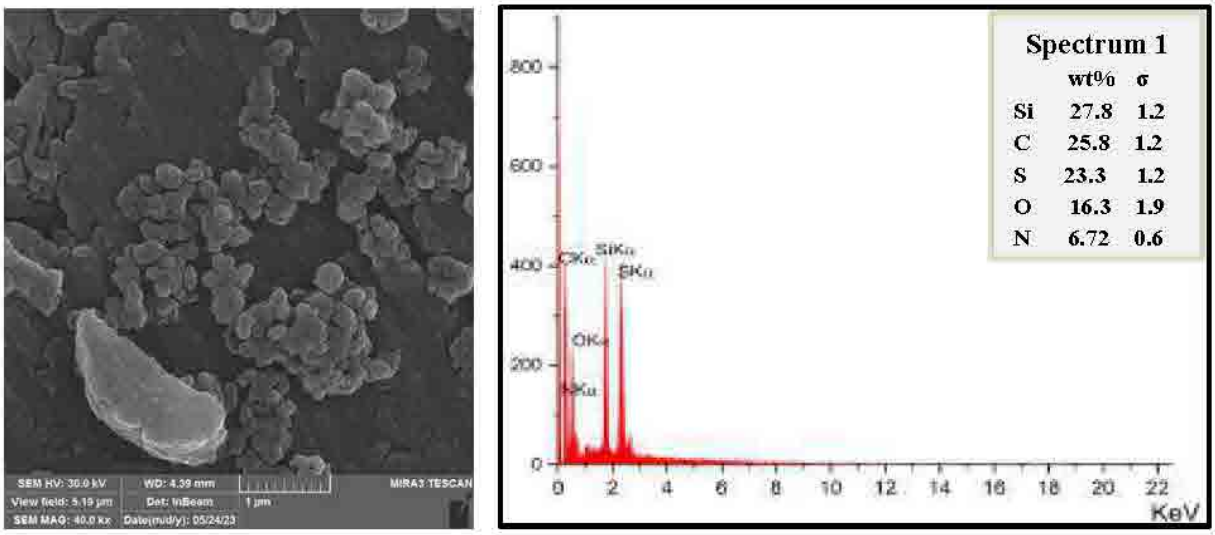

Fig. 3.8: FESEM and EDS analysis of RH-SiO_2PrANSA.

3.2.6 CHN Analysis

The elemental analysis (CHN) of the RH-SiO_2PrCl compound showed that the percentage of carbon and hydrogen reached 16.24% and 5.3%, respectively, as shown in Table 3.1. The elemental analysis of the RH-SiO_2PrANSA compound indicated that the percentage of carbon, hydrogen, nitrogen, and sulfur was 29.41%, 7.3%, 3.5%, and 4.65%, respectively, where the high percentage of carbon, nitrogen, and hydrogen as well as the percentage of sulfur are due to the association of RH-SiO_2PrANSA with 1-Amino2-naphthol4-sulfonic acid.

Table. 3.1: Elemental analysis (CHNS) of the RH-SiO_2PrCl and RH-SiO_2PrANSA

Sample	C (%)	H (%)	N (%)	S (%)
RH-SiO_2PrCl	16.24	5. 3	-	-
RH-SiO_2PrANSA	29.41	7.3	3.5	4.6

3.2.7 AFM images of RH-SiO_2PrCl and RH-SiO_2PrANSA

AFM images of RH-SiO2PrCl are shown in Figure 3.9. The structures appear pyramidal in shape and irregular pore arrangements, showing an average roughness modulus (Ra) of 1.295 nm and a root mean square roughness (Rrms) of 845 pm for RH-SiO_2PrCl. These results can be attributed to the immobilization of CPTES in sodium silicate.

AFM images of RH-SiO_2PrANSA are shown in Figure 3.10. The structures appear to be hierarchical in shape, the pore arrangements are irregular, and the hierarchical structure of RH-SiO_2PrANSA is more compact. The results show an average roughness modulus (Ra) of 1.433 nm, and root mean square roughness (Rrms) of 934 pm for the RH-SiO_2PrANSA catalyst. These results can be attributed to successfully modifying the surface of RH-SiO_2PrCl by 1-Amino-2-naphthol-4-sulphonic acid.

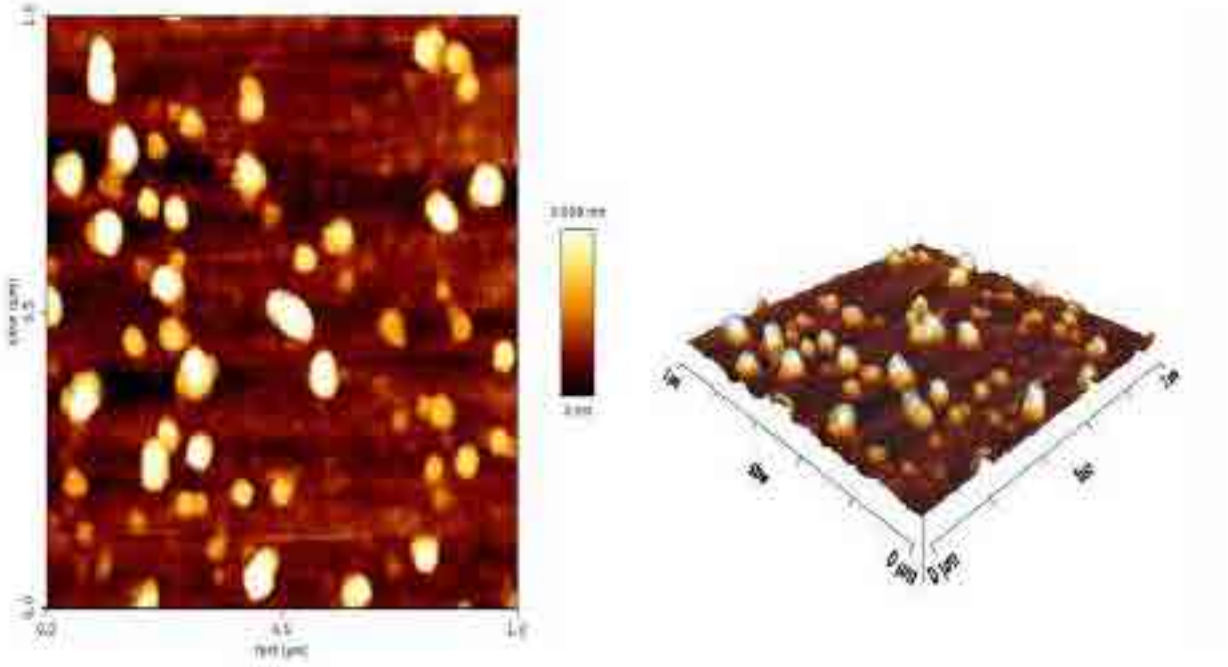

Fig. 3.9: AFM images of RH-SiO_2PrCl

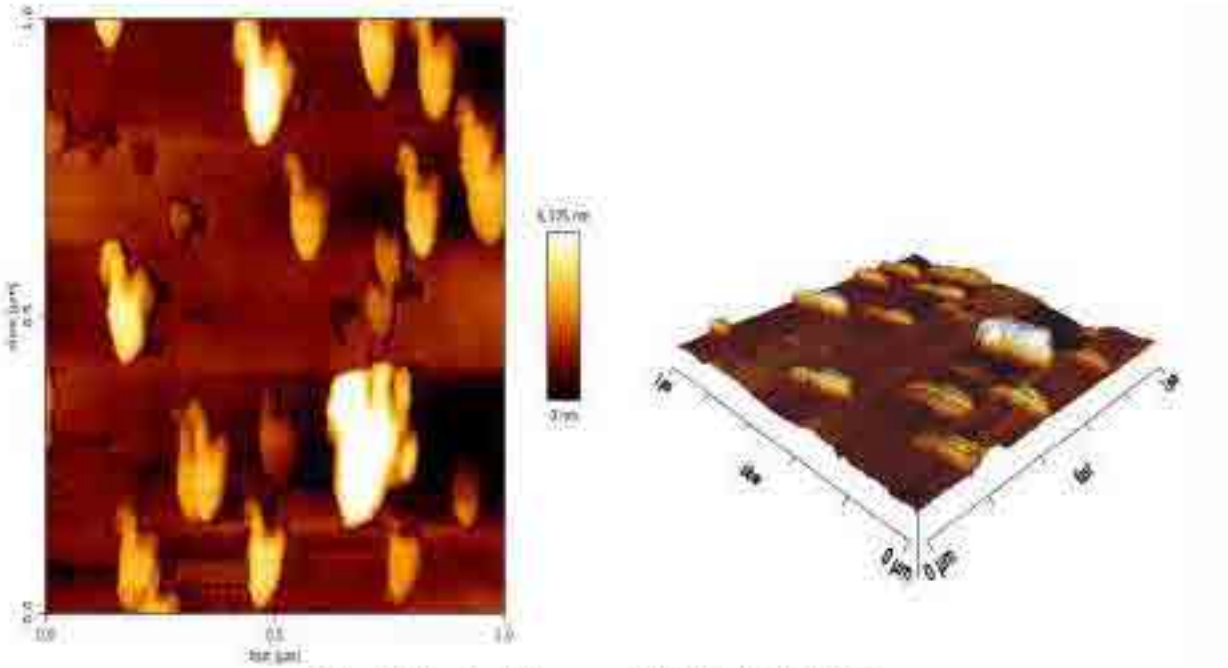

Fig. 3.10: AFM images of RH-SiO_2PrANSA.

3.2.8 Transmission Electron Macroscopy (TEM)

The TEM results are shown in the micrographs of the RH-SiO_2PrCl composite composed of amorphous silica in Figure 3.11. It can be observed that the particles and pores were well distributed, although interparticle aggregates also occurred. The estimated pore diameter measured according to the program Fiji ImageJ is approximately 4nm. This result is in good agreement with that obtained from the BET analysis.

Figure 3.12 shows TEM images of the new material RH-SiO_2PrANSA. The distribution of particles on the surfaces of the material can be observed, as it is more porous than the distribution of particles on the surfaces of functionalized silica RH-SiO_2PrCl, and it may be a result of treating this with 1-amino-2-naphthol-4-sulfonic acid. The estimated pore diameter measured according to the program Fiji ImageJ is approximately 5nm. This result is consistent with that obtained from BET analysis, which gives the impression that RH-SiO_2PrANSA is a porous material.

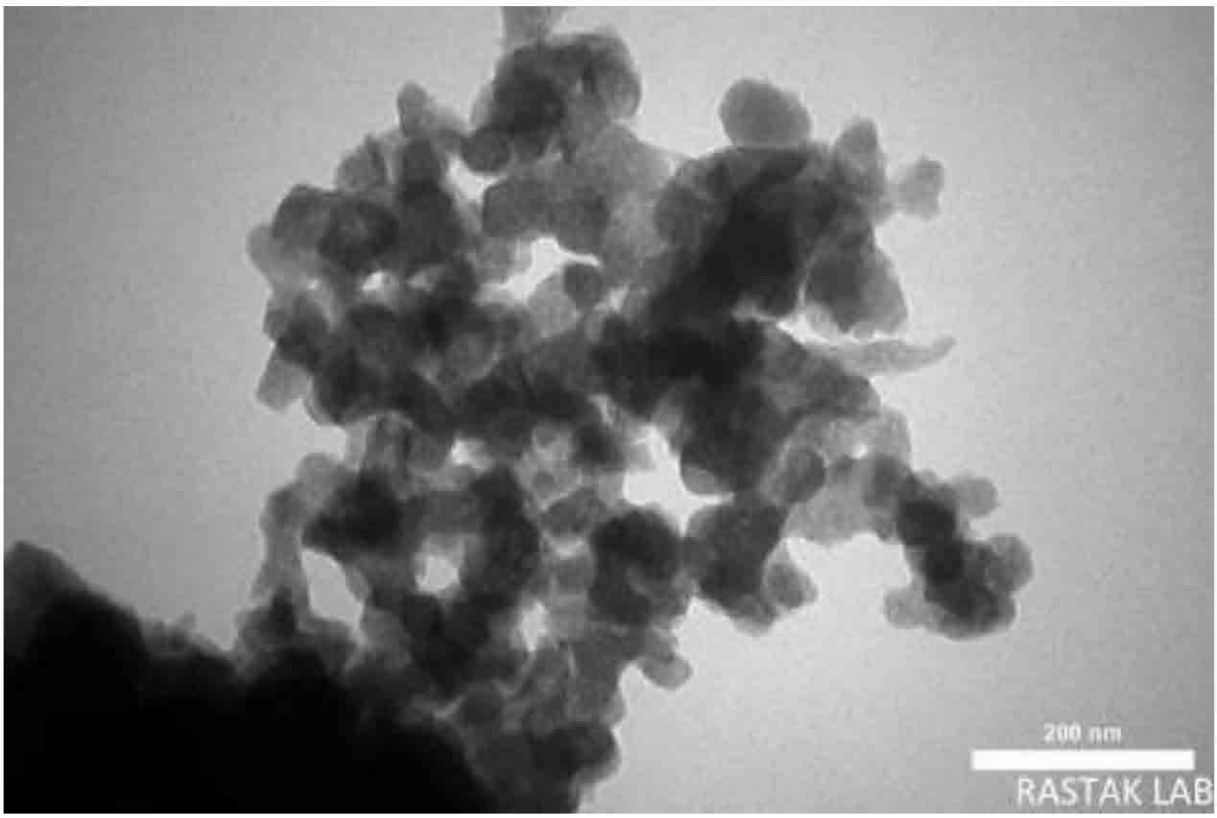

Fig.3.11: TEM images of RH-SiO_2PrCl.

Fig. 3.12: TEM images of RH-SiO_2PrANSA.

3.3 Synthesis of some useful 2,4,5-trisubstituted imidazole derivatives using RH-SiO_2PrANSA as catalyst

RH-SiO_2PrANSA as the catalyst was used to synthesize some 2,4,5-trisubstituted imidazole derivatives via reaction between various aldehydes, benzil and ammonium acetate (Scheme 3.2). The new methodology provides good yields through simple work in addition to the mild conditions and easy synthesis of the new catalyst.

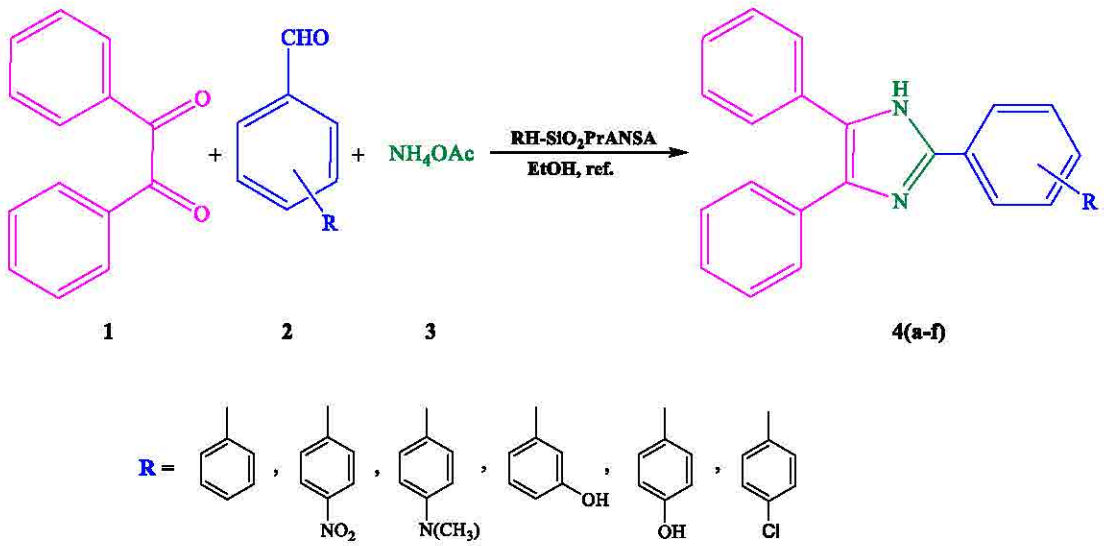

Scheme. 3.2: Synthesis of some useful 2,4,5-trisubstituted imidazole derivatives using RH-SiO_2PrANSA as catalyst

3.3.1 Optimization of reaction conditions

The benzaldehyde, ammonium acetate, and benzil reaction **(4a)** was selected as a model reaction to investigate the most favorable reaction conditions (Scheme 3.5). The investigation encompassed an examination of several solvents and molar ratios for the reaction, with the outcomes being consolidated in Table 3.2 and Table 3.3, correspondingly. The greatest percentage yield was attained when ethanol was used as the solvent, as indicated in Table 3.2, Entry 3. According to the molar ratio analysis, it was determined that the optimal and most appropriate choice for the reaction was a ratio of 1:1:5, as indicated in Table 3.3, Entry 5. Furthermore, the experimental procedure for the model reaction **(4a)** involved the utilization of different quantities of the catalyst, as indicated in Table 3.4, Entry 4, and that was demonstrated to improve outcomes by utilizing 0.08 g of

the catalyst. A set of 2,4,5-triphenyl imidazole derivatives **(4a–f)** was synthesized after the effective optimization of the reaction conditions.

Table .3.2: Effect of solvent on the synthesis of 2,4,5-triphenylimidazole **(4a)**

Entry	Solvent	Yield %
1	H_2O	72
2	Methanol	20
3	Ethanol	**97**
4	CH_3CN	58
5	THF	40

Table. 3.3: Effect of mole ratio on the synthesis of 2,4,5-triphenylimidazole **(4a)**

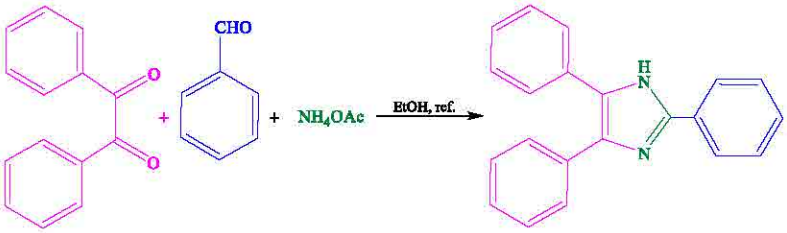

A **B** **C**

Entry	Mole ratio (A:B:C)	Yield %
1	1:1:1	32
2	1:1:2	51
3	1:1:3	69
4	1:1:4	84
5	1:1:5	**88**

Table. 3.4: Effect of the catalyst amount on synthesis of 2,4,5-triphenylimidazole **(4a)**

Entry	Catalyst	Yield (%)
1	0.01	64
2	0.02	77
3	0.04	87
4	0.08	**95**
5	0.16	74

3.3.2 Characterization of 2,4,5-trisubstituted imidazole derivatives

In this study, an innovative and effective synthetic process for the production of 2,4,5-trisubstituted imidazole derivatives from various aldehydes, ammonium acetate, and benzil with RH-SiO_2PrANSA as a catalyst is reported. The synthesis of imidazole derivatives is shown in Scheme 3.5. The FT-IR spectra of all derivatives (4a-f) showed two important bands, one at 3437-3313 cm^{-1} due to N–H stretching and the other at 1666-1600 cm^{-1} attributed to C=N stretching while the NMR spectra exhibited a peak at 13.16-12.32 ppm for the N–H of the ring of imidazole. Moreover, one compound peaked at 2.97 ppm for C–H of the aliphatic group, and two appeared to peak at 9.56 and 9.70 ppm due to O–H of hydroxyl groups [13-15]. The spectral data for all products (4a-f) are as follows:

1) 2,4,5-triphenylimidazole (4a)

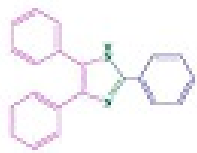

The condensation reaction of benzil with benzaldehyde and ammonium acetate in the presence of the new catalyst according to the general procedure in (Section 2.2.5.).

IR (KBr) $\bar{\nu}$ (cm^{-1}): 3317 (NH), 3063 (Ar–H), 1662 (C=N).

^{1}H NMR (400 MHz, DMSO-d_6) δ (ppm): 12.79 (s,1H, NH), 8.10 (d, J = 8.0 Hz, 2H, Ar–H), 7.57–7.21 (m, 13H, Ar–H).

MS (ESI): m/z = Found 296.3 [M^+], calculated 296.1.

2) 2-(4-nitrophenyl)-4,5-diphenylimidazole (4b)

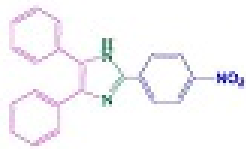

The condensation reaction of benzil with nitrobenzaldehyde and ammonium acetate in the presence of the new catalyst according to the general procedure in (Section 2.2.5.).

IR (KBr) δ (cm^{-1}): 3375 (NH), 3059 (Ar–H), 1600 (C=N), 1516 and 1338 (NO2).

^{1}H NMR (400 MHz, DMSO-d_6) δ (ppm): 13.16 (s,1H, NH), 8.37–8.33 (m, 3H, Ar–H), 8.32–7.26 (m, 11H, Ar–H).

MS (ESI): m/z = Found 341.1 [M^+], calculated 341.3.

3) 4-(4,5-diphenylimidazol-2-yl)-*N,N*-dimethylaniline (4c)

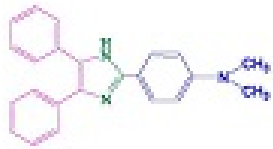

The condensation reaction of benzil with dimethyl benzaldehyde and ammonium acetate in the presence of the new catalyst according to the general procedure in (Section 2.2.5.).

IR (KBr) δ (cm^{-1}): 3375 (NH), 3036 (Ar–H), 2939, 2877 and 2800 (C–H), 1612 (C=N).

^{1}H NMR (400 MHz, DMSO-d_6) δ (ppm): 12.32 (s, 1H, NH), 7.92–7.89 (m, 2H, Ar–H), 7.51–7.30 (m, 10H, Ar–H), 6.81–6.78 (m, 2H, Ar–H), 2.97 (s, 6H, N(CH3)2).

MS (ESI): m/z = Found 339.2 [M^+], calculated 339.2.

4) 3-(4,5-diphenylimidazol-2-yl)phenol (4d)

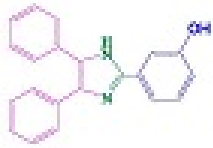

The condensation reaction of benzil with *m*-Hydroxybenzaldehyde and ammonium acetate in the presence of the new catalyst according to the general procedure in (Section 2.2.5.).

IR (KBr) ū (cm^{-1}): 3313 (OH), 3185 (NH), 3063 (Ar–H), 1662 (C=N).

^{1}H NMR (400 MHz, DMSO-d_6) δ (ppm): 12.61 (s, 1H, NH), 9.56 (s, 1H, OH), 7.55–7.20 (m, 12H, Ar–H), 6.79–6.77 (m, 2H, Ar–H).

MS (ESI): m/z = Found 312.1 [M^+], calculated 312.1.

5) 4-(4,5-diphenylimidazol-2-yl)phenol (4e)

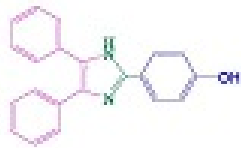

The condensation reaction of benzil with 4-Hydroxybenzyldehyde and ammonium acetate in the presence of the new catalyst according to the general procedure in (Section 2.2.5.).

IR (KBr) ū (cm^{-1}): 3313 (OH), 3167 (NH), 3063 (Ar–H), 1666 (C=N).

^{1}H NMR (400 MHz, DMSO-d_6) δ (ppm): 12.41 (s, 1H, NH), 9.70 (s, 1H, OH), 7.91–7.88 (m, 2H, Ar–H), 7.54–7.19 (m, 10H, Ar–H), 6.87–6.83 (m, 2H, Ar–H).

MS (ESI): m/z = Found 312.3 [M^+], calculated 312.1.

6) 2-(4-chlorophenyl)-4,5-diphenylimidazole (4f)

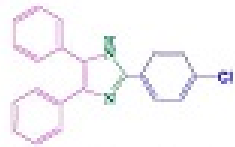

The condensation reaction of benzil with Chlorobenzaldehyde and ammonium acetate in the presence of the new catalyst according to the general procedure in (Section 2.3.1.).

IR (KBr) ū (cm^{-1}): 3437 (NH), 3066 (Ar–H), 1600 (C=N).

^{1}H NMR (400 MHz, DMSO-d_6) δ (ppm): 12.79 (s, 1H, NH), 8.10 (d, J = 8.0 Hz, 2H, Ar–H), 7.57–7.52 (m, 9H, Ar–H), 7.50–7.32 (m, 2H, Ar–H), 7.31–7.21 (m, 1H, Ar–H).

MS (ESI): m/z = Found 330.3 [M^+], calculated 330.1.

3.3.3 Catalyst reusability

A feature of utilizing the new catalyst, RH-SiO_2PrANSA, is that utilized again, rendering it both ecologically sustainable and cost-effective. In order to investigate the potential for catalyst reusability, a typical response was selected and examined using identically enhanced circumstances. Following the completion of the interaction, the catalyst was readily separated by use of the reaction combination by a straightforward filtration process and subsequently washed with dichloromethane. The catalyst that was retrieved underwent a drying process and was put through three more times of testing (Figure 3.17). Reusability the third time, the activity of the catalyst decreased. This is due to leaching in the catalyst solution upon reusability[141].

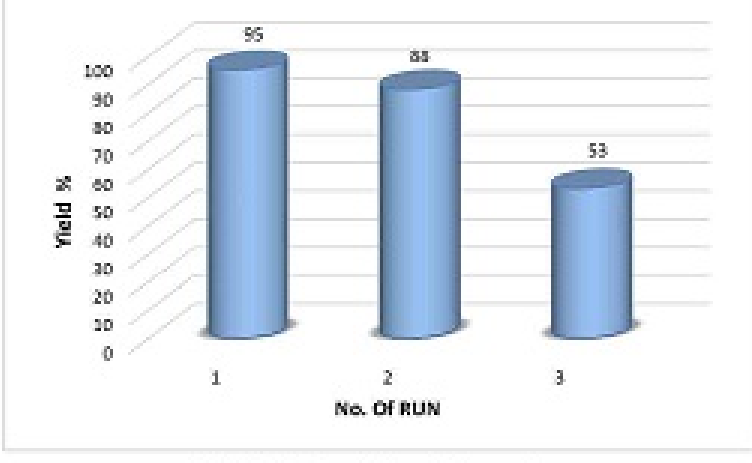

Fig. 3.13: Reusability of the catalyst.

3.4 Characterization of RH-SiO_2PrOPDA and RH-SiO_2PrOPDA-SO_4H

o-Phenylenediamine was functionalized with RH-SiO_2PrCl by replacing the chloro group with the *o*-phenylenediamine. In this reaction, 30 mL of toluene was used as a solvent and triethylamine were used as a scavenger for HCl molecule, mixture was refluxed for 24 hours at 110°C, producing the products shown in Scheme 3.3. The stabilization of sulfuric acid in RH-SiO_2PrOPDA was carried out by stirring. In this reaction, distilled water was used, the sample was washed, filtered and dried for 24 hours at 110 °C, producing the products shown in Scheme 3.3.

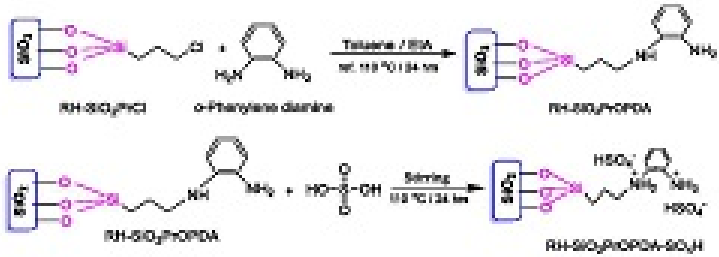

Scheme. 3.3: Synthesis reaction of RH-SiO_2PrOPDA and RH-SiO_2PrOPDA-SO_4H.

3.4.1 FT-IR of RH-SiO_2PrOPDA and RH-SiO_2PrOPDA-SO_4H

The FTIR spectra in Figure 3.18 showed that the RH-SiO_2PrCl complex did not show broad and good peaks as mentioned previously in comparison with the first catalyst, and the peaks did not appear well and were weak compared to the second catalyst RH-SiO_2PrOPDA when adding *o*-Phenylenediamine, and it was observed when adding sulfuric acid to the second catalyst that the peaks appeared well and clearly.

FT-IR spectrum of the RH-SiO_2PrOPDA (Figure 3.14) showed the presence of a band 3047 cm^{-1}, which is the stretching vibration of the hydroxyl group in (Si-OH) and adsorbed water on the surface of silica [142]. A band at 2935 cm^{-1}, which indicates the presence of vibrations belonging to the C-H stretching group.

Also refers band 1600 cm^{-1} to N-H bending. There is an absorption band at 1138 cm^{-1}, which indicates the C-N stretching group vibrations. There is a group of bands 1080, 810, and 435 cm^{-1}, indicating the stretching vibration of siloxane (Si–O–Si) [143]. The presence of the above bands indicates the successful stabilization of o-phenylenediamine onto the silica matrix.

While, the FT-IR spectrum of the new catalyst RH-SiO_2PrOPDA-SO_3H in Figure 3.14 showed the presence of a band 3433 cm^{-1}, which is the stretching vibration of the hydroxyl group in (Si-OH) and adsorbed water on the surface of silica [144]. The band 2947 cm^{-1} also indicates the presence of C-H stretching group vibration [145]. A stretching vibration of siloxane (Si–O–Si) appeared at 1111 cm^{-1}. At the same time, the functional group of sulfonic acid in the silica matrix appears with different absorption bands of S–O stretching modes, which are in the range of 1000-1300 cm^{-1}, and the S-O vibration that appears at about 613 cm^{-1}. This indicates the successful immobilization of sulfonic acids [146] into the surfaces of RH-SiO_2PrOPDA-SO_3H.

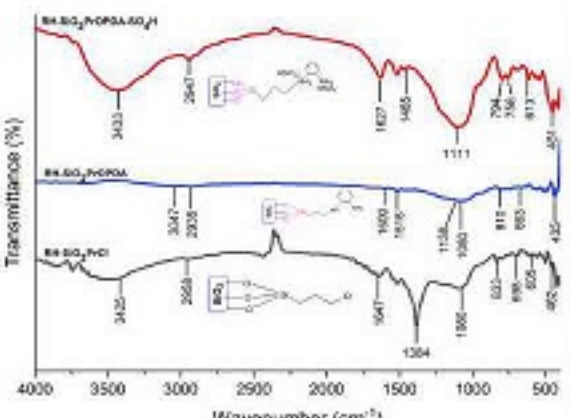

Fig. 3.14: FT-IR spectrum of RH-SiO_2PrOPDA and RH-SiO_2PrOPDA-SO_3H.

3.4.2 X-ray diffraction of RH-SiO_2PrOPDA and RH-SiO_2PrOPDA-SO_4H.

The XRD spectrum of RH-SiO_2PrOPDA is shown in Figure 3.15. A broad peak appears at 2θ = 22°, this indicates the amorphous nature of the prepared RH-SiO_2PrOPDA sample [147], a few sharp peaks in different pattern are observed this could be as a result of immobilizing o-phenylenediamine onto silica which shows some crystallinity on the RH-SiO_2PrOPDA.

The XRD spectrum of the catalyst RH-SiO_2PrOPDA-SO_4H is shown in Figure 3.15. A broad peak appears at 2θ = 22°, where no absorption of any crystalline structure can be seen through the absence of sharp peaks despite the immobilization of sulfuric acid on the catalyst RH-SiO_2PrOPDA. It is worth noting that the broad peak at 2θ = 22° is due to the amorphous nature of silica [148], and this is consistent with much of the previous literature.

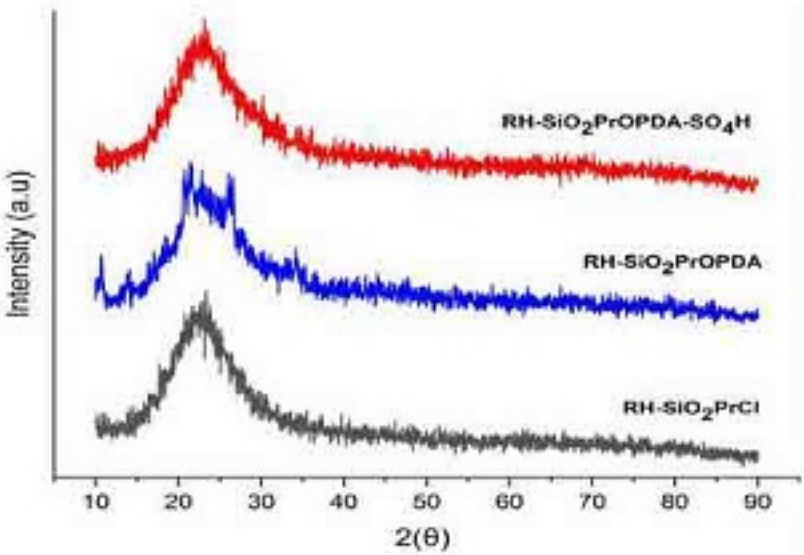

Fig. 3.15: X-ray diffraction of RH-SiO_2PrOPDA and RH-SiO_2PrOPDA-SO_4H.

3.4.3 Thermal analysis TGA/DSC of RH-SiO_2PrOPDA

Thermogravimetric analysis (TGA) was used to ascertain the thermal stability of the RH-SiO_2PrOPDA. The TGA thermogram Figure 3.16 shows two distinct phases, in the first phase, at a temperature ranging from 50 to 200 °C,

attributed to the loss of water adsorbed on the compound sample surface (about 16%). Decomposition of groups the o-phenylenediamine bonded to the silica (about 60%) for the second mass loss at a temperature from 200 to 600 °C, at high-temperature silanol groups were aggregated, as seen between 600 and 900 °C (about 20%).

Thermogravimetric analysis (TGA) was used to ascertain the thermal stability of the catalyst RH-SiO_2PrOPDA-SO_4H. The TGA thermogram Figure 3.17. shows two distinct phases in the first phase, at a temperature ranging from 150 to 300 °C, which is attributed to the loss of water adsorbed on the compound sample surface (about 15%). Decomposition of groups the o-phenylenediamine and sulfuric acid bonded to the silica (about 50%) for the second mass loss at a temperature from 200 to 650 °C. These results indicate that the acid catalyst is stable at the abovementioned temperature. moreover, the water adsorption tendency on the catalyst surface increases after Bronsted acid immobilization in silica.

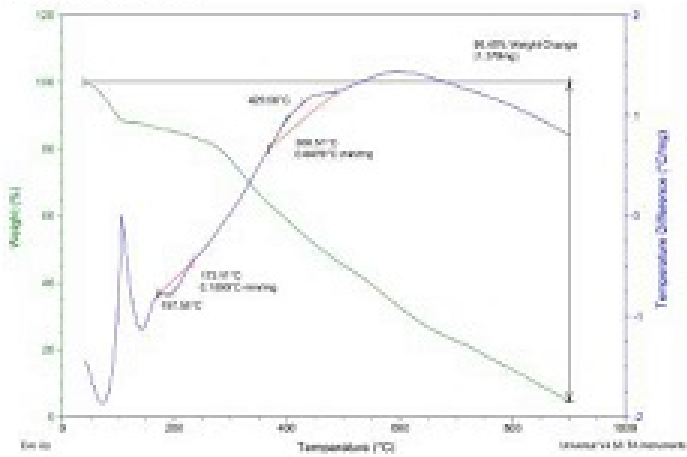

Fig. 3.16: TAG analysis of RH-SiO_2PrOPDA.

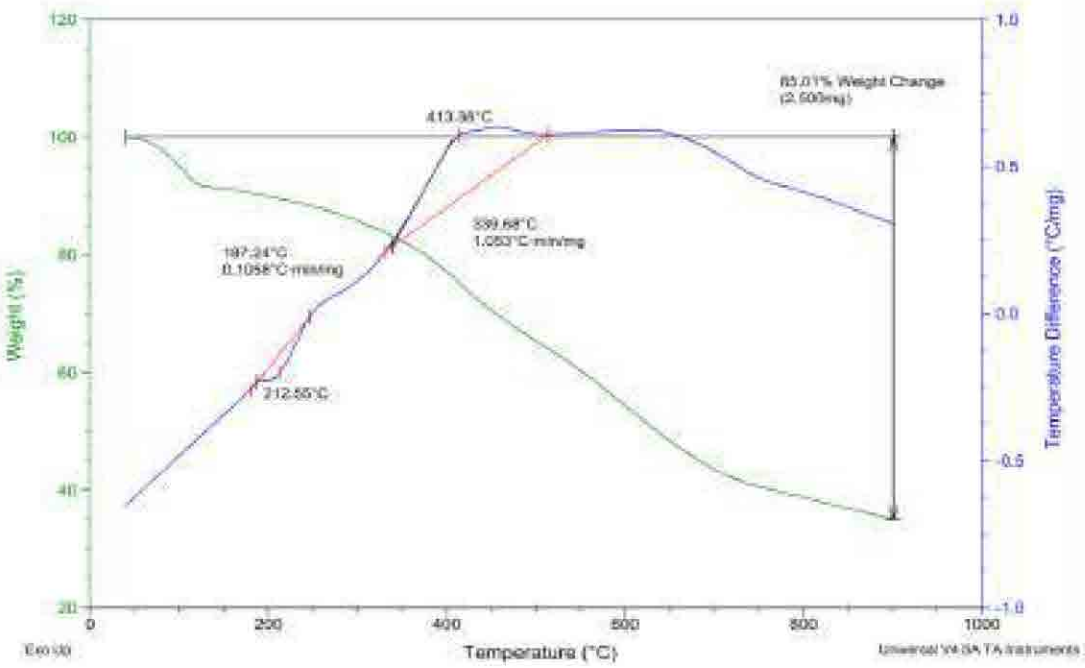

Fig.3.17: TAG analysis of RH-SiO_2PrOPDA-SO_4H.

3.3.4 Nitrogen adsorption/desorption analysis

In Figure 3.18, the results for nitrogen adsorption/desorption are shown, where the pore diameter of the catalyst formed RH-SiO_2PrOPDA was 3.6 nm, as well as the surface area of the same compound was 190 $m^2 . g^{-1}$, and these results are within the IUPAC classification. The hysteresis loops of the formed compound are of the H2 type, and the nitrogen isotherm of the sample appears to be of the (IV) type [28]. The decrease in the value of surface area for the RH-SiO_2PrOPDA could be due to the immobilization of *o*-phenylenediamine molecules on the silica surface, which causes a closure in some of the pores. The pore size distribution was shown in the inset of Figure 3.20, the RH-SiO_2PrOPDA showed distribution of pores width ranging from 5–20 nm and was within the mesoporous materials.

In Figure 3.19, the results for nitrogen adsorption/desorption are shown, where the pore diameter of the catalyst formed RH-SiO_2PrOPDA-SO_4H was 3.5 nm, as well as the surface area of the same compound was 170 $m^2 . g^{-1}$, and these results are within the IUPAC classification. The hysteresis loops of the formed compound are of the H2 type, and the nitrogen isotherm of the sample appears to be of the (IV) type.

A decrease in the surface area of the catalyst was observed as a result of the introduction of sulfuric acid into the RH-SiO$_2$PrCPTDA catalyst matrix, and Adam and Andar observed a similar result [25]. RH-SiO$_2$PrCPTDA-SO$_3$H showed a distinct pore size distribution between 2 - 20 nm. These fall within the mesoporous region.

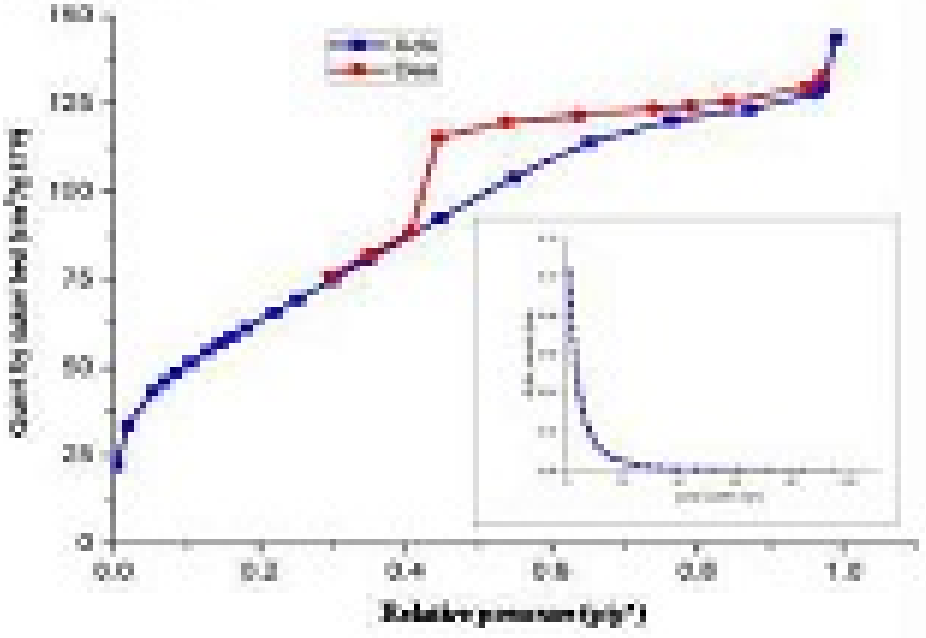

Fig. 3.18: Nitrogen adsorption/desorption analysis of RH-SiO$_2$PrCPTDA.

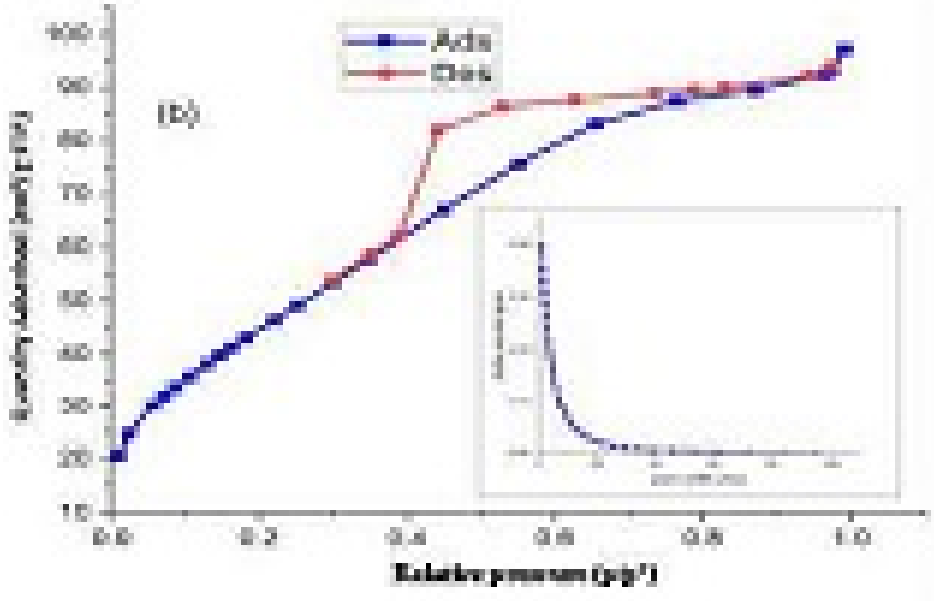

Fig. 3.19: Nitrogen adsorption/desorption analysis of RH-SiO$_2$PrCPTDA-SO$_3$H.

3.4.5 FESEM/EDS of RH-SiO$_2$PrOPDA and RH-SiO$_2$PrOPDA-SO4H

Field emission scanning electron microscopy (FESEM) of the new catalyst RH-SiO$_2$PrOPDA are also shown in Figure 3.20. The particles appear as irregular shapes with small porosity distributed on the surfaces of the catalyst, with an average diameter of 52.9 nm. and the EDX analysis in Figure 3.20 for the RH-SiO$_2$PrOPDA catalyst shows a peak density of silica at 46.72%, Oxygen at 24.90%, nitrogen at 18.97%, and carbon at 9.41%. The components manufactured for this catalyst indicate that the ratio of nitrogen and carbon is the result of the treatment of silica supported with o-phenylenediamine.

Field emission scanning electron microscopy (FESEM) images of the new catalyst RH-SiO$_2$PrOPDA-SO$_4$H are also shown in Figure 3.21 The surfaces are less porous than those of the Previous compound RH-SiO$_2$PrOPDA, with an average diameter of 61.3. nm. EDX analysis is shown in Figure 3.21. The EDX spectrum showed peak silica density at 40.78%, Oxygen at 22.16%, nitrogen at 15.93%, carbon at 11.36 and sulfur at 9.77%. Spectral analysis showed that the catalyst contains nitrogen and sulfur in addition to the elements oxygen, silicon, and carbon in the catalyst, as a result of the silica matrix being supported by sulfuric acid [139].

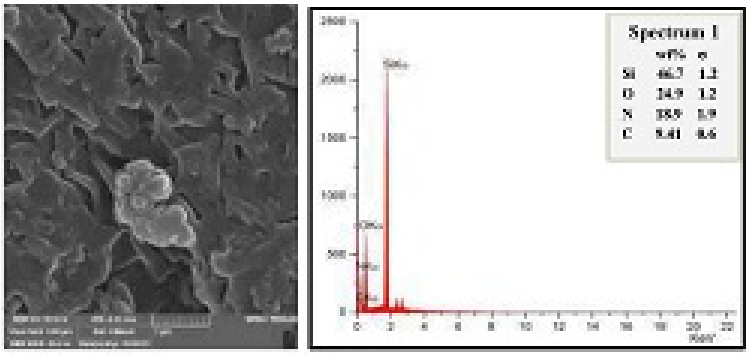

Fig. 3.20: FESEM and EDS analysis of RH-SiO$_2$PrOPDA.

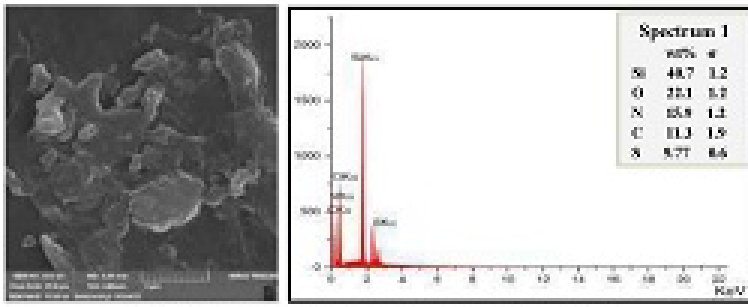

Fig. 3.21: FESEM and EDS analysis of $SiO_2PrOPDA-SO_3H$.

3.4.6 CHN Analysis

The elemental analysis (CHNS) of the RH-SiO2PrOPDA compound showed that the percentages of carbon, hydrogen and nitrogen reached 21.85 %, 10.57%, and 2.2%, respectively, as shown in Table 3.5. The elemental analysis of the RH-$SiO_2PrOPDA-SO_3H$ compound indicated that the percentage of carbon, hydrogen, nitrogen, and Sulfur was 22.60%, 11.12 %,4%, and 2%; Elemental analysis of the compound showed the presence of sulfur elements in addition to an increase in the proportion of elements as a result of supporting the RH-$SiO_2PrOPDA$ catalyst with sulfuric acid.

Table 3.5: (CHN) of the RH-SiO_2PrCl, RH-$SiO_2PrOPDA$ and RH-$SiO_2PrOPDA-SO_3H$

Sample	C (%)	H (%)	N (%)	S (%)
RH-SiO_2PrCl	16.24	5. 3	-	-
RH-$SiO_2PrOPDA$	21.85	10.57	2.2	-
RH-$SiO_2PrOPDA-SO_3H$	22.60	11.22	4	2

3.4.7 AFM images of RH-$SiO_2PrOPDA$ and $SiO_2PrOPDA-SO_3H$

AFM images of RH-$SiO_2PrOPDA$ are shown in Figure 3.22. The structures appear needle-pointed in shape, and the pore arrangements are irregular. The results of the RH-$SiO_2PrOPDA$ catalyst show an average roughness modulus (Ra) of 855 pm and root mean square roughness (Rrms) of 626 pm, which is lower than the average roughness modulus and root mean roughness of RH-SiO_2PrCl functionalized silica.

These results can be attributed to the successful surface modification of RH-SiO_2PrCl by *o*-phenylenediamine.

AFM images of RH-$SiO_2PrOPDA$-SO_4H are shown in Figure 3.23. The structures appear irregularly pyramidal. The estimated average roughness modulus (Ra) is 1.915 nm, and the root mean square roughness (Rrms) is 1.363 nm for the RH-$SiO_2PrOPDA$-SO_4H catalyst, which is larger than the roughness modulus and root square roughness of RH-SiO_2PrCl and RH-$SiO_2PrOPDA$ catalyst. This is attributed to the addition of sulfuric acid in the RH-$SiO_2PrOPDA$ catalyst.

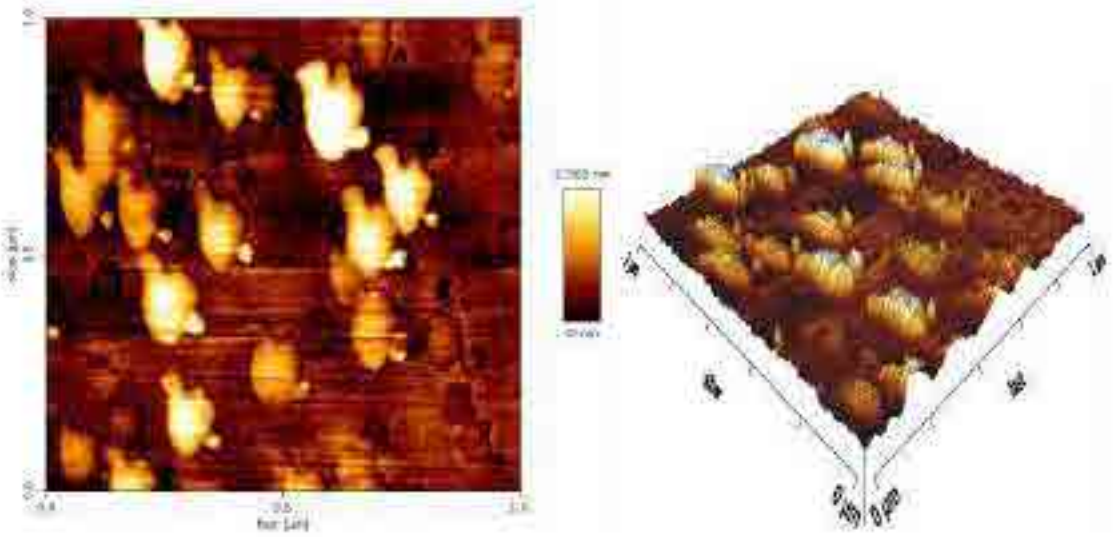

Fig. 3.22: AFM images of RH-$SiO_2PrOPDA$.

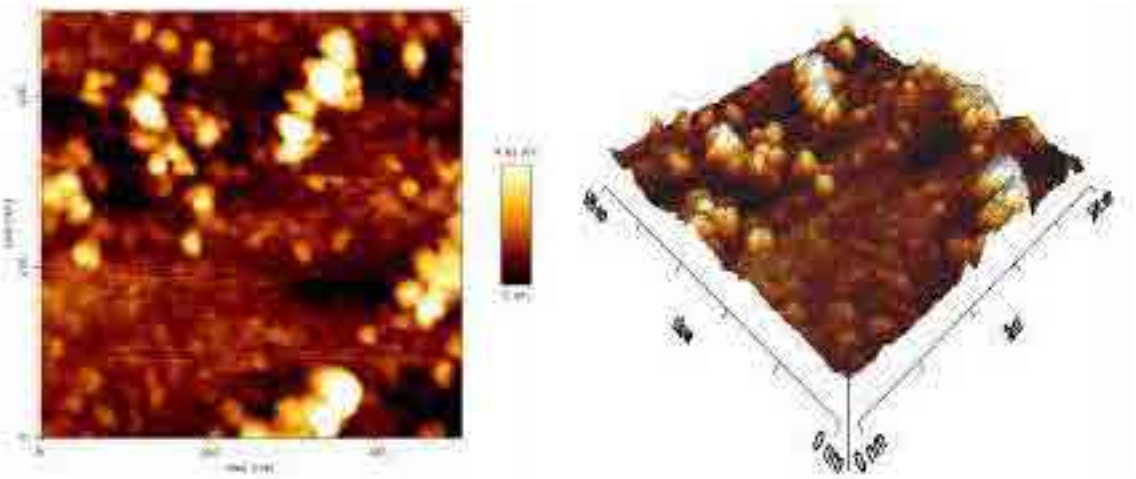

Fig. 3.23: AFM images of RH-$SiO_2PrOPDA$-SO_4H.

3.4.8 TEM images of RH-SiO_2PrOPDA and RH-SiO_2PrOPDA-SO_4H

Figure 3.24 shows TEM images of the RH-SiO_2PrOPDA catalyst, and it can be seen that the distribution of particles on the groove surfaces appears less porous than the distribution of particles on the RH-SiO_2PrCl functionalized silica surfaces. As a result of the treatment of this porosity-reducing *o*-phenylenediamine catalyst, the estimated pore diameter measured according to the program Fiji ImageJ is approximately 4nm. This result is consistent with that obtained from BET analysis, which gives the impression that RH-SiO_2PrOPDA is a porous material.

Figure 3.25 shows TEM images of the new RH-SiO_2PrOPDA-SO_4H catalyst. It can be observed that the distribution of particles on the surfaces of the catalyst is more dispersed than the distribution of particles on the surfaces of the functionalized silica RH-SiO_2PrCl and the catalyst RH-SiO_2PrOPDA, and this may be a result of treating this catalyst with sulfuric acid [149]. The estimated pore diameter measured according to the program Fiji ImageJ is approximately 4nm. This result is consistent with that obtained from BET analysis, which gives the impression that RH-SiO_2PrOPDA-SO_4H is a porous material.

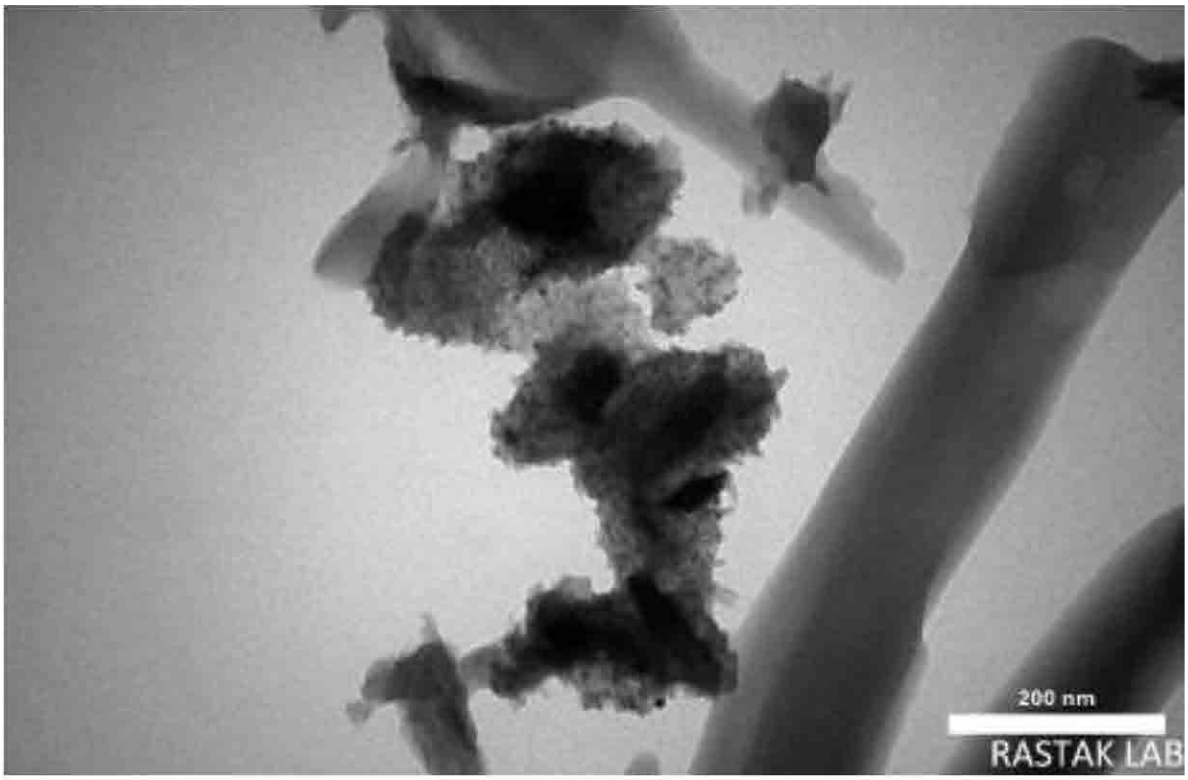

Fig.3.24: TEM images of RH-SiO_2PrOPDA.

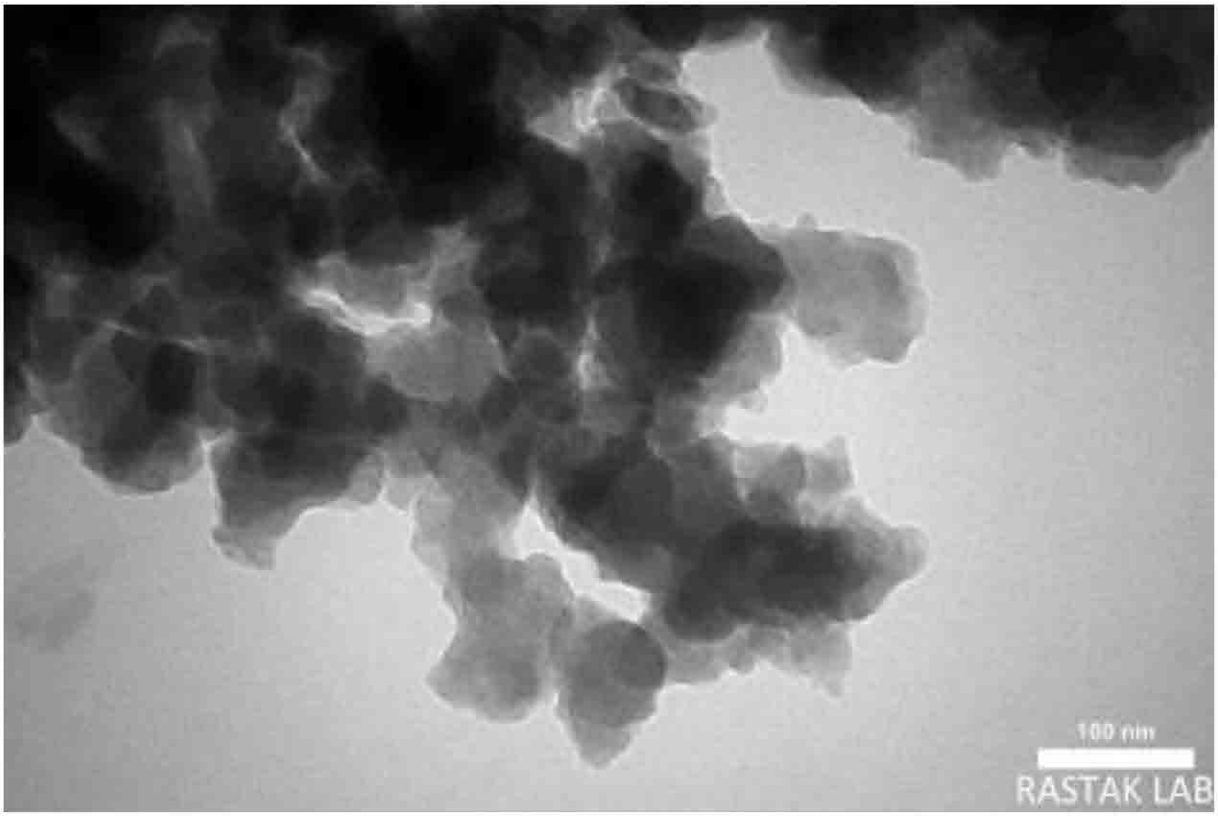

Fig.3.25: TEM images of RH-SiO_2PrOPDA-SO_4H.

3.5 Synthesis of some useful 2,4,5-trisubstituted imidazole derivatives using RH-SiO_2PrOPDA-SO_4H as catalyst

Reaction of benzil, different aldehydes with ammonium acetate by using RH-SiO_2PrOPDA-SO_4H as the catalyst to synthesize some useful 2,4,5-trisubstituted imidazole derivatives.

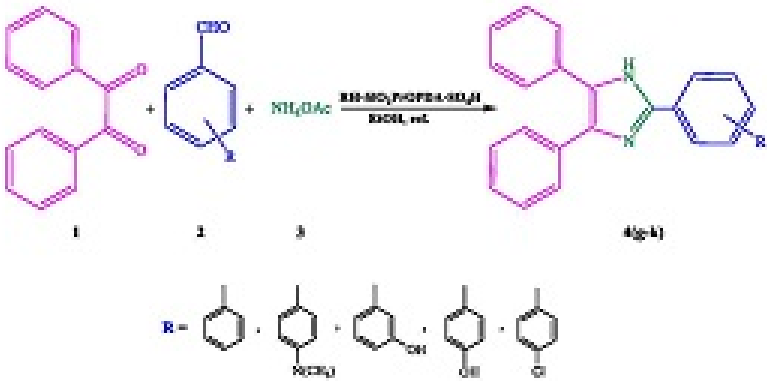

Scheme. 3.4: Synthesis of some useful 2,4,5-trisubstituted imidazole derivatives using RH-SiO_2PrOPDA-SO_4H as catalyst

3.5.1 Optimization of reaction conditions

The reaction between benzaldehyde, ammonium acetate, and benzil were selected as an example of a reaction that is intended to be studied (4g). The most effective conditions (Scheme 3.6) were determined as a result. Several different solvents and various molar ratios were examined for this process. The findings are listed in Table 3.6 and Table 3.7. The highest yield percentage was achieved using ethanol as the solvent (Table 2.6, Entry 3). The molar ratio demonstrated that the most effective and practical choice for the reaction was 1:1:5 (Table 3.7, Entry 5). Additionally, the model reaction (4g) was conducted with different amounts of catalyst (Table 3.8). The highest percentage product was achieved when 0.04 g of catalyst was employed. (Table 3.8, Entry 3). After successfully

optimizing the reaction conditions, a series of 2,4,5-trisubstituted imidazole derivatives **(4g-k)** were prepared.

Table. 3.6: Effect of solvent on the synthesis of 2,4,5-triphenyl-1*H*-imidazole **(4g)**

entry	Solvent	Yield %
1	H_2O	35
2	Methanol	46
3	Ethanol	**99**
4	CH_3CN	28
5	THF	71

Table. 3.7: Effect of mole ratio on the synthesis of 2,4,5-triphenyl-1*H*-imidazole **(4g)**

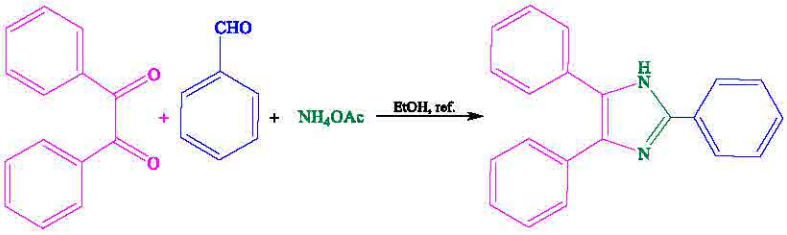

A **B** **C**

Entry	Mole ratio (A:B:C)	Yield %
1	1:1:1	92
2	1:1:2	39
3	1:1:3	42
4	1:1:4	96
5	1:1:5	**99**

Table. 3.8: Effect of the catalyst amount on synthesis of 2,4,5-triphenyl-1*H*-imidazole **(4g)**

Entry	Catalyst	Yield (%)
1	0.01	56
2	0.02	78
3	0.04	**99**
4	0.08	35
5	0.16	53

3.5.2 Characterization of 2,4,5-trisubstituted imidazole derivatives

The spectral analyses of synthesized products were confirmed by comparison with those reported in the literature, and melting points (Table 2.4) were also recorded and compared with known compounds [19-20]. ^{1}H NMR spectra exhibited the N–H proton of the imidazole ring in the downfield region while FT-IR spectra of the compounds **(4g-k)** showed pecks at 3480–3174 and 1666–1604 cm^{-1} for the (N–H) and (C=N) groups, respectively. The spectral data for all products **(4g-k)** are as follows:

1) 2,4,5-triphenyl-1*H*-imidazole **(4g)**

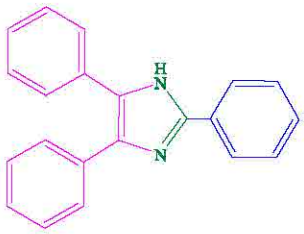

The condensation reaction of benzil with benzaldehyde and ammonium acetate in the presence of the new catalyst according to the general procedure in (Section 2.2.7.).

IR (KBr) ῡ (cm^{-1}): 3315 (NH), 3063 (Ar–H), 1662 (C=N).

^{1}H NMR (400 MHz, DMSO) δ (ppm): 12.79 (s, 1H, NH), 8.10 (d, J = 8.0 Hz, 2H, Ar–H), 7.57 – 7.54 (m, 3H, Ar–H), 7.52 – 7.33 (m, 8H, Ar–H), 7.29 – 7.21 (m, 2H, Ar–H).

MS (ESI): m/z = Found 296.2 [M$^+$], calculated 296.1.

2) 4-(4,5-diphenyl-1*H*-imidazol-2-yl)-*N,N*-dimethylaniline **(4h)**

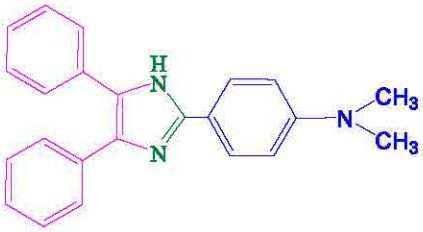

The condensation reaction of benzil with dimethyl benzaldehyde and ammonium acetate in the presence of the new catalyst according to the general procedure in (Section 2.2.7.).

IR (KBr) $\bar{\upsilon}$ (cm^{-1}): 3480 (NH), 3059 (Ar–H), 2939, 2866 and 2800 (C–H), 1612(C=N).

^{1}H NMR (400 MHz, DMSO) δ (ppm): 12.31 (s, 1H, NH), 7.90 (d, *J* = 8.0 Hz, 2H, Ar–H), 7.50–7.20 (m, 10H, Ar–H), 6.79 (d, *J* = 8.0 Hz, 2H, Ar–H), 2.96 (s, 6H, N(CH3)2).

MS (ESI): m/z = Found 339.4 [M^+], calculated 339.2.

3) 3-(4,5-diphenyl-1*H*-imidazol-2-yl) phenol **(4i)**

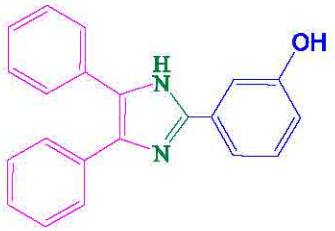

The condensation reaction of benzil with *m*-Hydroxybenzaldehyde and ammonium acetate in the presence of the new catalyst according to the general procedure in (Section 2.2.7.).

IR (KBr) $\bar{\upsilon}$ (cm^{-1}): 3317 (OH), 3190 (NH), 3063 (Ar–H), 1666 (C=N).

^{1}H NMR (400 MHz, DMSO) δ (ppm): 12.61 (s, 1H, NH), 9.56 (s, 1H, OH), 7.55 – 7.49 (m, 5H, Ar–H), 7.44 (t, *J* = 8.0 Hz, 2H, Ar–H), 7.39 – 7.20 (m, 5H, Ar–H), 6.78 (d, *J* = 8.0 Hz, 2H, Ar–H).

MS (ESI): m/z = Found 312.2 [M^+], calculated 312.1.

4) 4-(4,5-diphenyl-1*H*-imidazol-2-yl)phenol **(4j)**

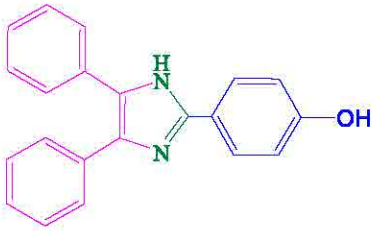

The condensation reaction of benzil with 4-Hydroxybenzyldehyde and ammonium acetate in the presence of the new catalyst according to the general procedure in (Section 2.2.7.).

IR (KBr) $\bar{\upsilon}$ (cm^{-1}): 3313 (OH), 3174 (NH), 3032 (Ar–H), 1604 (C=N).

^{1}H NMR (400 MHz, DMSO) δ (ppm): 12.40 (s, 1H, NH), 9.69 (s, 1H, OH), 7.89 (d, J = 8.0 Hz, 2H, Ar–H), 7.53 (d, J = 8.0 Hz, 2H, Ar–H), 7.49 – 7.41 (m, 4H, Ar–H), 7.37 – 7.18 (m, 4H, Ar–H), 6.84 (d, J = 8.0 Hz, 2H, Ar–H).

MS (ESI): m/z = Found 312.3 [M^+], calculated 312.1.

5) 2-(4-chlorophenyl)-4,5-diphenyl-1*H*-imidazole **(4k)**

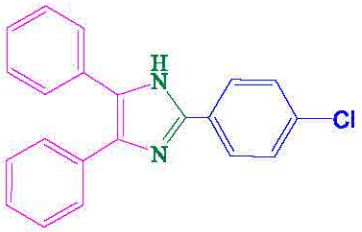

The condensation reaction of benzil with Chlorobenzaldehyde and ammonium acetate in the presence of the new catalyst according to the general procedure in (Section 2.2.7.).

IR (KBr) $\bar{\upsilon}$ (cm^{-1}): 3182 (NH), 3063 (Ar–H), 1666 (C=N).

^{1}H NMR (400 MHz, DMSO) δ (ppm): 12.69 (s, NH), 8.08 (d, J = 8.0 Hz, 2H, Ar–H), 7.53–7.46 (m, 8H, Ar–H), 7.39–7.36 (m, 4H, Ar–H).

MS (ESI): m/z = Found 330.3 [M^+], calculated 330.1.

3.5.3 Reusability of the catalyst

The advantage of employing a novel catalyst (RH-SiO_2PrOPDA-SO_4H) that is reusable is that it was both economical and ecologically benign. Selected typical reactions that happen in the same way under the same optimised conditions were investigated to look at the catalyst's recyclability. The catalyst may be readily filtered out of the mixture when the reaction is finished, and dichloromethane can then be used to wash it. The dried catalyst was re-tested three times (Figure 3.34). Reusability the third time, the activity of the catalyst decreased. This is due to leaching in the catalyst solution upon reusability[141].

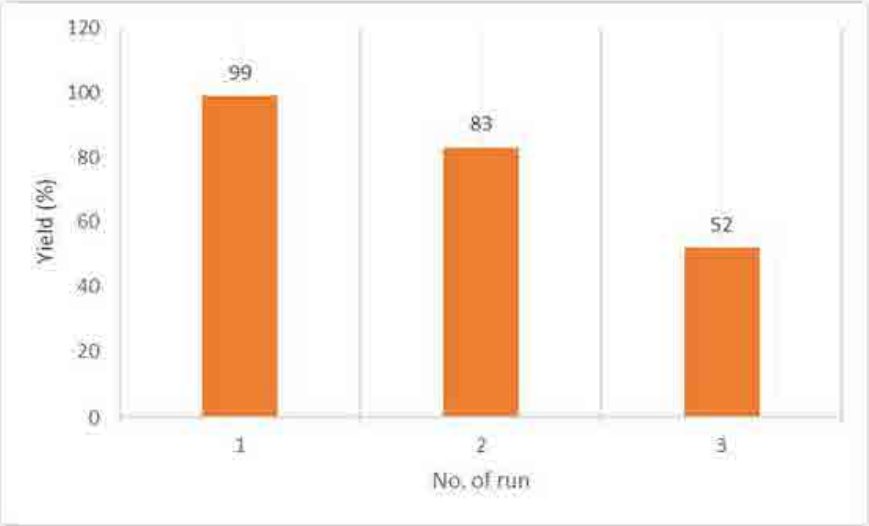

Fig. 3.26: Reusability of the catalyst

3.6 Conclusions

1) This study relied on preparing heterogeneous solid catalysts. It was used to synthesize 2,4,5-trisubstituted imidazole derivatives, where extracted silica (rice husks) was prepared from Iraqi rice husks by soaking and drying at room temperature for two days. After that extracted silica was functionalized with 3-(Chloropropyl)triethoxysilane (CPTES) via titration to prepare RH-SiO_2PrCl. RH-SiO_2PrCl reacted with 1-Amino-2-naphthol-4-sulfonic acid, *o*-Phenylenediamine, and sulfuric acid to prepare RH-SiO2PrANSA, RH-SiO_2PrOPDA, and RH-SiO_2PrOPDA-SO_4H, respectively, through reflux.
2) The XRD diffraction pattern showed a strong and broad peak diffused with maximum intensity at 22-23° (2θ) indicating the amorphous nature of 4. RH-SiO_2PrCl, RH-SiO_2PrANSA and RH-SiO_2PrOPDA-SO_4H.
3) The functionalized particles are granular and irregularly shaped, as demonstrated by the FESEM pictures. For RH-SiO_2PrANSA and RH-SiO_2PrOPDA-SO_4H, the average diameter is around 61.8 nm and 61.3 nm, respectively.
4) EDX analysis showed the presence of nitrogen and sulfur for RH-SiO_2PrANSA and RH-SiO_2PrOPDA-SO_4H respectively, which can be regarded as further evidence of the effective incorporation of the organic molecules on the silica surface.
5) Nitrogen adsorption/desorption analysis showed that the specific surface area of RH-SiO_2PrANSA and RH-SiO_2PrOPDA-SO_4H less than the specific surface area of RH-SiO_2PrCl, due to large molecules attached to the surfaces of the functional silica matrix.
6) The TGA/DSC ranged from 50 to 600°C and showed two decomposition stages for the RH-SiO_2PrANSA and RH-SiO_2PrOPDA-SO_4H.
7) Using RH-SiO_2PrANSA and RH-SiO_2PrOPDA-SO_4H as new catalysts, an effective and convenient one-pot three-component synthesis of 2,4,5-tri-substituted imidazole derivatives has been developed. This process is reusable

under reflux at room temperature and involves the condensation reaction of benzil, various aldehydes, and ammonium acetate in ethanol.

8) FTIR, ^{1}HNMR, and mass spectrometry were used to characterise all of the synthesised 2,4,5-trisubstituted imidazole derivatives (see Appendix). The method has a number of benefits, including high yields, quick reaction times, ease of setup, safer reaction conditions, and the catalyst's reusability. It's also cost-effective and ecologically friendly, with moderate settings and straightforward catalyst synthesis.

3.7 Future works

1) **Preparation, characterization and study of new catalysts and benefit from them in a synthesis of imidazole derivatives from different compounds using simple, safe and rapid methods.**
2) **Extracting silica from various sources such as corn, wheat and sunflower.**

References

References

1. Hang X, Ha X, Fang F (2011) Porous inorganic materials. Encycl Inorg Bioinorg Chem
2. Little MA, Cooper AI (2020) The chemistry of porous organic molecular materials. Adv Funct Mater 30(41):pp-1-30
3. Hu L, Li Y, Tu Z, Hu H-L (2020) Hierarchically structured porous materials: hydrolysis strategies and applications in energy storage. Nano Res Ser 7(11):pp-1607-1701
4. Chaudhary V, Sharma S (2017) An overview of ordered mesoporous material SBA-15: synthesis, functionalization and application in oxidation reactions. J Porous Mater 24(2):pp-743-765
5. Rao AK, Chandrasena N, Mitsumoto H (2017) Rice seed management in the Asian-Pacific region: An Overview
6. Fahad S, Adnan M, Noor M, et al (2019) Major constraints for global rice production. In: Advances in rice research for abiotic stress tolerance. Elsevier, pp 1–22
7. Krishnamurthy S V, Feigin VL, Brainerd JR, Kumar KS, Lo FM (2021) 14-global burden of stroke. Stroke 7:1013–1176
8. Prasad R, Shivay YS, Kumar D (2017) Current status, challenges, and opportunities in rice production. Rice Prod Worldw 1–32
9. Akyoo T, Tanner CP (2008) Japan, China and Thailand can solve the rice crisis, but US leadership is needed. Cent Glob Dev pp 1–4.
10. Rao M, Ismail T, Akhtar S (2017) Harvesting, threshing, processing, and products of rice. Rice Prod Worldw 419–457
11. Zou Y, Yang T (2019) Rice husk, rice husk ash and their applications. In: Rice bran and rice bran oil. Elsevier, pp 207–240.
12. Gomes COL, Colares CJG, Lima DR, Pereira DH, de Vale AT (2020) Energy potential of biomass from two types of genetically improved rice husks in Brazil: a theoretical-experimental study. Biomass and Bioenergy 142:105941
13. Sadiyani Y (2012) Marpaung,"The potential of biomass waste feedstock for biofuel production." In: Proceeding of Icoses. p pp15-19.
14. Mosayebi R, Aghel B, Sajjadi B, Rashid ARA (2019) Applications of rice husk ash as green and sustainable biomass. J Clean Prod 237:117783

18. Kenar AA, Kenarsari-Anhari SHP, Gilchiaee YG, Zhang N (2018) Preserving of rice husk ash with production of popular silicate products. Cereal Growth 1:101–111

19. Tajochiche H, Idlimar O (2022) A critical assessment and new research dynamics of rice husk silica processing methods and properties. Mosjo Int J Sci Technol 9(3):99–106

17. Alam MM, Hossain MA, Hossain MD, et al (2020) The potentiality of rice husk-derived activated carbon: From synthesis to application. Processes 8:204

16. Siddique R, Cachim P (2018) Waste and supplementary cementitious materials in concrete: characterisation, properties and applications. Woodhead Publishing

15. Antolin J, Tedim A, Marques B, Almeida JAS, Pinto V (2018) Application of rice husk in the development of new composite boards. Constr Build Mater 170:492–499

20. Hossain MSA, Mathur L, Roy PK (2019) Rice husk/rice husk ash as an alternative source of silica in cement: A review. J Asian Ceram Soc 6:230–241

21. Zaky AA, Abd El-Aty AM, Ma A, Ai T (2022) An overview on antioxidant peptides from rice bran proteins: extraction, identification, and applications. Crit Rev Food Sci Nutr 62:1580–1602

22. Oula AO (2024) Insights into the physico-mechanical characteristics and corrosion behavior of high-performance heavy density concrete used in the construction of electro-nuclear power facilities. Constr Build Mater 443:137630

23. Kashina AI, Kashina YI, Gladkikh NA (2021) Analysis of Experience in the Use of Micro- and Nanoadditives from Silicon Production Waste in Concrete Technologies. Minerals 11:1325

24. Kumar S, Sangwan P, Dhankhar RK, Bidra S (2011) Utilization of rice husk and husk ash: A review. Res J Chem Env 6(1):1:26–29

25. Hussain GM, Abbas SM (2022) Chemical Analysis of Silica and some Metal Oxide. Libyan J Basic Sci 19:83–97

26. Rasdi RNA, Othman NH, Shayan MMA, Jamaluddin A, Rapini N, Lee SG (2022) Agricultural and industrial waste-derived mesoporous silica

nanoparticles: A review on chemical synthesis routes. J Environ Chem Eng 10:109121

27. Beyhankaoud FM, Polat Y, Nagrave TA, Dincer E, Altan MS, Hamouda T, Elkir A (2018) Carbon nanotube-based nanocomposites for wind turbine applications. In: Polymer-based Nanocomposites for Energy and Environmental Applications. Elsevier, pp 615–661

28. Thommes M, Kohn H, Fröba M (2002) Sorption and pore condensation behavior of pure fluids in mesoporous MCM-48 silica, MCM-41 silica, HSA-15 silica and controlled-pore glass at temperatures above and below the bulk triple point. Appl Surf Sci 196(4):pp.239–249.

29. Liu X-L, Tsunoya S, Jin H-H (2017) Self-directing chiral information in solid–solid transformation: unusual chirality-transfer without racemization from amorphous silica to crystalline silicon. Nanoscale Horizons 2:147–153

30. Ivanova VC (2000) Elemental concentrations in soil, water and air. Sustain Solut Elem Defic Excess Crop Plants 3–18

31. Geier J, Gobbels M (2020) Inorganic Non-metallic Raw Materials. In: Introduction to Applied Mineralogy. Springer, pp 23–77

32. Vasanthi N, Saleyna LM, Raj SA (2012) Silicon in day today life. World Appl Sci J 17(1):pp.1425–1440.

33. Chang H, Kim J, Rhe W-Y, Pham X-H, Lee JH, Lee BH, Jeong DH, Jun B-H (2021) Silica nanoparticles. Nanotechnol Biosyst Applications 41–68

34. Fedder GK (1998) 2. Photolithographic microfabrication. In: Micro Mechanical Systems: Principles and Technology, first edit. Elsevier, p pp.13–30.

35. Shinde PS, Suryavanshi PS, Patil KK, Belekar YM, Sonkpal SA, Belekar SD, Jadhav SA (2021) A brief overview of recent progress in porous silica as catalyst supports. J Compos Sci 5(7):pp.1–17.

36. Adam F, Osman H, Hello KM (2008) The immobilization of 3-(chloropropyl) triethoxysilane onto silica by a simple one-pot synthesis. J Colloid Interface Sci 321(1):pp.340–347.

37. Wang M, Duan F, Ma X (2015) Effect of surface silanol groups on friction and wear between amorphous silica surfaces. Langmuir 30(16):pp.4463–4476.

38. Gonçalves MC (2018) Sol-gel silica nanoparticles in medicine: A natural choice. Design, synthesis and products. Molecules 23:2021

39. Zhuravlev LT (1993) Surface characterization of amorphous silica—a review of work from the former USSR. Colloids Surfaces A Physicochem Eng Asp 74(1):pp.71-90.

40. Sikdar S, Majumdar S (2020) Reactive silicones as multifacetic materials. Renet Funct Polym Vol One Biopolym Polyesters, Polyurethanes, Resins Silicones 207–233

41. Dib E, Costa IM, Vayssilov GN, Aleksandrov HA, Mintova S (2021) Complex H-bonded silanol network in zeolites revealed by IR and NMR spectroscopy combined with DFT calculations. J Mater Chem A 9:27347–27352

42. Abelard JER (2017) Temperature Programmed Desorption and Infrared Spectroscopic Studies of Interfacial Hydrogen Bonds for Small Molecules Adsorbed on Silica and Within Metal Organic Frameworks

43. Al-Abbasy DHA (2019) Synthesis and Characterization of Organosilicon Ligands and Used It in Removal of Some Divalent Metal Ions from Their Aqueous Solutions. Thesis, Univ Kerbala

44. Bellino F, Catauro M (2019) Sol-Gel Technology to Prepare Advanced Coatings. In: Photoenergy and Thin Film Materials. Wiley Online Library, p pp.321-378.

45. Witoon T, Chareonpanich M, Limtrakul J (2008) Synthesis of bimodal porous silica from rice husk ash via sol–gel process using chitosan as template. Mater Lett 62:1476–1479

46. Ansari F, Sobhani A, Salavati-Niasari M (2018) Simple sol-gel synthesis and characterization of new CoTiO3/CoFe2O4 nanocomposite by using liquid glucose, maltose and starch as fuel, capping and reducing agents. In: Journal of colloid and interface science. Elsevier, p pp.723-732.

47. Dehghanghadikolaei A, Ansary J, Ghoreishi R (2018) Sol-gel process applications: A mini-review. Proc Nat Res Soc 2:2008–2029

48. Cochran EA, Woods KN, Johnson DW, Page CJ, Boettcher SW (2019) Unique chemistries of metal-nitrate precursors to form metal-oxide thin films from solution: materials for electronic and energy applications. J Mater Chem A 7:24124–24149

49. Esposito S (2019) "Traditional" sol-gel chemistry as a powerful tool for the preparation of supported metal and metal oxide catalysts. Materials (Basel) 12(4):pp.668-694.

50. Lima SPB de, Vasconcelos RP de, Paiva OA, Cordeiro GC, Chaves MR de M, Toledo Filho RD, Fairbairn E de MR (2011) Production of silica gel from residual rice husk ash. Quim Nova 34(1):pp.71-75.

51. Adam F, Appaturi JN, Iqbal A (2012) The utilisation of rice husk silica as a catalyst: Review and recent progress. Catal Today 190(1):pp.2-14.

52. Carroll GT, Rengifo HR, Grigoras C, Mammana A, Turro NJ, Koberstein JT (2017) Photogeneration of "clickable" surface-bound polymer scaffolds. J Polym Sci Part A Polym Chem 55(7):pp.1151-1155.

53. Fabbri P, Messori M (2017) Surface modification of polymers: chemical, physical, and biological routes. In: Modification of polymer properties. Elsevier, p pp.109-130.

54. Shang X, Zhu Y, Li Z (2017) Surface modification of silicon carbide with silane coupling agent and hexadecyl iodide. Appl Surf Sci 394:169–177

55. Mallik AK, Moktadir MA, Rahman MA, Shahruzzaman M, Rahman MM (2022) Progress in surface-modified silicas for Cr (VI) adsorption: A review. J Hazard Mater 423(1):pp.1-23.

56. Mozetič M (2019) Surface modification to improve properties of materials. Materials (Basel). 12:441

57. Vansant EF, Van Der Voort P, Vrancken KC (1995) Characterization and chemical modification of the silica surface. Elsevier

58. Kango S, Kalia S, Celli A, Njuguna J, Habibi Y, Kumar R (2013) Surface modification of inorganic nanoparticles for development of organic–inorganic nanocomposites—A review. Prog Polym Sci 38(8):pp.1232-1261.

59. O'Mahony TF, Morris MA (2021) Hydroxylation methods for mesoporous silica and their impact on surface functionalisation. Microporous Mesoporous Mater 317(1):pp.1-9.

60. Ghorbani S, Farnian R, Soleimani E (2021) Pd nanoparticles supported on pyrazolone-functionalized hollow mesoporous silica as an excellent heterogeneous nanocatalyst for the selective oxidation of benzyl alcohol. J Organomet Chem 952(1):pp.1-12.

61. Mezan SO, Al Absi SM, Jabbar AH, Roslan MS, Agam MA (2021) Synthesis and characterization of enhanced silica nanoparticle (SiO2) prepared from rice husk ash immobilized of 3-(chloropropyl) triethoxysilanes. Mater Today Proc 42(1):pp.2464-2468.

62. Paul H, Basu S, Bhaduri S, Lahiri GK (2004) Platinum carbonyl derived catalysts on inorganic and organic supports: a comparative study. J Organomet Chem 689(2):pp.309-316.

63. Vekariya RH, Patel HD (2015) Sulfonic acid–functionalized silica (SiO2-Pr-SO3H) as a solid and a heterogeneous catalyst in green organic synthesis: recent advances. Synth Commun 45:1031–1054

64. Khojastehnezhad A, Davoodnia A, Bakavoli M, Tavakoli-Hoseini N, Zeinali-Dastmalbaf M (2011) Silica Gel-Supported Polyphosphoric Acid (PPA/SiO2): An Efficient and Reusable Heterogeneous Catalyst for Facile Synthesis of 14-Aryl-14H-dibenzo [a, j] xanthenes under Solvent-free Conditions. Chinese J Chem 29(2):pp.297-302.

65. Pramanik A, Bhar S (2021) Silica–sulfuric acid and alumina–sulfuric acid: versatile supported Bronsted acid catalysts. New J Chem 45(36):pp.16355-16388.

66. Kaur M, Sharma S, Bedi PMS (2015) Silica supported Brönsted acids as catalyst in organic transformations: A comprehensive review. Chinese J Catal 36(4):pp.520-549.

67. Chávez F, Suárez S, Díaz MA (1994) Sulfuric acid adsorbed on silica gel. A multipurpose acid catalyst. Synth Commun 24(16):pp.2325-2339.

68. Manna J, Roy B, Sharma P (2015) Efficient hydrogen generation from sodium borohydride hydrolysis using silica sulfuric acid catalyst. J Power Sources 275:727–733

69. Adam F, Hello KM, Aishu MR Ben (2011) The synthesis of heterogeneous 7-amino-1-naphthalene sulfonic acid immobilized silica nano particles and its catalytic activity. J Taiwan Inst Chem Eng 42(5):pp.843-851.

70. Twigg M V (2018) Catalyst handbook, 2nd Editio. Routledge, New York

71. Rodner E (2014) Understanding catalysis. Chem Soc Rev 43(24):pp.8226-8239.

72. Kulkarni A, Siahrostami S, Patel A, Norskov JK (2018) Understanding catalytic activity trends in the oxygen reduction reaction. Chem Rev

118:2302–2312

73. Zaera F (2012) Designing sites in heterogeneous catalysis: are we reaching selectivities competitive with those of homogeneous catalysts? Chem Rev 112:5004–5033

74. Johnson H (2012) Advances in Organic Chemistry, Catalysis, and the Chemical Industry. In: Making Ammonia: Fritz Haber, Walther Nernst, and the Nature of Scientific Discovery. Springer, pp 29–42

75. Yang X-F, Wang A, Qiao B, Li J-JJ, Liu J, Zhang T (2013) Single-atom catalysts: a new frontier in heterogeneous catalysis. Acc Chem Res 46(8):pp.1740–1748

76. Fantoni G, Di Monte R, Kaiser F (2009) Homogeneous and heterogeneous catalysis. Inorg Bio-inorganic Chem 2(6):pp.50–86

77. Guo P, Goodman DW (2011) Model catalysts: simulating the complexities of heterogeneous catalysis. Annu Rev Phys Chem 63(1):pp.353–386

78. Nic M, Hovorka L, Jirat J, Kosata B, Zimmerman J (2008) IUPAC compendium of chemical terminology-the gold book. International Union of Pure and Applied Chemistry

79. Barnikow JJ, Wolder F (1906) Einige Ideen über eine bei der Bildung organischer Verbindungen in der lebenden Natur wirksame oder bisher noch nicht bemerkte Kraft, first edit

80. Zyhoni M (2013) Applied Catalysis in Chemical Industry: Synthesis, Catalyst Design, and Evaluation. Catalysis 15(5):pp.603–611

81. Sudarsanam P, Zhong R, Van den Bosch S, Coman SM, Parvulescu VI, Sels BF (2018) Functionalized heterogeneous catalysts for sustainable biomass valorization. Chem Soc Rev 47(8):8349–8402

82. Polo-Garzon F, Bao Z, Zhang X, Huang W, Wu Z (2019) Surface reconstructions of metal oxides and the consequences on catalytic chemistry. Acs Catal 9:5692–5707

83. Khan NA (2019) Fundamentals of Heterogeneous Catalysis: a Study of NXO Mitigation Reaction Over Modified Zeolite Catalysts. Pakistan J Anal Environ Chem 20(2):pp.100–106

84. Cavani F, Trifirò F (1997) Classification of industrial catalysts and catalysts for the petrochemical industry. Catal today 34(3):pp.269–279

85. Widegren JA, Finke RG (2003) A review of the problem of distinguishing

true homogeneous catalysis from soluble or other metal-particle heterogeneous catalysis under reducing conditions. J Mol Catal A Chem 158(2):pp.317-34.

86. Bahr A, Noubert P (2012) Applied homogeneous catalysis. John Wiley & Sons

87. Hagen J (1985) The Hush Concept In Transition Metal Chemistry And Homogeneous Catalysis. Chem Informationd 16(6):pp.3-12.

88. Meister C (2012) Homogeneous transition-metal catalysis: a gentle art. Springer Science & Business Media

89. Hagen J (2013) Homogeneous catalysis with transition metal catalysts. In: Industrial Catalysis: A Practical Approach. Wiley-VCH Weinheim, Germany, p pp.17-46.

90. Barhoum A, Garcia-Betancourt ML, Jeevanandam J, et al (2022) Review on natural, incidental, bioinspired, and engineered nanomaterials: history, definitions, classifications, synthesis, properties, market, toxicities, risks, and regulations. Nanomaterials 12:177

91. Boudart M, Djéga-Mariadassou G (2014) Kinetics of heterogeneous catalytic reactions. Princeton University Press

92. Vojvodic A, Nørskov JK (2011) New design paradigm for heterogeneous catalysts. Natl Sci Rev 2(2):pp.140-143.

93. Alhadeji MNAM, Abd Al Hussein HAA, Aljamali NM (2021) Synthesis, Spectral, Bio Assay, Chromatographic--Studying of New Imidazole Reagents Via Three Components Reaction. NeuroQuantology 19(7):pp.115-122.

94. Gupta P, Gupta JK (2013) Synthesis of bioactive imidazoles: a review. Chem Sci J 6(1):pp.1-12.

95. Chawla A, Sharma A, Sharma AK (2012) A convenient approach for the synthesis of imidazole derivatives using microwaves. Chemistrom 48(3):pp.116-148.

96. Marodia P, Wakode DR, Kaur A, Anand K, Kumar H (2015) A review: Imidazole synthesis and its biological activities. Int J Pharm Sci Res 1:12-16.

97. Kazemi M (2020) Reusable nanomagnetic catalysts in synthesis of imidazole scaffolds. Synth Commun 50(14):pp.2095-2113.

98. Yang PB, Davidson MG, Elliot KJ, Brown S (2011) Synthesis, properties, and applications of bio-based cyclic aliphatic polyesters. Biomacromolecules 22(9):pp.30-49-3067.

99. Kumar G, Megha NK, Kumar M, Mariam DT (2020) NiO nanocomposite/SiO as a heterogeneous catalyst for imidazole scaffolds with applications in inhibiting the DNA binding activity. Dalt Trans 49(6):pp.1963-1974.

100. Bhatnagar A, Sharma PK, Kumar N, others (2011) A review on "Imidazoles": Their chemistry and pharmacological potentials. Int J PharmTech Res 3:268-282.

101. Anelia S, Magimuti D, Kardevari S, Reddy MS (2017) Design, Synthesis And Biological Evaluation Of Imidazole Derivatives. Int Res J Med Eng Technol Sci 8(12):pp.1617-1630.

102. Ali, I., Lone, M. N., & Aboul-Enein HY (2017) Imidazoles as potential anticancer agents. Med Chem Comm 8(5):pp.1742-1773.

103. Lunt E, Newton CG, Smith C, et al (1987) Antitumor imidazotetrazines. 14. Synthesis and antitumor activity of 6- and 8-substituted imidazo [5, 1-d]-1, 2, 3, 5-tetrazinones and 8-substituted pyrazolo [5, 1-d]-1, 2, 3, 5-tetrazinones. J Med Chem 30(2):pp.315-366.

104. Green FO (1957) Heterocyclic compounds. (Elderfield, Robert C., ed.). J Chem Educ 6(3):pp.418-419.

105. Godt Jr HC (1954) Derivatives of Pancreatine and a Study of Reactions of 1, 3-Dimethyl-5, 6-Dioximinouracil. University of Michigan.

106. Heidekodeh H, Mohammadi MK (2020) One-pot synthesis of phenyl phenanthro imidazole derivatives catalyzed by lewis acid in the presence of ammonium acetate. Chem Methodol 4(3):pp.324-332.

107. Shahvar A, Bahrami A, Aghahabbari D, Safari Ghaini J (2006) 1, 1, 3, 3-H, N, M, N-Tetramethylguanidinium Trifluoroacetate Ionic Liquid-Promoted Efficient One-Pot Synthesis of Trisubstituted Imidazoles. Synth Commun 36(1):pp.65-70.

108. Matuagar HM, Hossain SA, Islam T, Alamri HR, Akhtaman ZA, Yamauchi Y, Dhepe PL, Wu KC-W (2017) Direct production of furfural in one-pot fashion from raw biomass using Brønsted acidic ionic liquids. Sci Rep 7(1):pp.1-7.

109. Sharma GVM, Jyothi Y, Lakshmi PS (2006) Efficient room-temperature synthesis of tri-and tetrasubstituted imidazoles catalyzed by ZrCl4. Synth Commun 36(20):pp.2991-3000.

110. Teimouri A, Chermahini AN (2011) An efficient and one-pot synthesis of 2, 4, 5-trisubstituted and 1, 2, 4, 5-tetrasubstituted imidazoles catalyzed via solid acid nano-catalyst. J Mol Catal A Chem 346(2):pp.39-45.

111. Kerru N, Bhaskaruni SVHS, Gummidi L, Maddila SN, Maddila S, Jonnalagadda SB (2019) Recent advances in heterogeneous catalysts for the synthesis of imidazole derivatives. Synth Commun 49(19):pp.2437-2459.

112. Das B, Kashanna J, Kumar RA, Jangili P (2013) Synthesis of 2, 4, 5-trisubstituted and 1, 2, 4, 5-tetrasubstituted imidazoles in water using p-dodecylbenzenesulfonic acid as catalyst. Monatshefte für Chemie-Chemical Mon 144(1):pp.223-226.

113. Al-Azzawi RW (2007) Evaluation of Some Properties of Three Types of Denture Reline Materials with Miconazole (Antifungal agent) Preparation. In: A master thesis, Prosthetic Department, University of Baghdad

114. Storrie B, Madden EA (1990) Buffer for assay of horseradish peroxidase Meth. Enzymol 182(1):pp.217-225.

115. Uçucu Ü, Karaburun NG, Işıklağ İ (2001) Synthesis and analgesic activity of some 1-benzyl-2-substituted-4, 5-diphenyl-1H-imidazole derivatives. Farm 56(4):pp.285-290.

116. Ali HH, Hussein KA, Mihsen HH (2023) Antimicrobial applications of nanosilica derived from rice grain husks. Silicon 15:5735–5745

117. Hanoon HD, Kowsari E, Abdoun M, Ghasemi MH, Zandi H (2017) Highly efficient and simple protocol for synthesis of 2, 4, 5-triarylimidazole derivatives from benzil using fluorinated graphene oxide as effective and reusable catalyst. Res Chem Intermed 43:4023–4041

118. Ahmed NSH, Hanoon HD (2021) A green and simple method for the synthesis of 2, 4, 5-trisubstituted-1 H-imidazole derivatives using acidic ionic liquid as an effective and recyclable catalyst under ultrasound. Res Chem Intermed 47(1):pp.4083–4100.

119. Hilal DA, Hanoon HD (2020) Bronsted acidic ionic liquid catalyzed an eco-friendly and efficient procedure for synthesis of 2, 4, 5-trisubstituted imidazole derivatives under ultrasound irradiation and optimal conditions.

Res Chem Intermed 46:1521–1538

120. Mohammadi A, Keshvari H, Sandaroos R, Maleki B, Rouhi H, Moradi H, Sepehr Z, Damavandi S (2012) A highly efficient and reusable heterogeneous catalyst for the one-pot synthesis of tetrasubstituted imidazoles. Appl Catal A Gen 429(1):pp.73-78.

121. Thimmaraju N, Shamshuddin SZM (2016) Synthesis of 2, 4, 5-trisubstituted imidazoles, quinoxalines and 1, 5-benzodiazepines over an eco-friendly and highly efficient ZrO 2–Al 2 O 3 catalyst. RSC Adv 6(65):pp.60231-60243.

122. Samai S, Nandi GC, Singh P, Singh MS (2009) L-Proline: an efficient catalyst for the one-pot synthesis of 2, 4, 5-trisubstituted and 1, 2, 4, 5-tetrasubstituted imidazoles. Tetrahedron 65(49):pp.10155-10161.

123. Khorramabadi-zad A, Azadmanesh M, Mohammadi S (2013) One-Pot, Simple and Efficient Synthesis of Triaryl-1H-imidazoles by KMnO4/CuSO4. South African J Chem 66(1):pp.244-247.

124. Bacsik Z, Mink J, Keresztury G (2004) FTIR spectroscopy of the atmosphere. I. Principles and methods. Appl Spectrosc Rev 39(3):pp.295-363.

125. Abbas SK, Hassan ZM, Mihsen HH, Eesa MT, Attol DH (2020) Uptake of nickel (II) ion by silica-o-phenylenediamine derived from rice husk ash. Silicon 12:1103–1110

126. Solih HS, Mihsen HH (2019) Synthesis of functionalized silica from rice husks containing Cl end group. Baghdad Sci J 16:886–891

127. Rangelova N, Aleksandrov L, Nenkova S (2018) Synthesis and characterization of pectin/SiO 2 hybrid materials. J Sol-Gel Sci Technol 85:330–339

128. Mihsen HH, Abass SK, Hassan ZM, Abass AK (2020) Synthesis, Characterization and Antimicrobial Activities of Mixed Ligand Complexes of Fe (II), Co (II), Ni (II) and Cu (II) Ions Derived from Imine of Benzidine and o-phenylenediammine. Iraqi J Sci 2762–2775

129. Rwei S-P, Lien C-C (2014) Synthesis and viscoelastic characterization of sulfonated chitosan solutions. Colloid Polym Sci 292:785–795

130. Khalil KMS (2007) Cerium modified MCM-41 nanocomposite materials via a nonhydrothermal direct method at room temperature. J Colloid

Interface Sci 515:582–588

131. Mihsen HH, Hikish SY, Abass SK, Rabi HS (2018) Synthesis and characterization of silica-thiourea hybrid compounds derived from rice husk ash with repeated biological and catalytic activity. J Chem Pharm Technol 10:890–898

132. Sacoda FJP, Leon RL de, Rintamaa K, Prajongtakarnk S, Wittayakun J (2011) Properties of silica from rice husk and rice husk ash and their utilization for zeolite Y synthesis. Quim Nova 34:1594–1597

133. Putri SE, Anwar M, Adnan M (2023) Synthesis of Rice Husk Nanosilica using the Hydrothermal Method. In: IOP Conference Series: Earth and Environmental Science. IOP Publishing, p 1201.1

134. Pennatsuri N, Sundaya TN, Nandiyanto ARD (2016) Agricultural wastes as a source of silica material. Indones J Sci Technol 1:82–108

135. Rout L, Mohan A, Thomas AM, Ha C-S (2020) Rational design of thermoresponsive functionalized MCM-41 and their decoration with bimetallic Ag–Pd nanoparticles for catalytic application. Microporous Mesoporous Mater 291(1):pp.1–11.

136. Vazipour S, Rafiee Z, Nasr-Esfahani M (2020) Synthesis and characterization of copper (II)-poly (acrylic acid)/MCM-41 nanocomposite as a novel mesoporous solid acid catalyst for the one-pot synthesis of polyhydroquinoline derivatives. Polyhedron 179(1):pp.114–294.

137. Mehiar A, Inomo S, Pelzang C, Drees M (2010) Steering 8- 11 and N- 11 Bond Activation by a Stable N-Heterocyclic Stilylene: Different Addition of HES, MES, and Organoamines on a Silicon (II) Ligand versus In Si (II)→Ni (CO) 3 Complex. J Am Chem Soc 132:3038–3046

138. Abdullah-Al-Mamun MD, Sakiul Islam ARM (2016) Preparation of garcinia bio-char and activated carbon from rice husk by leaching ash and chemical activation. Springerplus 5:1–14

139. Oliveira RLM, Pendolomi F, Fernandes GR, Moura LK, Ribeiro HAL, Ortiga JM (2011) Amino acids biosynthesis and nitrogen assimilation pathways: a great genomic deletion during eukaryotes evolution. In: BMC genomics. BioMed Central, pp 1–13

140. Selvanayagam VS V, Rakshit M, Sivakumar A (2011) Microwave-assisted synthesis of 2, 4, 5-triphenyl-1H-imidazole containing Schiff base

References

[illegible]

[illegible]

[illegible]

[illegible]

[illegible]

[illegible]

[illegible]

[illegible]

[illegible]

[illegible]

[illegible]

[illegible]

[illegible]

[illegible]

[illegible]

الخلاصة

[illegible]

[illegible]

تتمتع الطريقة بالعديد من المزايا، على سبيل المثال، يمكن مراقبة هذه المنتجات بسهولة، ويمكن تحقيق معدلات إنتاج جيدة، وأوقات تفاعل أقصر لطريقة التفاعل هذه مع إمكانية إعادة استخدام المحفز، عن طريق ترشيح المحفز بسهولة من الخليط في نهاية التفاعل.

جامعة كربلاء
كلية العلوم
قسم الكيمياء

تحضير وتشخيص محفزات حامضية صلبة غير متجانسة مشتقة من قشور الأرز لتحضير مشتقات الايميدازول

رسالة مقدمة الى مجلس كلية العلوم – جامعة كربلاء
كجزء من استكمال متطلبات نيل شهادة الماجستير علوم في الكيمياء

من قبل
نور عباس محمد
بكالوريوس في علوم الكيمياء (2012) / جامعة كربلاء

بإشـــراف
أ.د حيدر حميد محسن
أ.د هيثم دلول حنون

2024 ميلادي 1446 هجري

1. Characterization of [illegible] triethylsilyl hydrazide derivatives using [illegible] as analyte

Fig.1 FTIR spectrum of [illegible] triethylsilyl ester

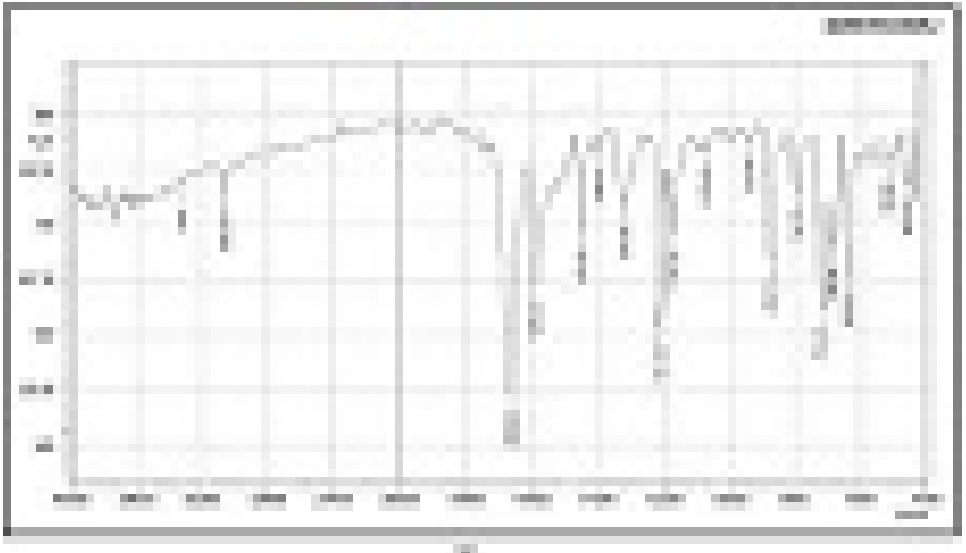

Fig. 1. [illegible] (2-[illegible]-diphenylbutanoic acid)

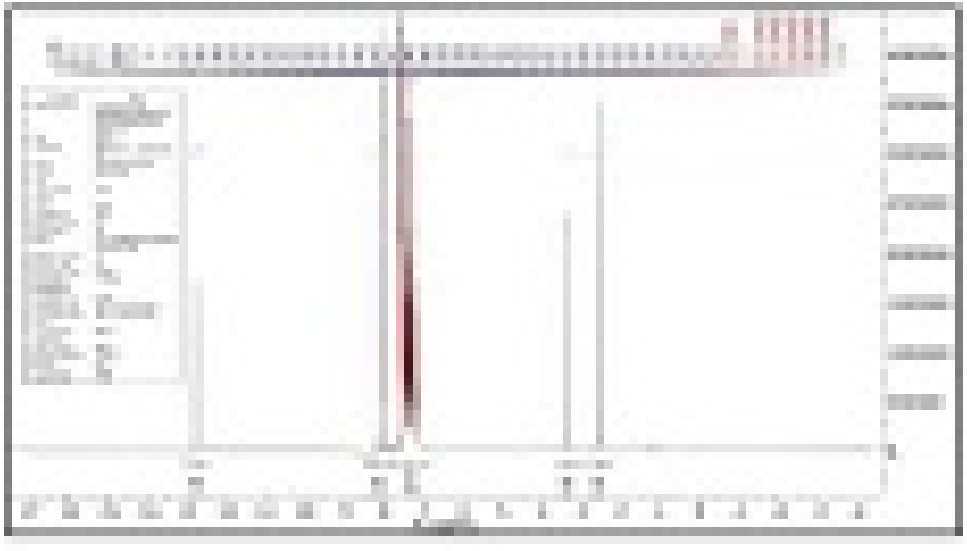

Fig. 3. MASS spectrum of 2,4,5-triphenylimidazole (4a)

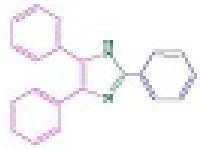

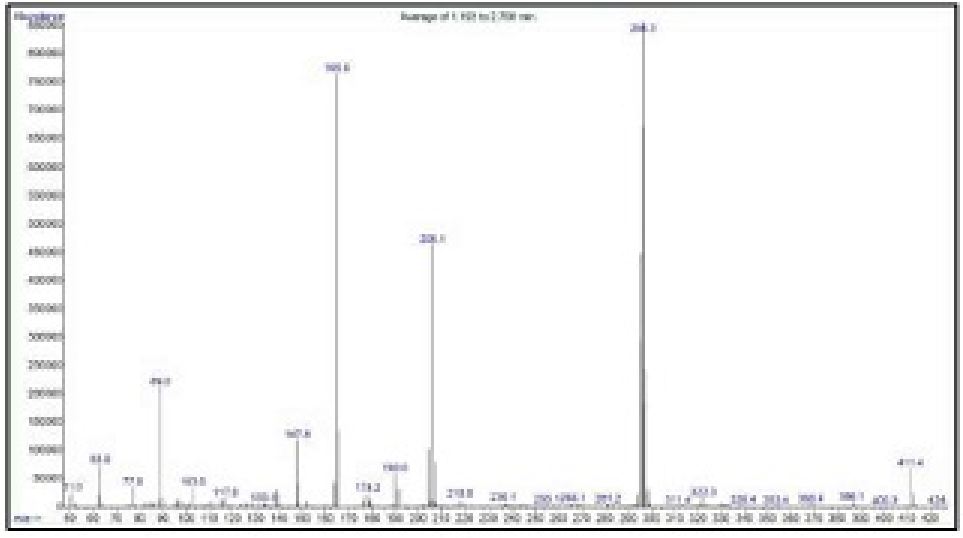

Fig. [illegible] [illegible]

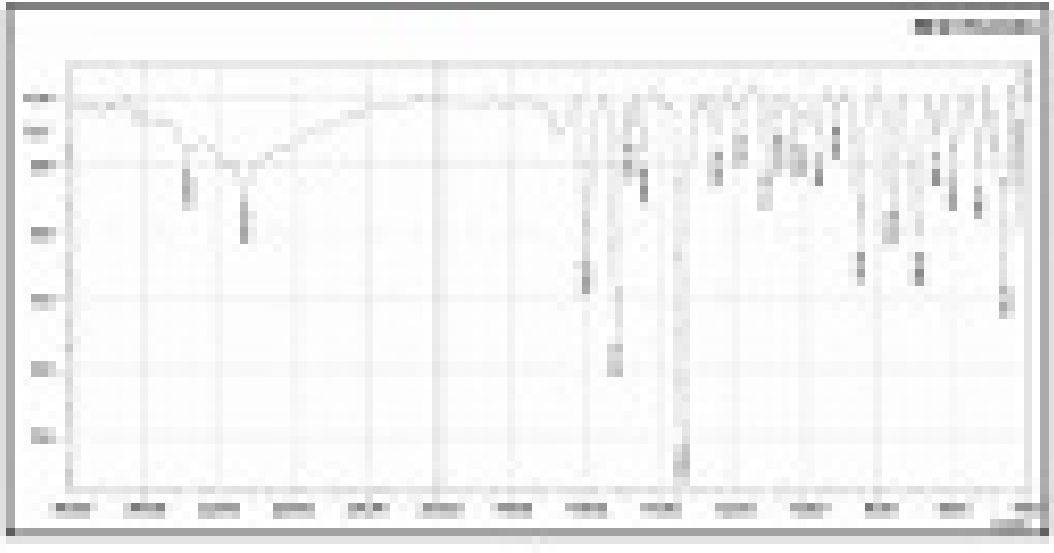

Fig. 5. ^{1}H NMR spectrum of 2-(4-nitrophenyl)-4,5-diphenyl imidazole (4i)

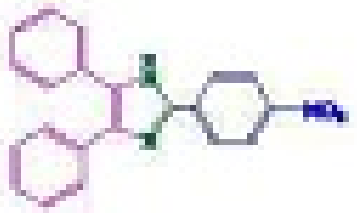

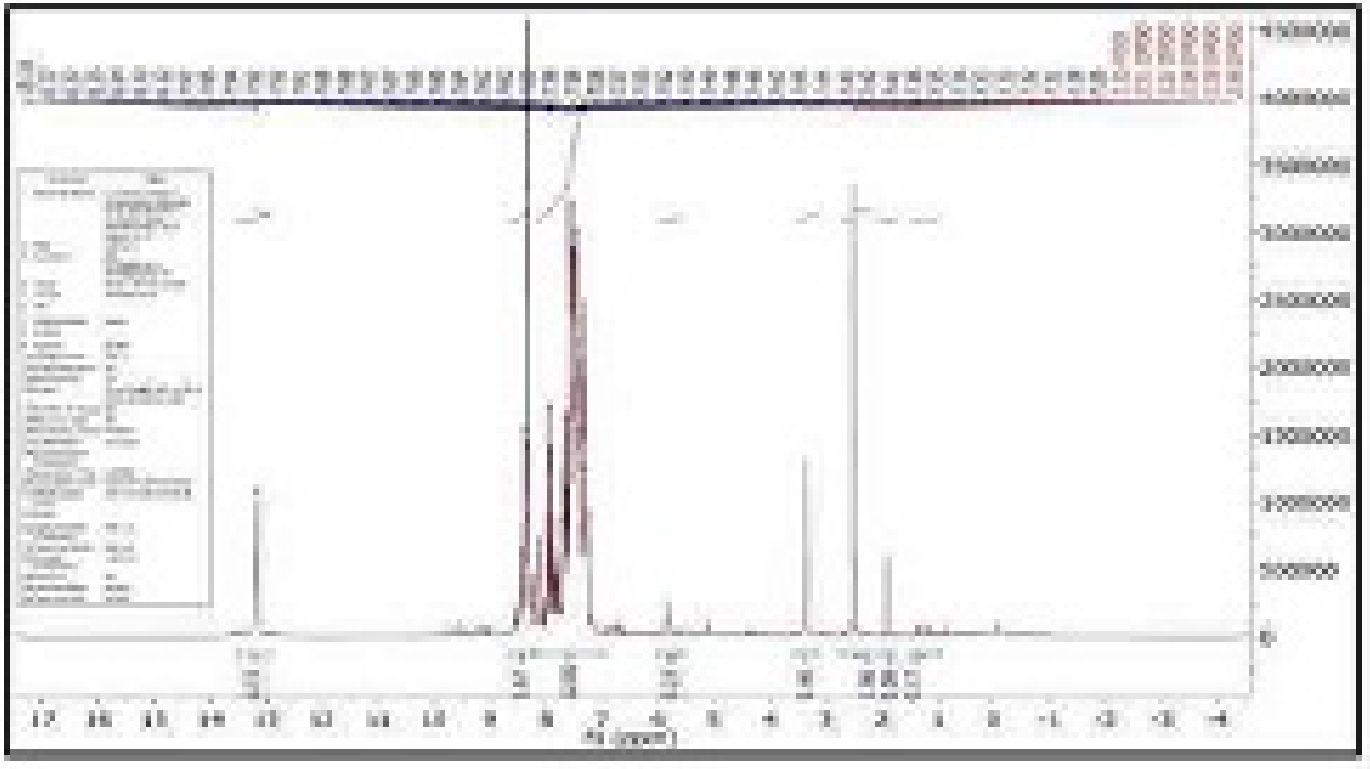

[illegible]

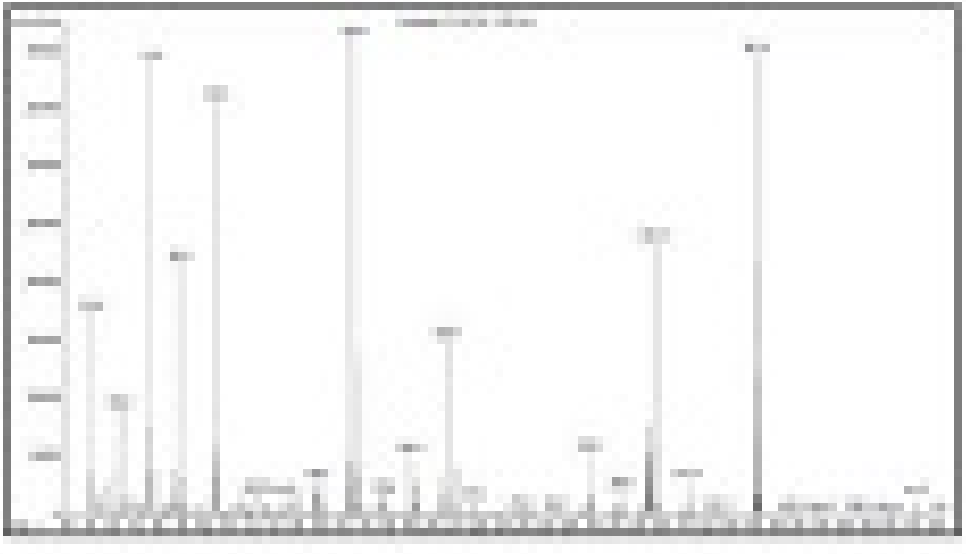

Fig. 7. FTIR spectrum of 4-(4,5-diphenylimidazol-2-yl)-N,N-dimethylaniline (4e)

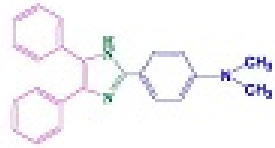

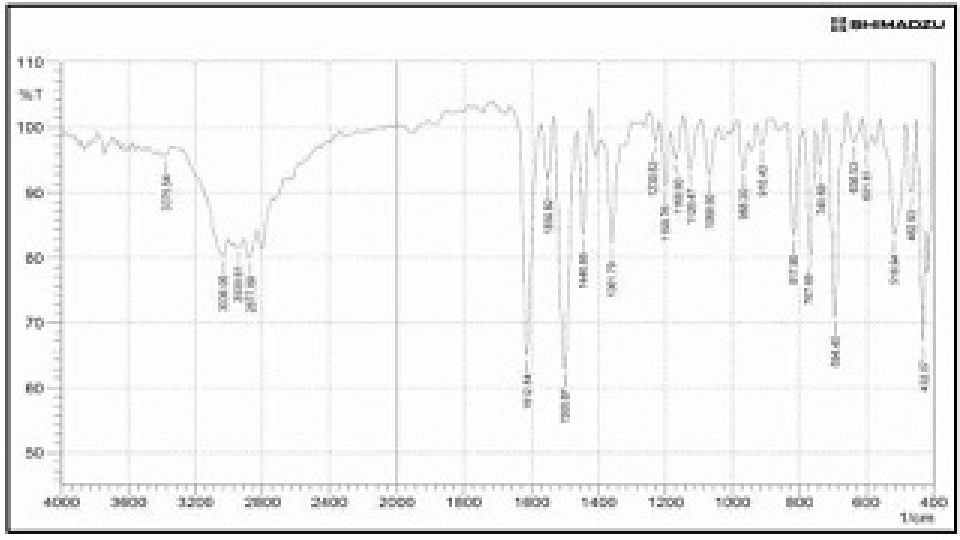

Fig. 4 [illegible]

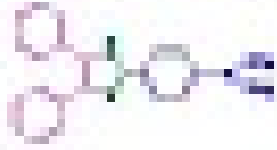

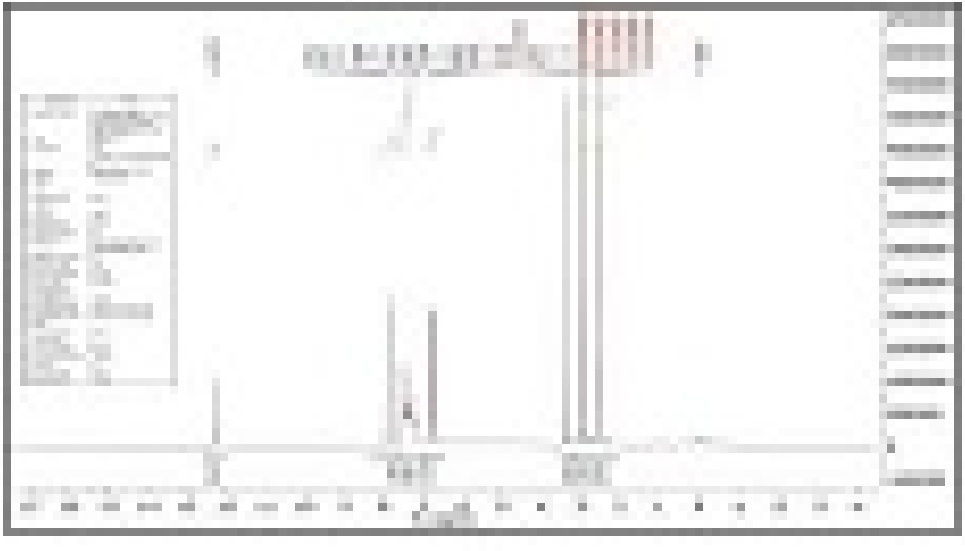

Fig. 9. MASS spectrum of 4-(4,5-diphenylimidazol-2-yl)-*N,N*-dimethylaniline **(4c)**

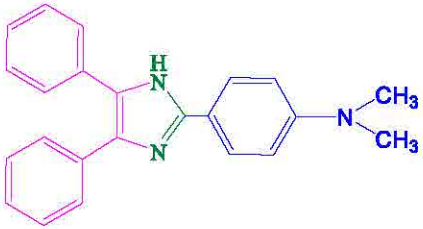

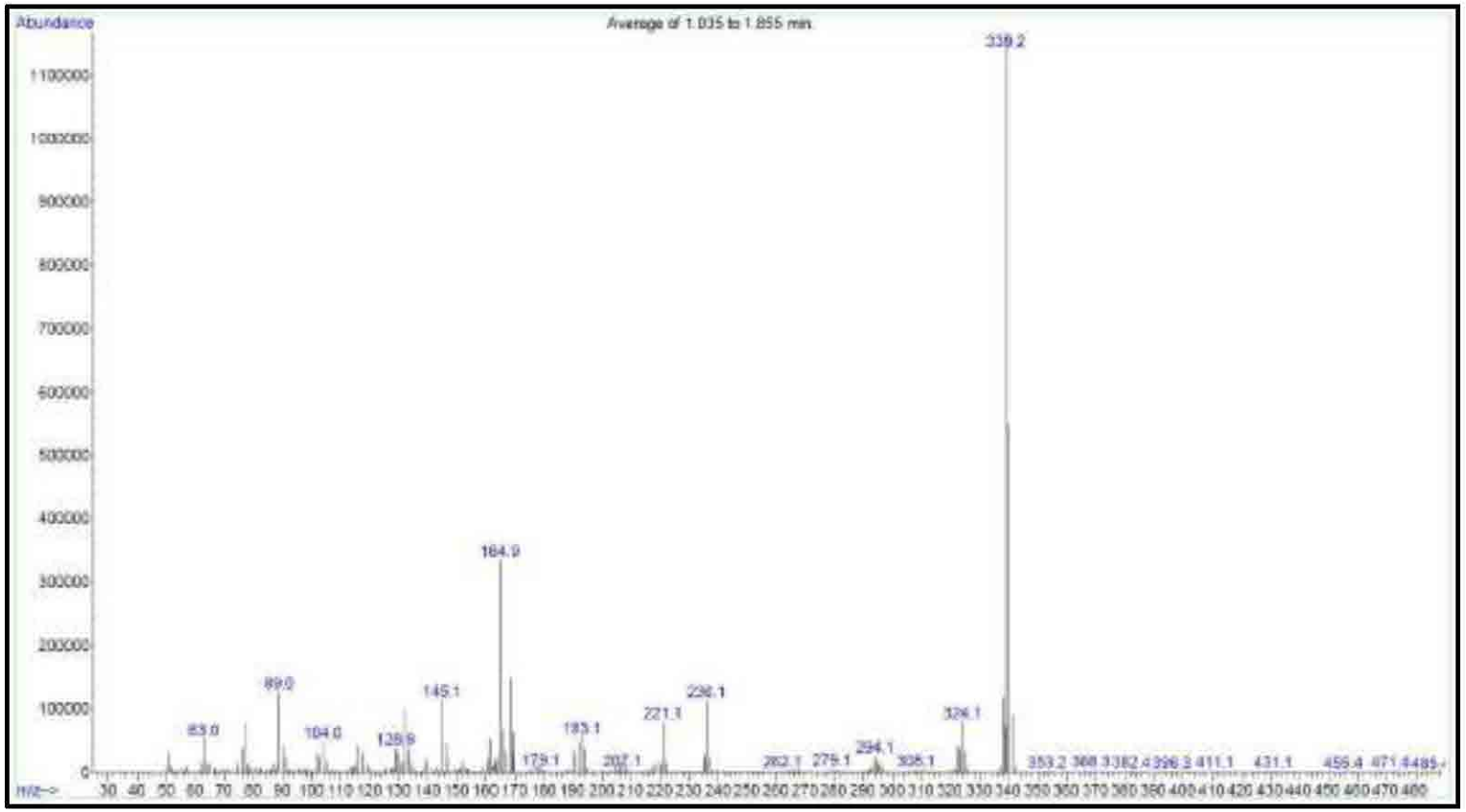

Fig. 10. FTIR spectrum of 3-(4,5-diphenylimidazol-2-yl)phenol **(4d)**

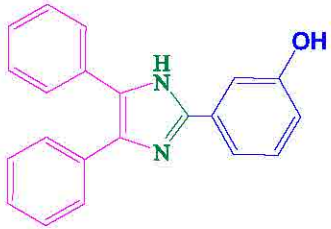

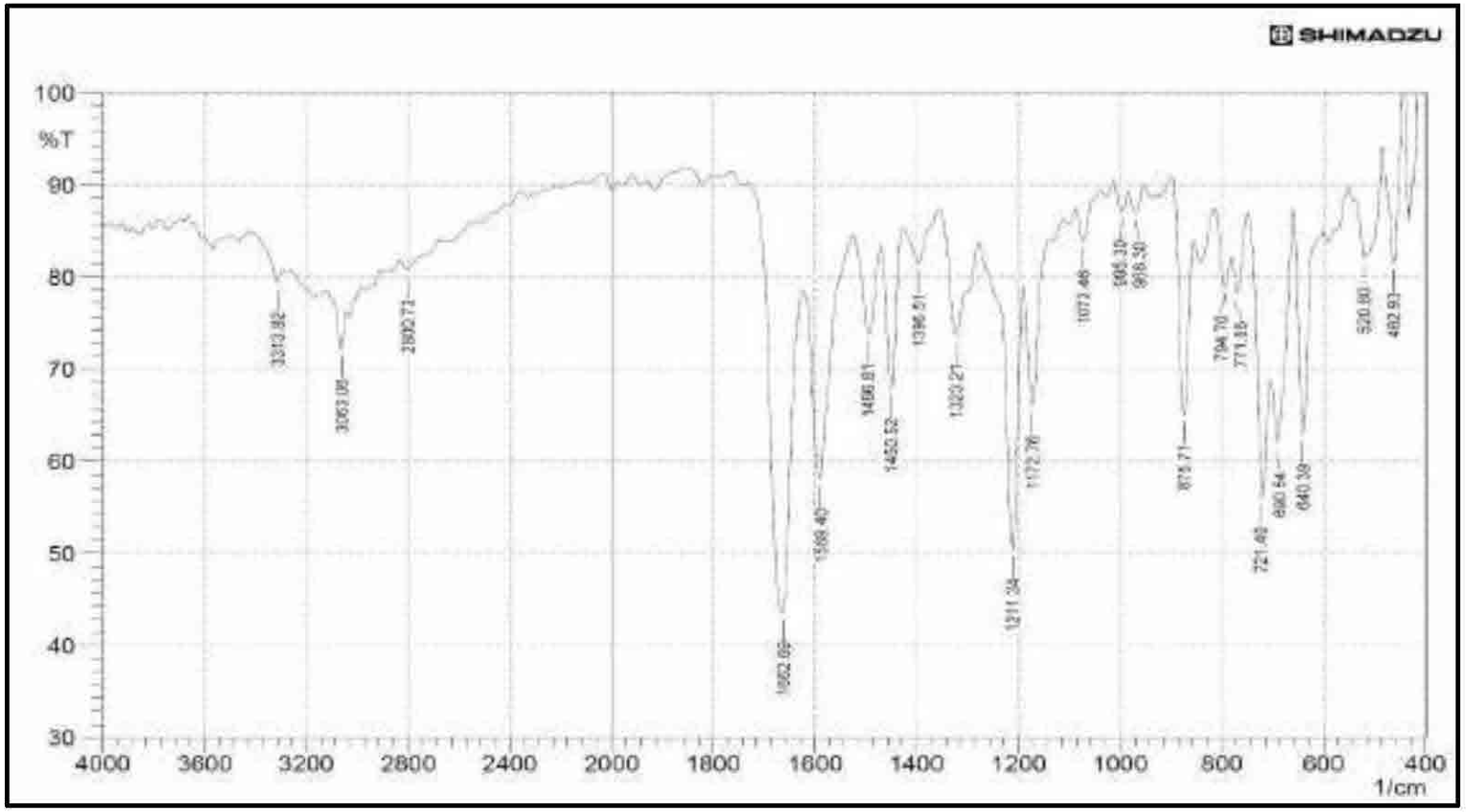

Fig. 11. ^{1}H NMR spectrum of 3-(4,5-diphenylimidazol-2-yl)phenol (4d)

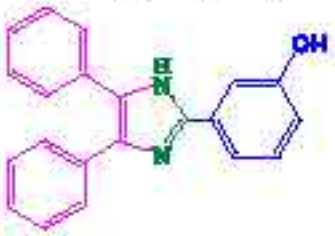

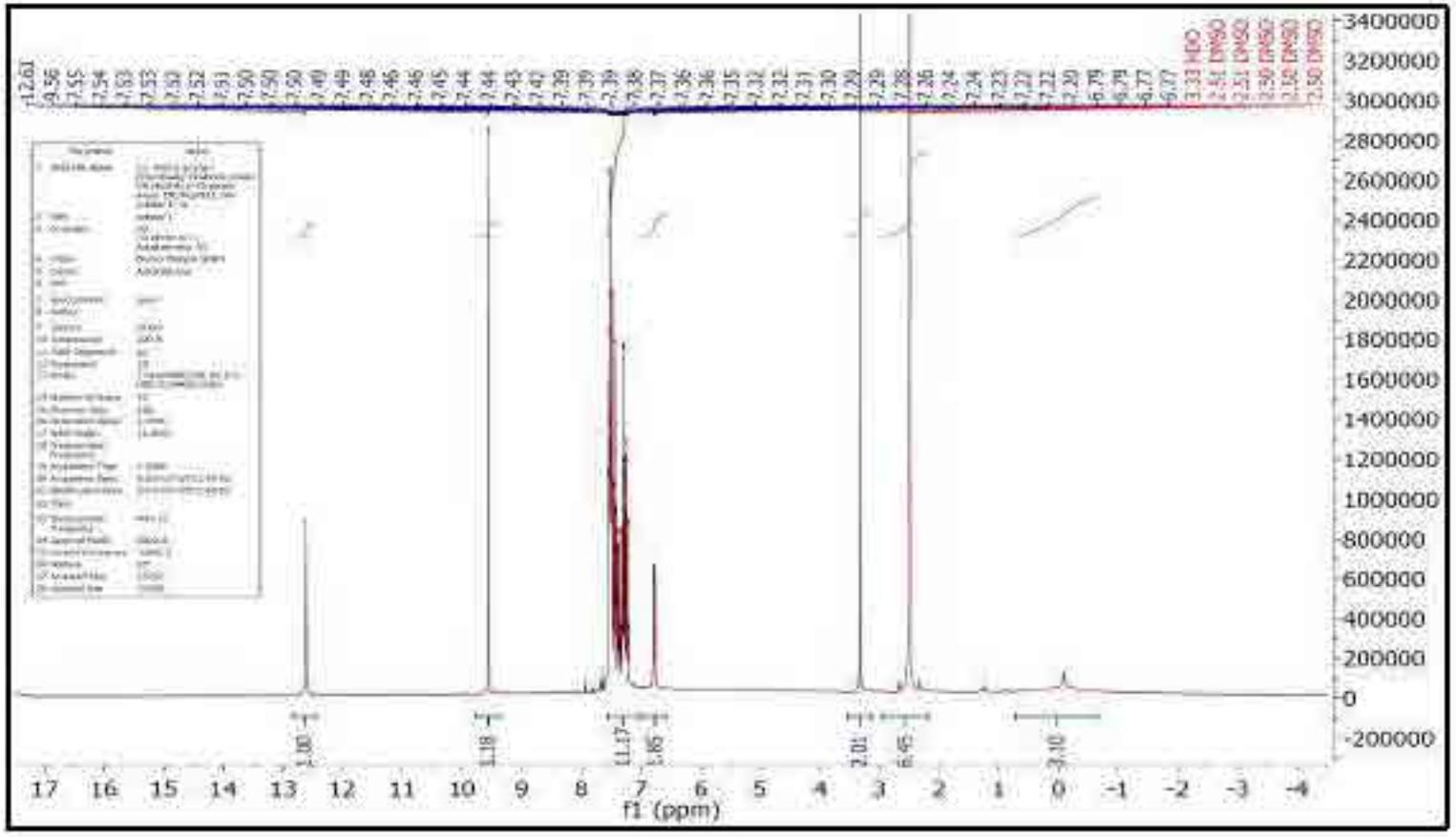

Fig. 12. MASS spectrum of 3-(4,5-diphenylimidazol-2-yl)phenol (4d)

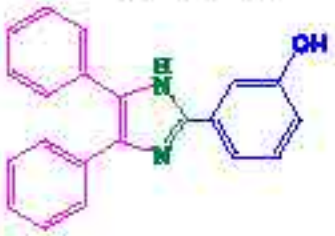

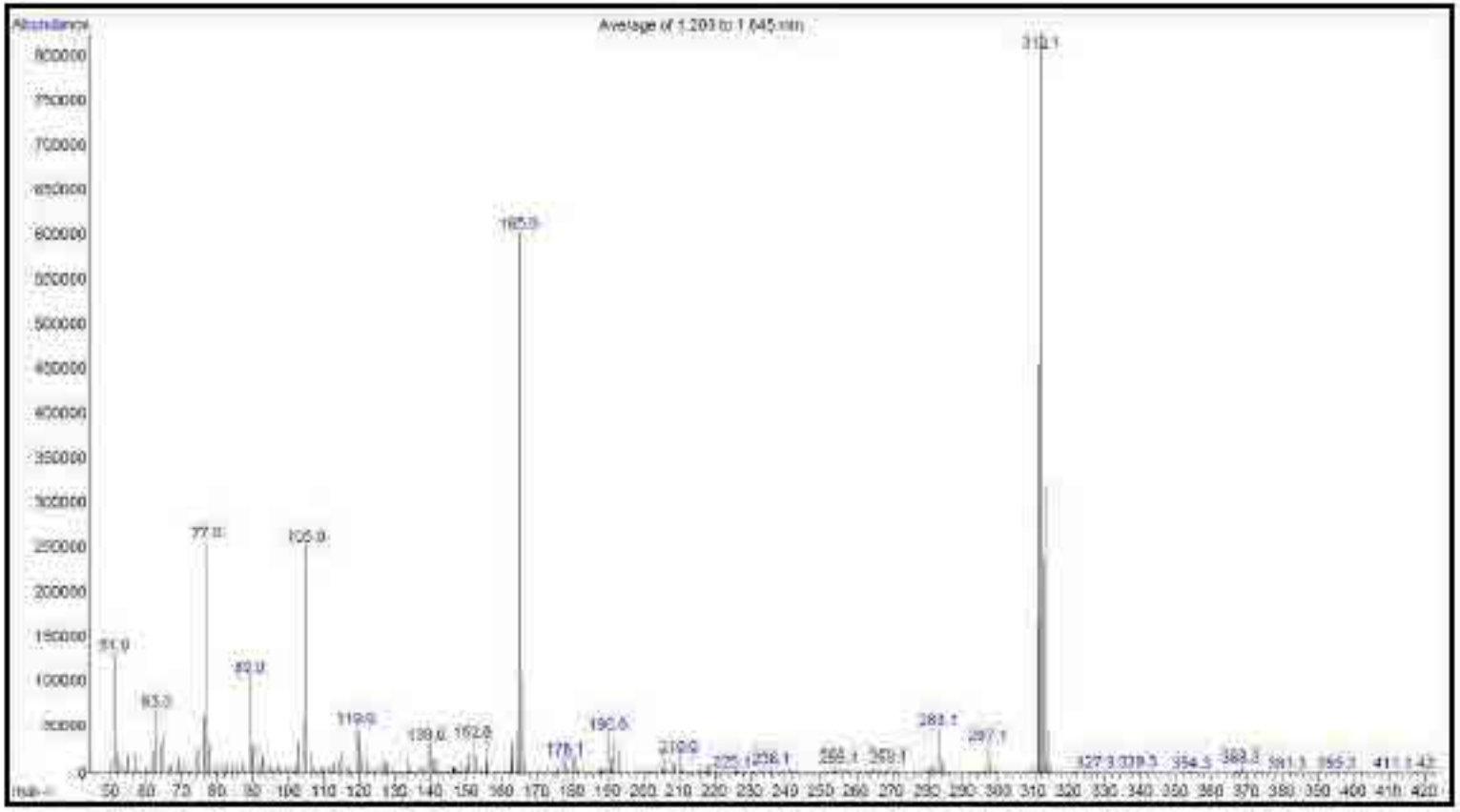

Fig. 13. FTIR spectrum of 4-(4,5-diphenylimidazol-2-yl)phenol **(4e)**

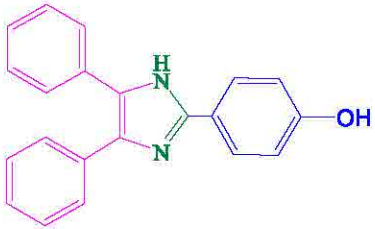

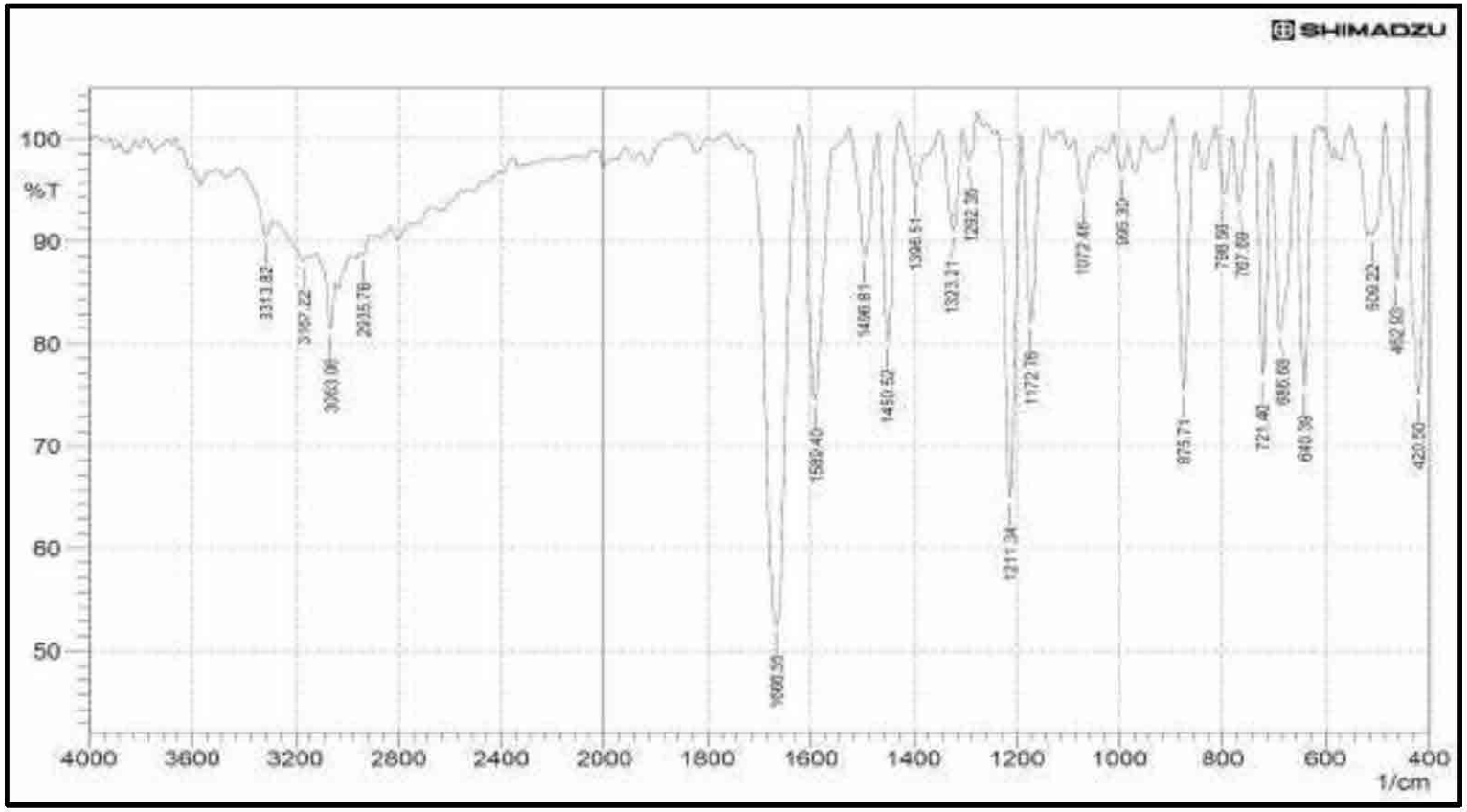

Fig. 14. ^{1}H NMR spectrum of 4-(4,5-diphenylimidazol-2-yl)phenol (4e)

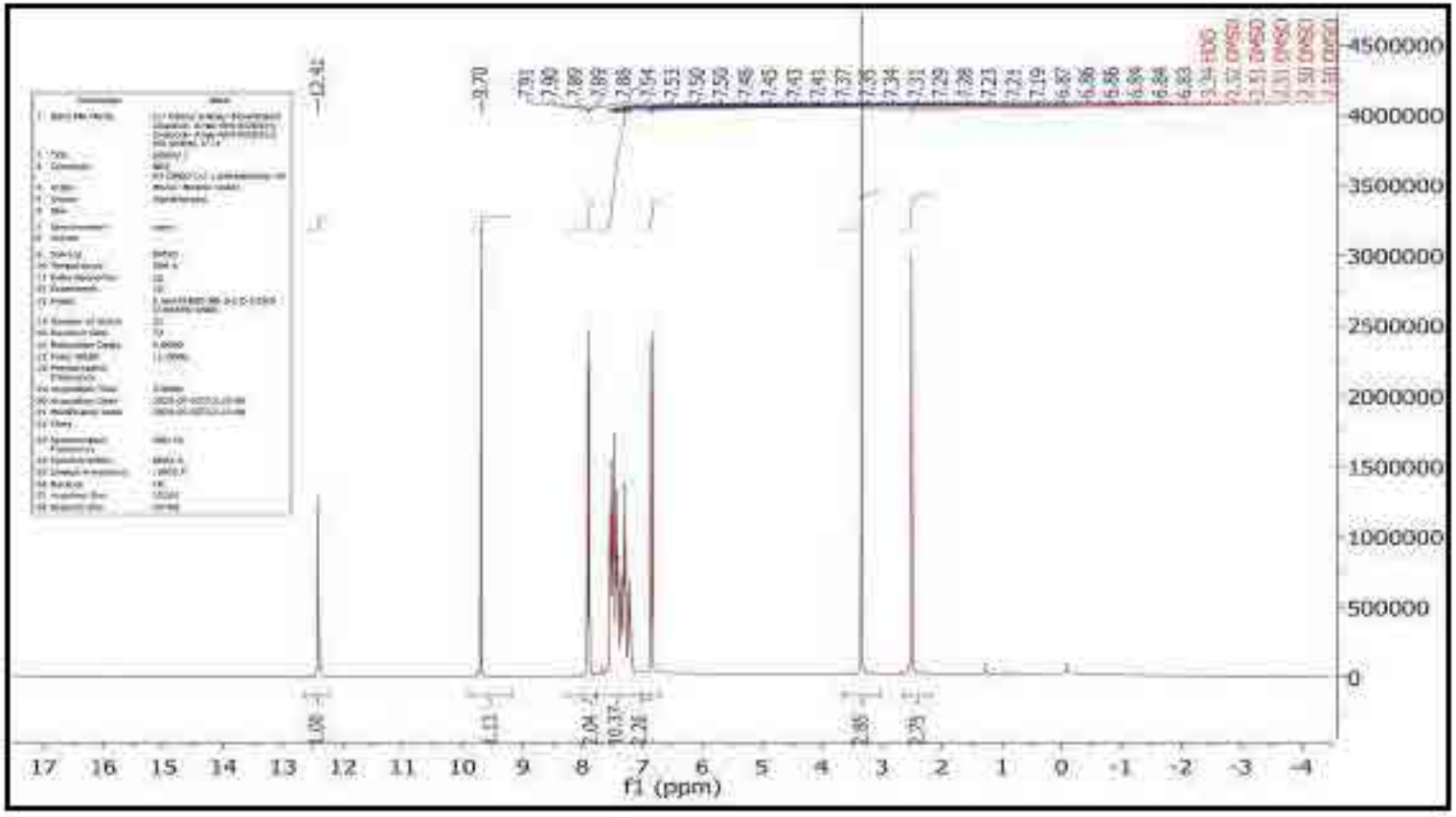

Fig. 15. MASS spectrum of 4-(4,5-diphenylimidazol-2-yl)phenol (4e)

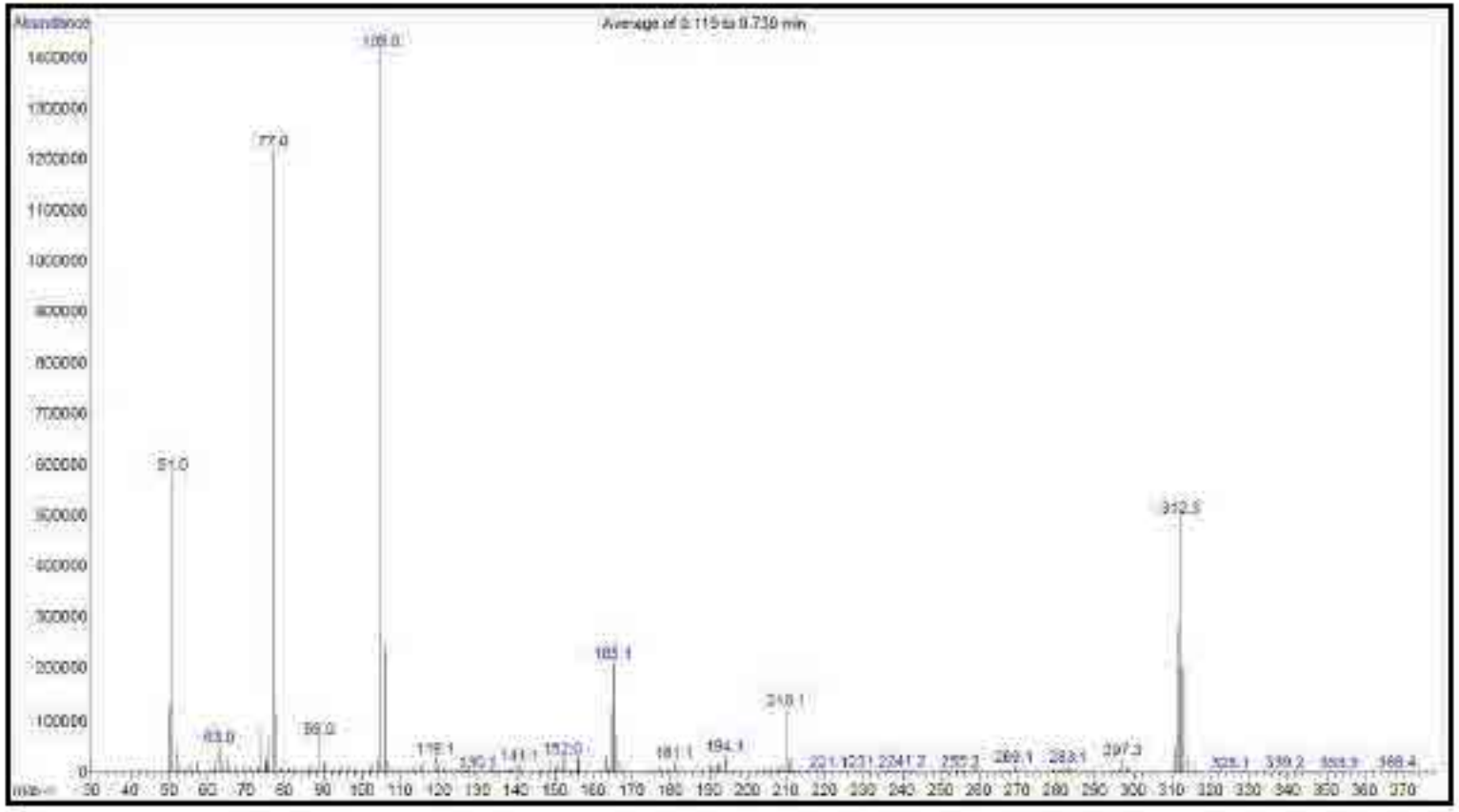

Fig. 16. FTIR spectrum of 2-(4-chlorophenyl)-4,5-diphenylimidazole (4f)

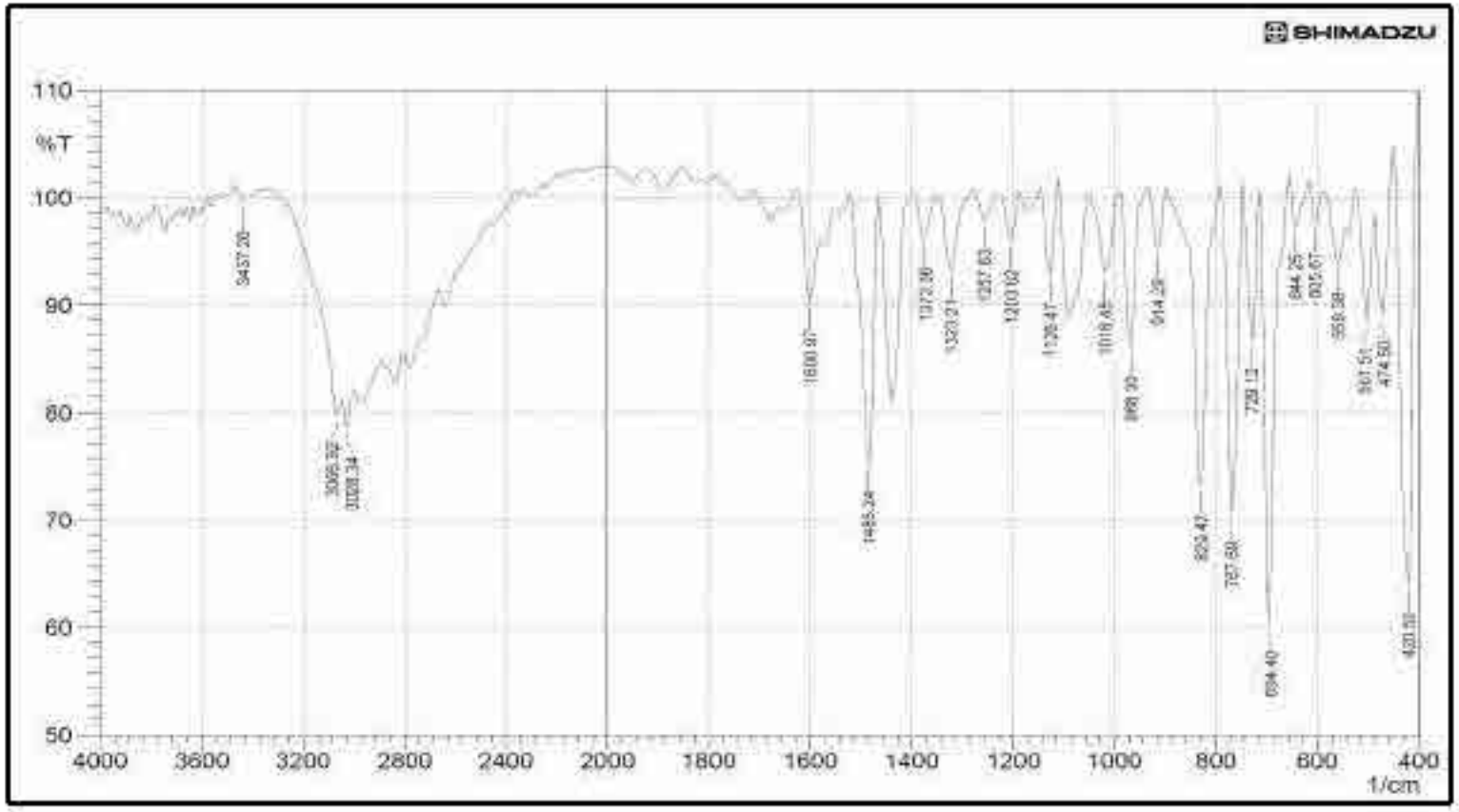

Fig. 17. ^{1}H NMR spectrum of 2-(4-chlorophenyl)-4,5-diphenylimidazole (4f)

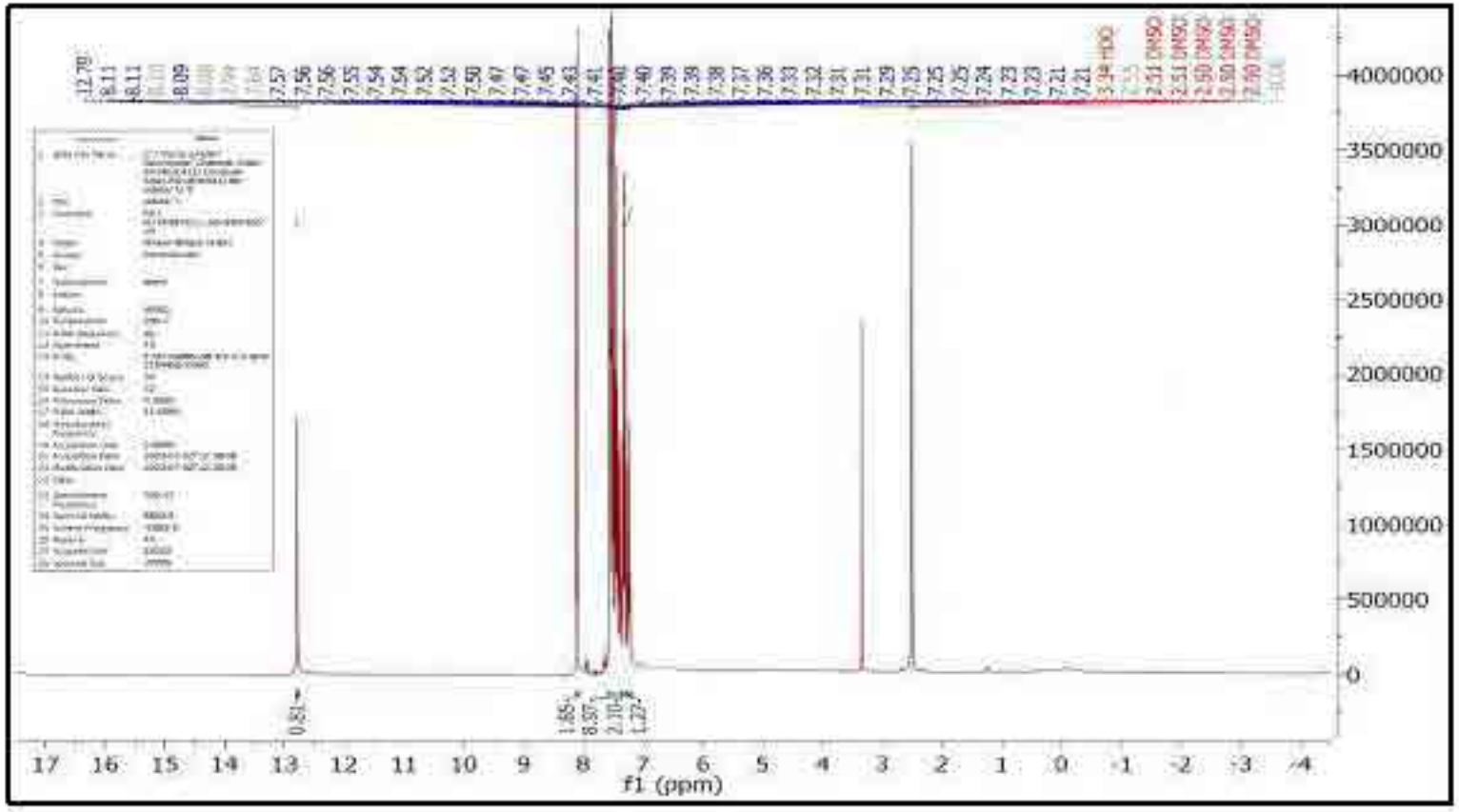

Fig. 18. MASS spectrum of 2-(4-chlorophenyl)-4,5-diphenylimidazole (4f)

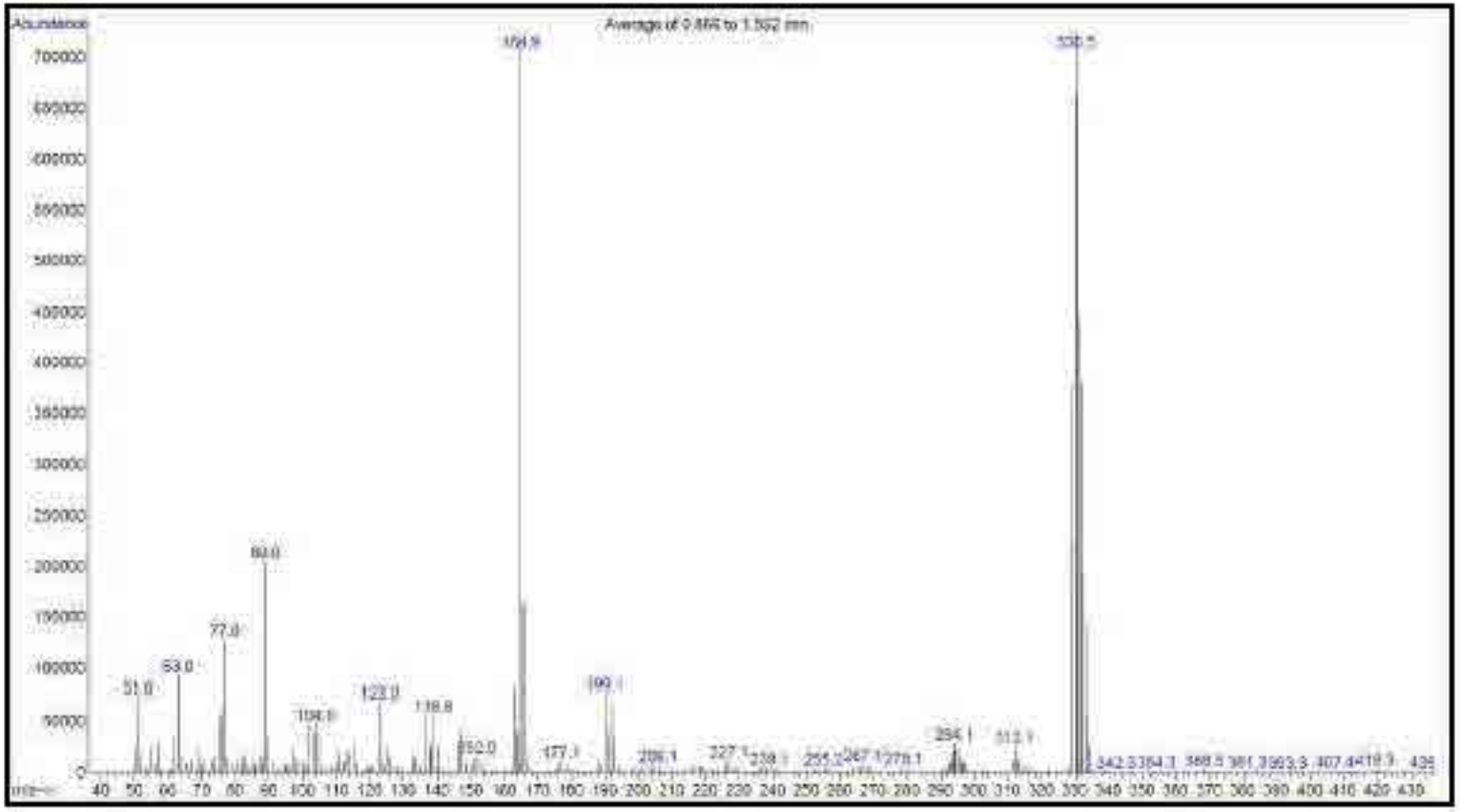

2. Characterization of 2,4,5-trisubstituted imidazole derivatives using $SiO_2PrOPDA$-SO_4H as catalyst

Fig. 19. FTIR spectrum of 2,4,5-triphenyl-1*H*-imidazole (4g)

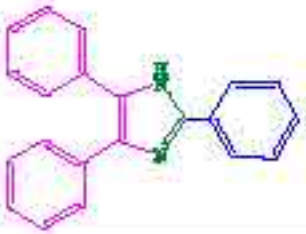

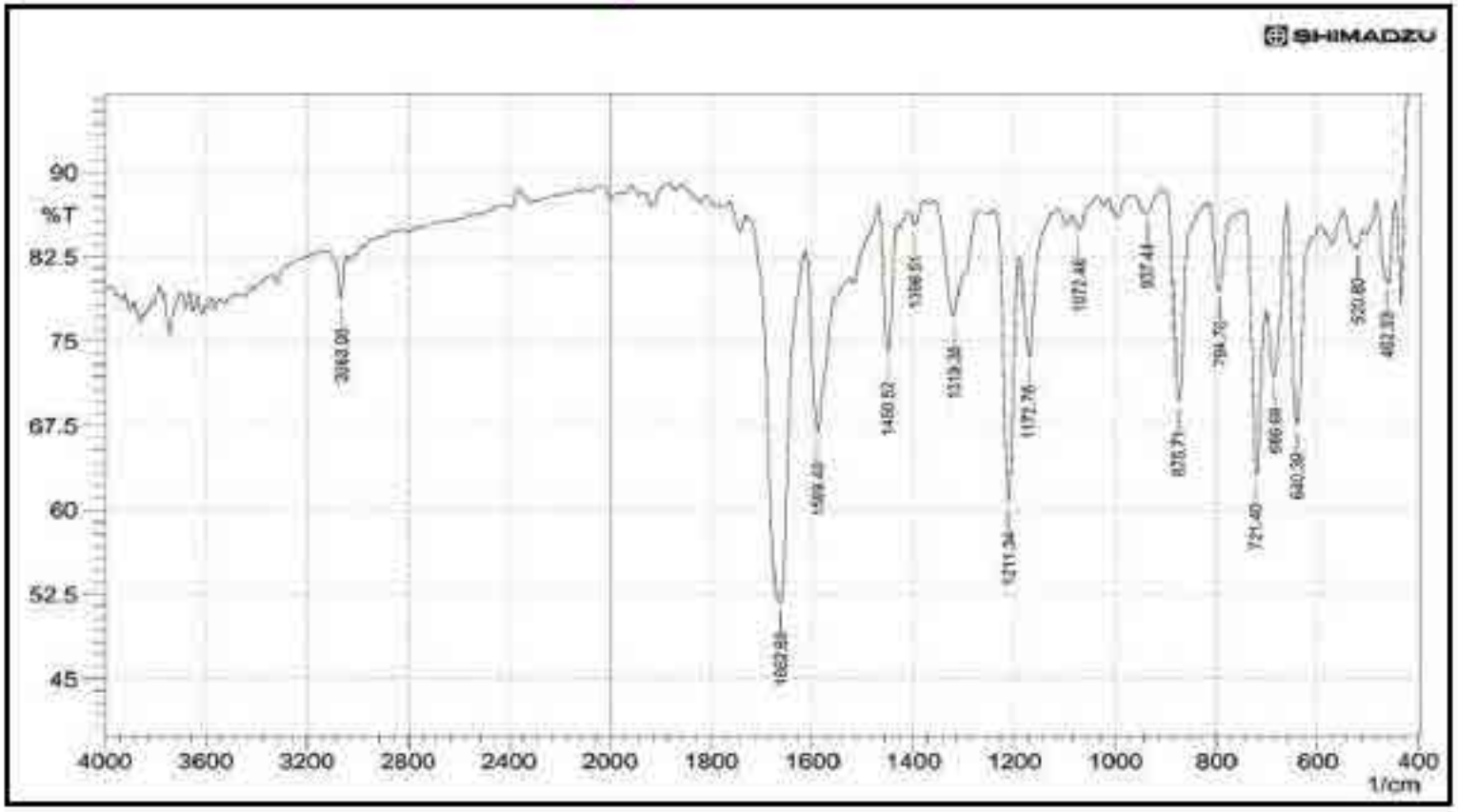

Fig. 20. ^{1}H NMR spectrum of 2,4,5-triphenyl-1*H*-imidazole (4g)

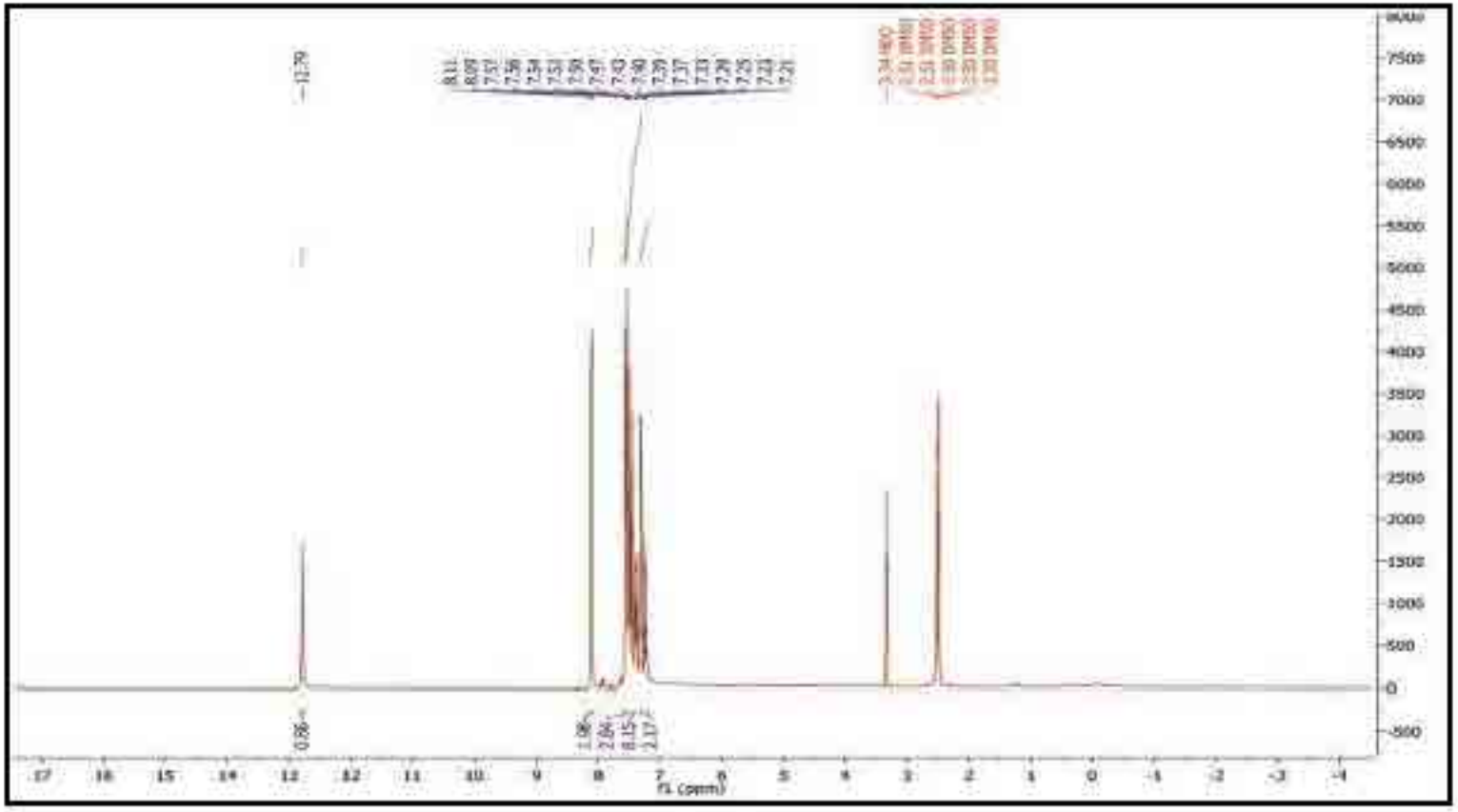

Fig. 21. MASS spectrum of 2,4,5-triphenyl-1*H*-imidazole **(4g)**

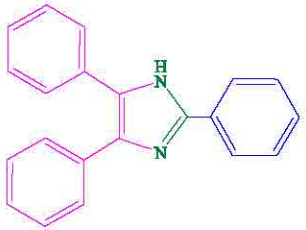

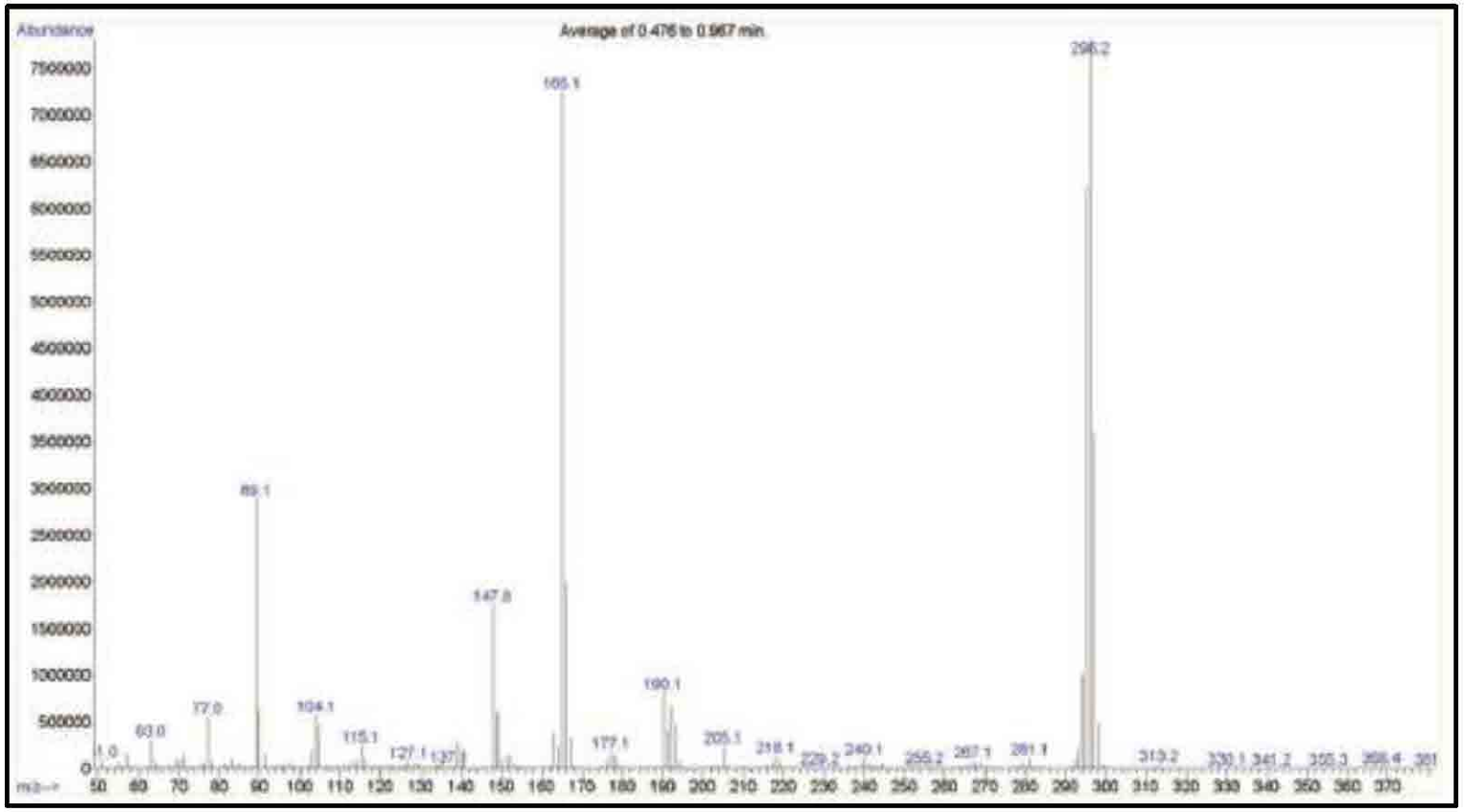

Fig. 22. FTIR spectrum of 4-(4,5-diphenyl-1*H*-imidazol-2-yl)-*N,N*-dimethylaniline (4h)

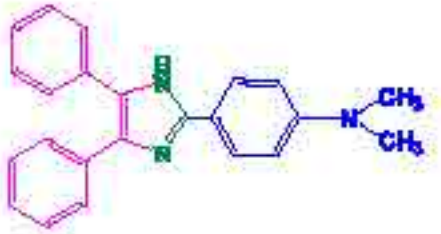

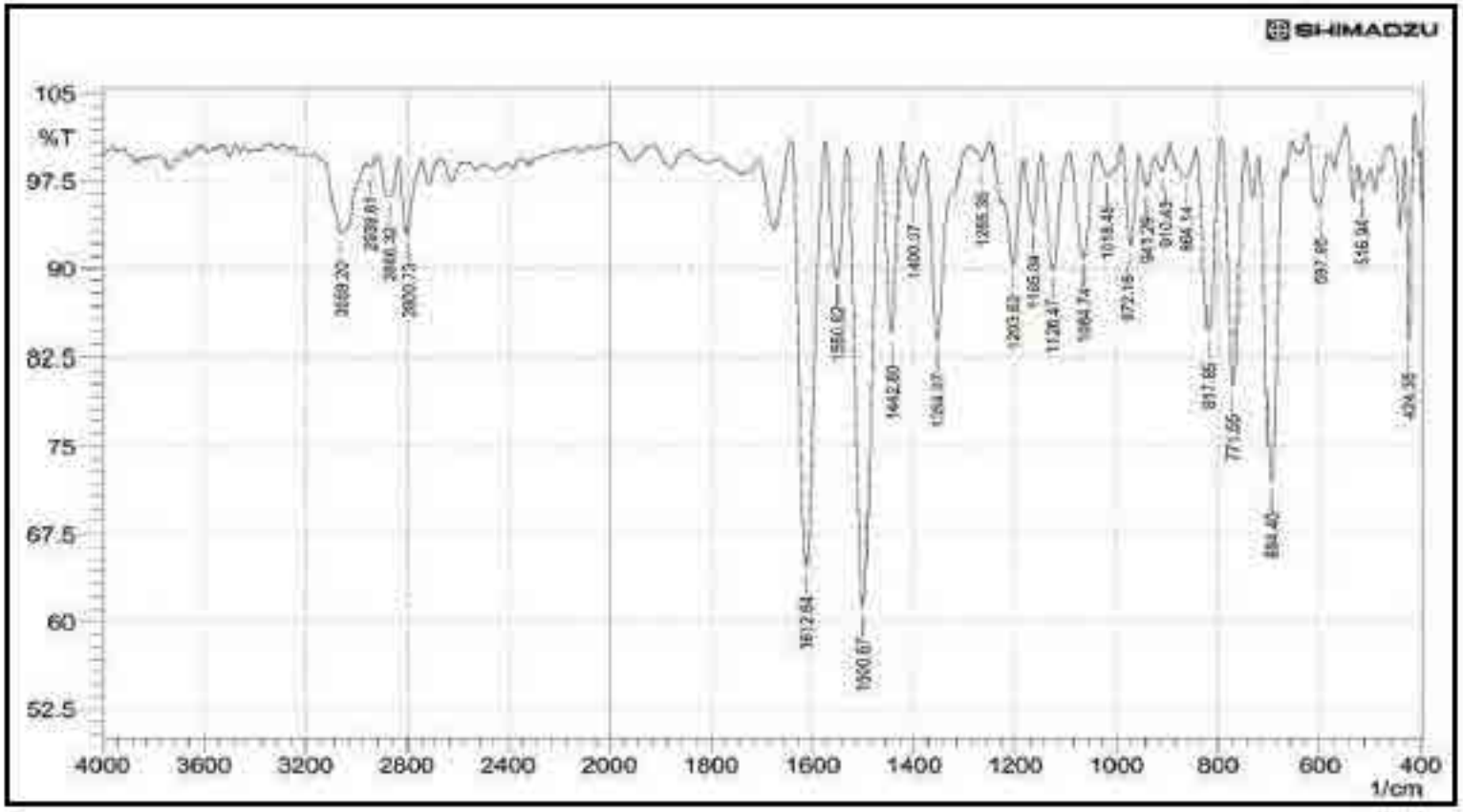

Fig. 23. ^{1}H NMR spectrum of 4-(4,5-diphenyl-1*H*-imidazol-2-yl)-*N*,*N*-dimethylaniline (4h)

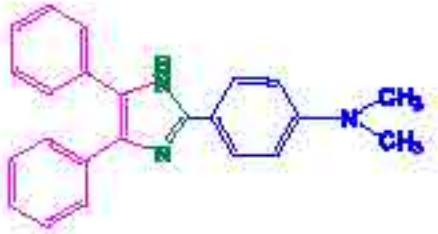

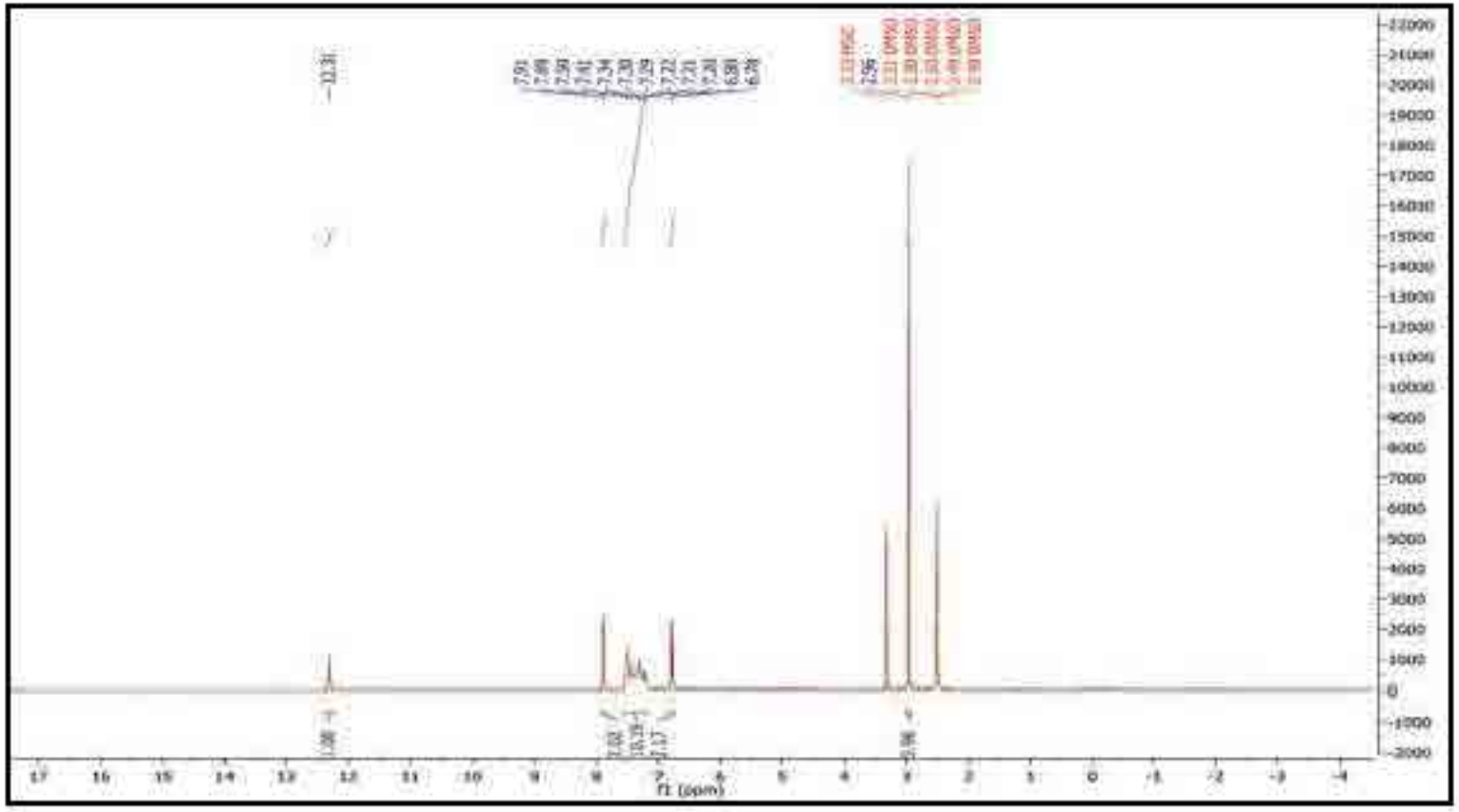

Fig. 24. MASS spectrum of 4-(4,5-diphenyl-1*H*-imidazol-2-yl)-*N*,*N*-dimethylaniline (4h)

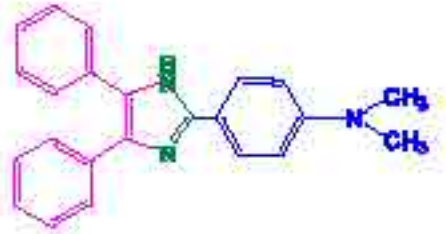

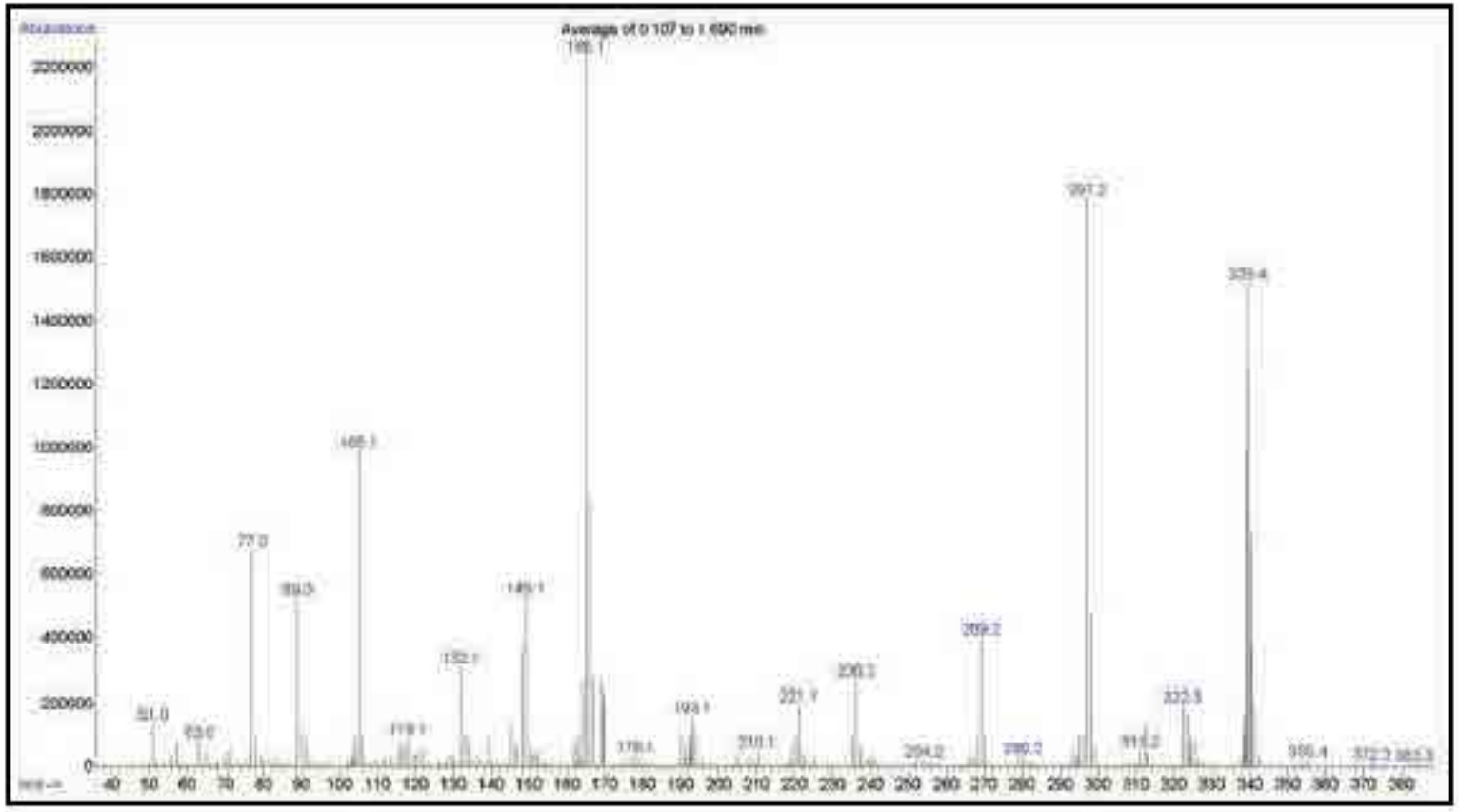

Fig. 25. FTIR spectrum of 3-(4,5-diphenyl-1*H*-imidazol-2-yl) phenol (4l)

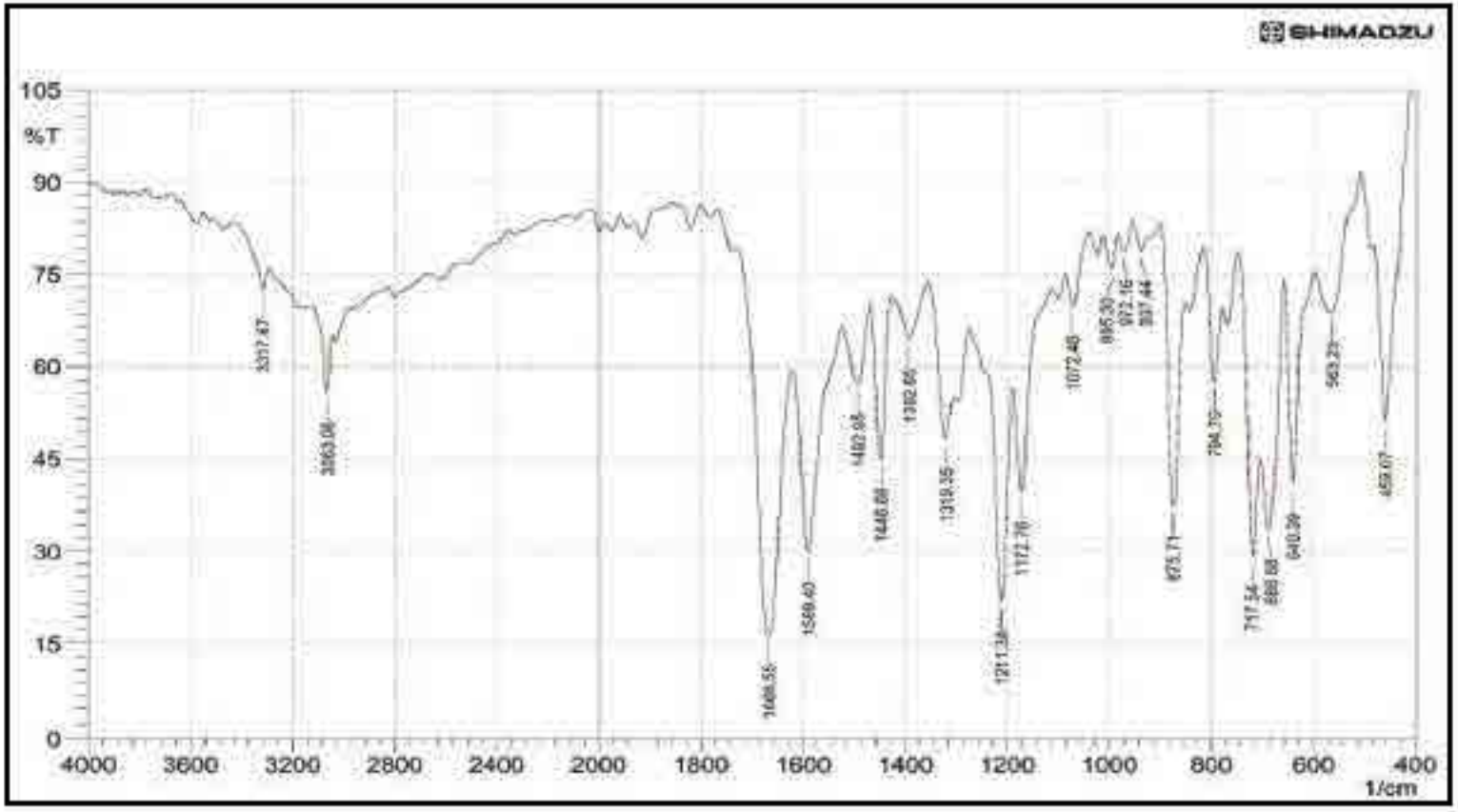

Fig. 26. ^{1}H NMR spectrum of 3-(4,5-diphenyl-1*H*-imidazol-2-yl) phenol (4l)

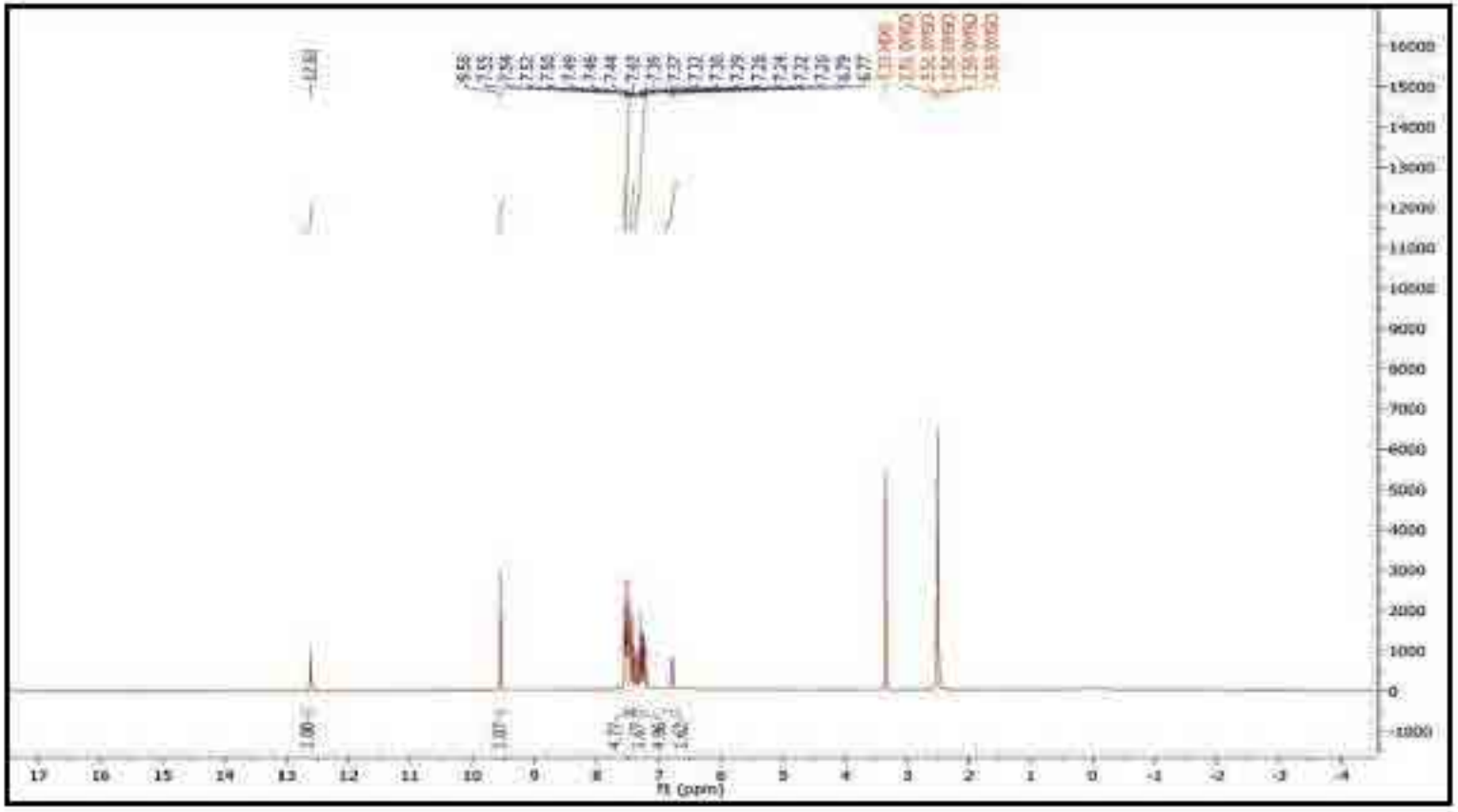

Fig. 27. MASS spectrum of 3-(4,5-diphenyl-1*H*-imidazol-2-yl) phenol (4l)

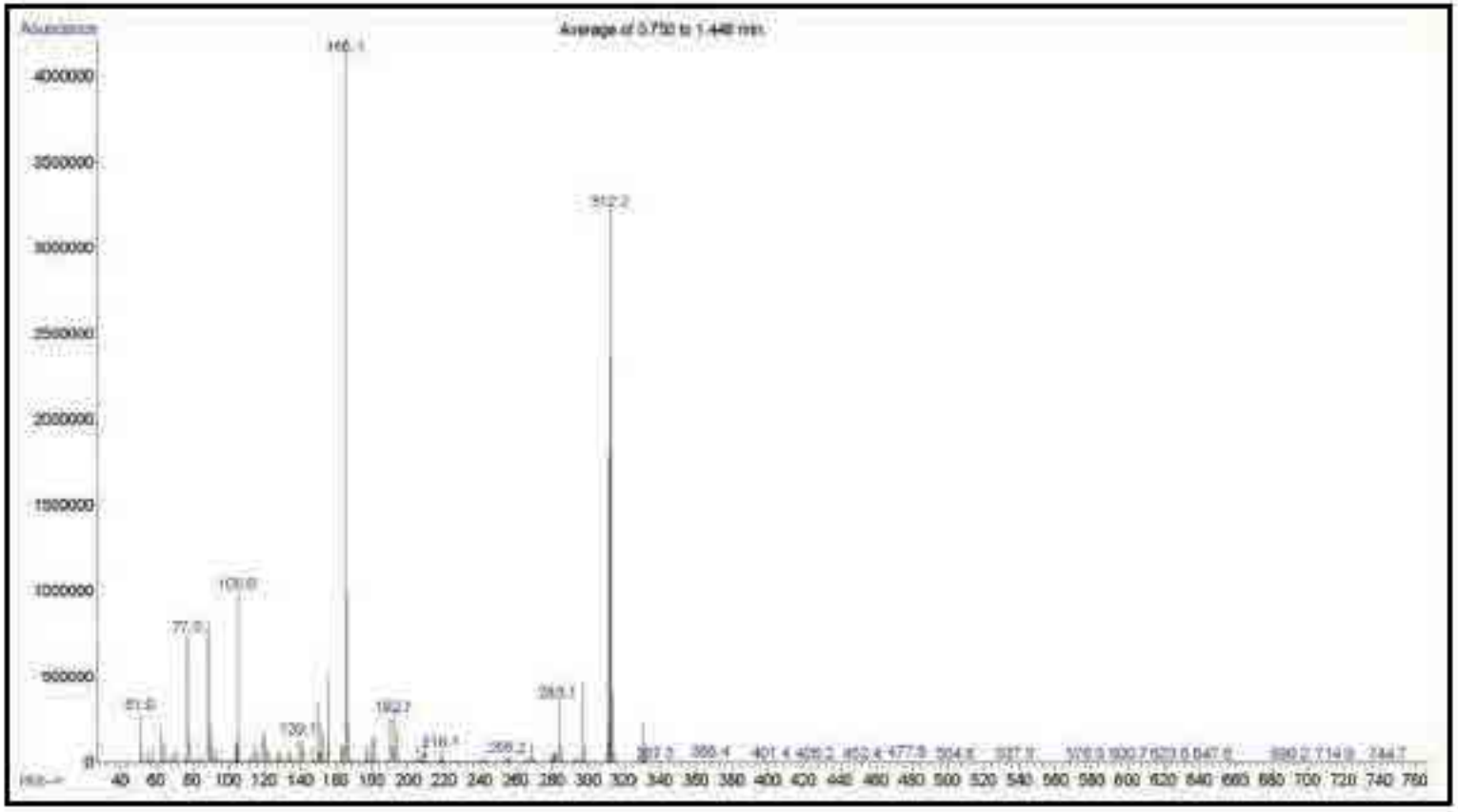

Fig. 28. FTIR spectrum of 4-(4,5-diphenyl-1*H*-imidazol-2-yl)phenol (4j)

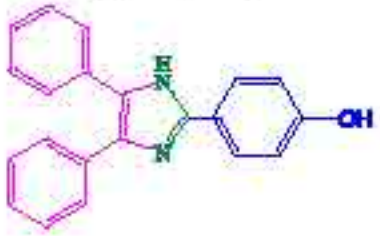

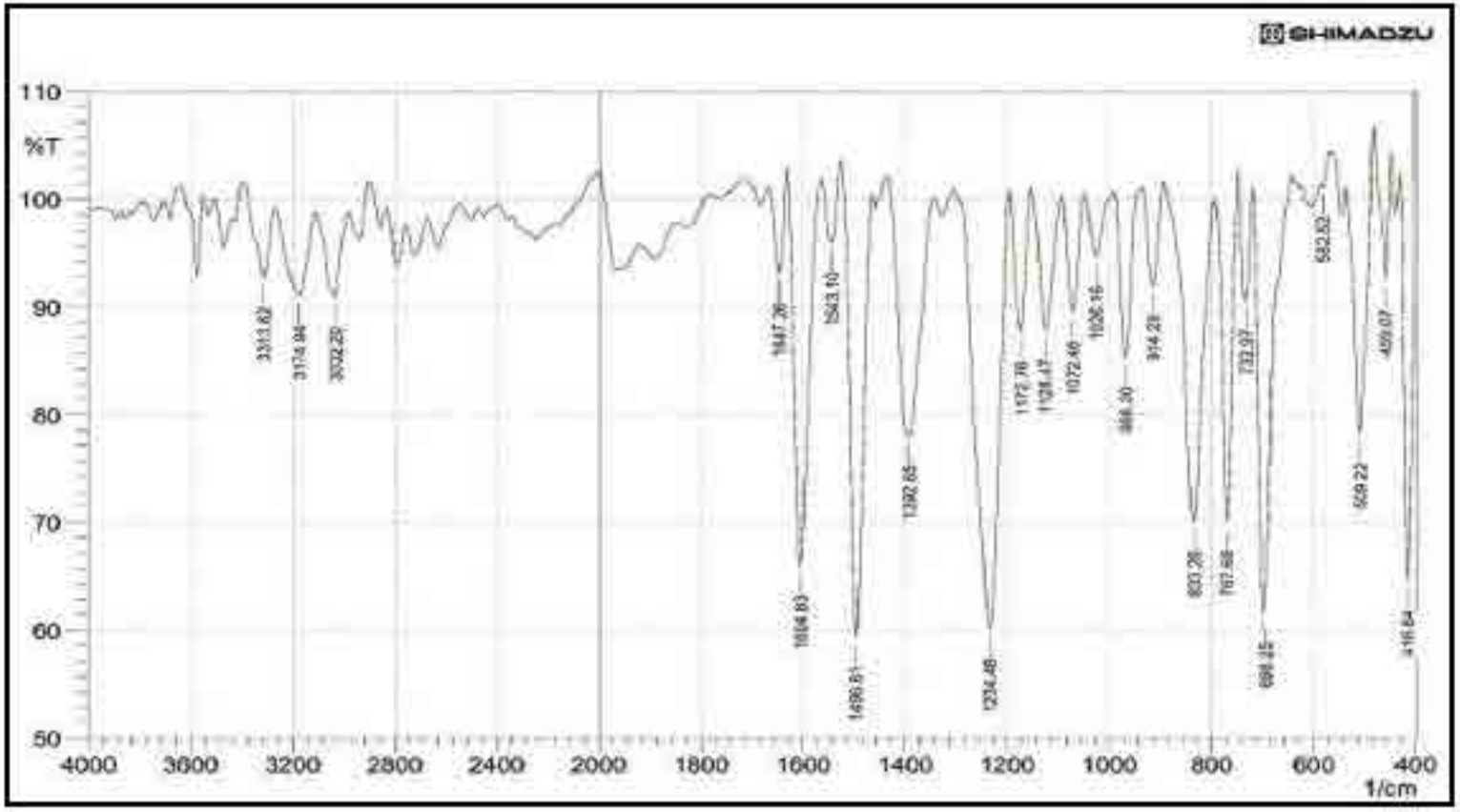

Fig. 29. ^{1}H NMR spectrum of 4-(4,5-diphenyl-1*H*-imidazol-2-yl)phenol **(4j)**

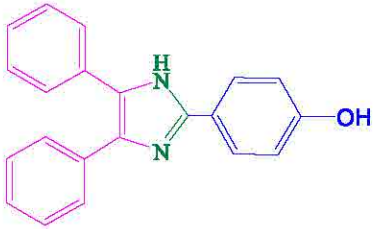

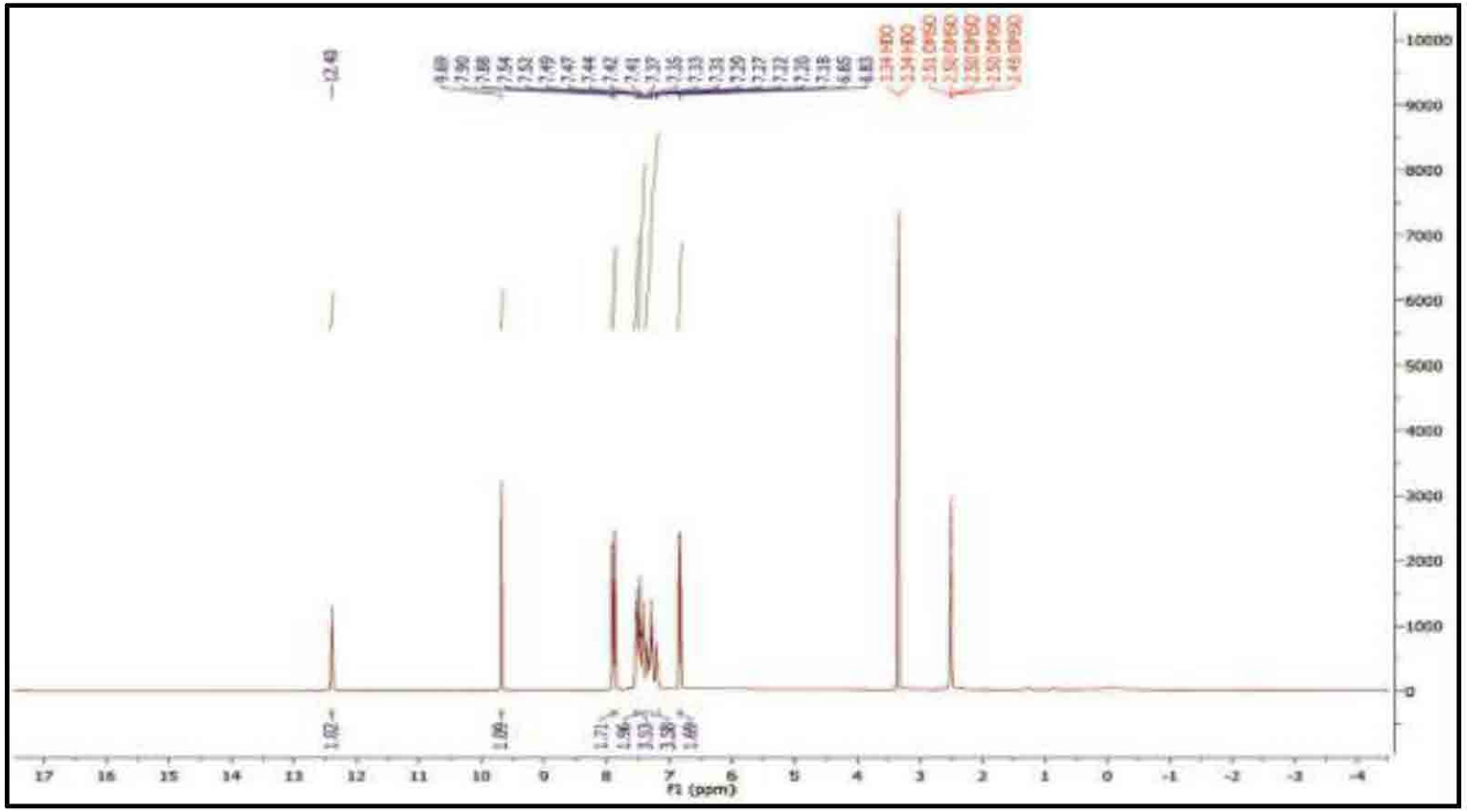

Fig. 30. MASS spectrum of 4-(4,5-diphenyl-1*H*-imidazol-2-yl)phenol (4j)

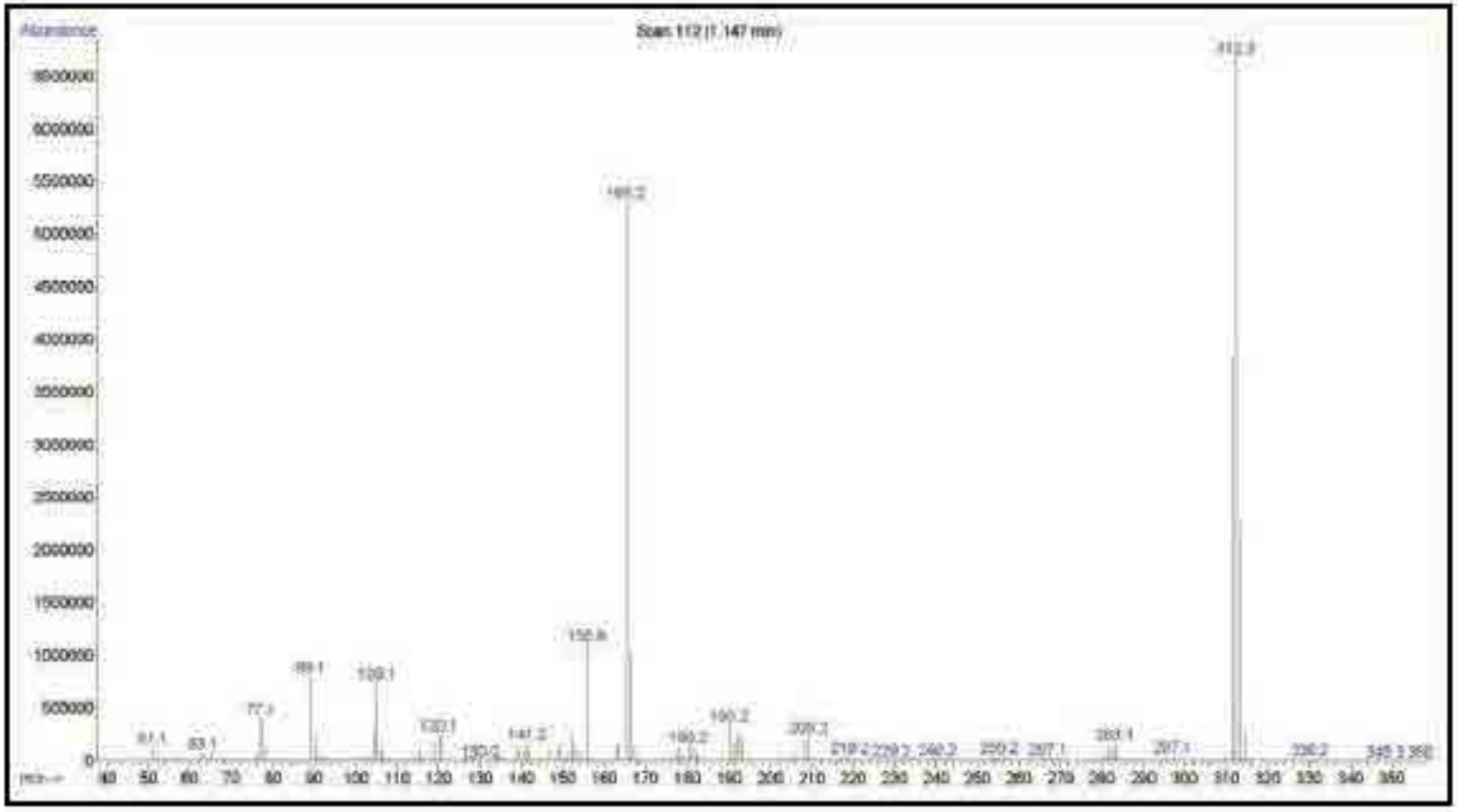

Fig. 31. FTIR spectrum of 2-(4-chlorophenyl)-4,5-diphenyl-1*H*-imidazole **(4k)**

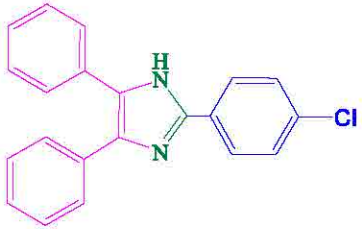

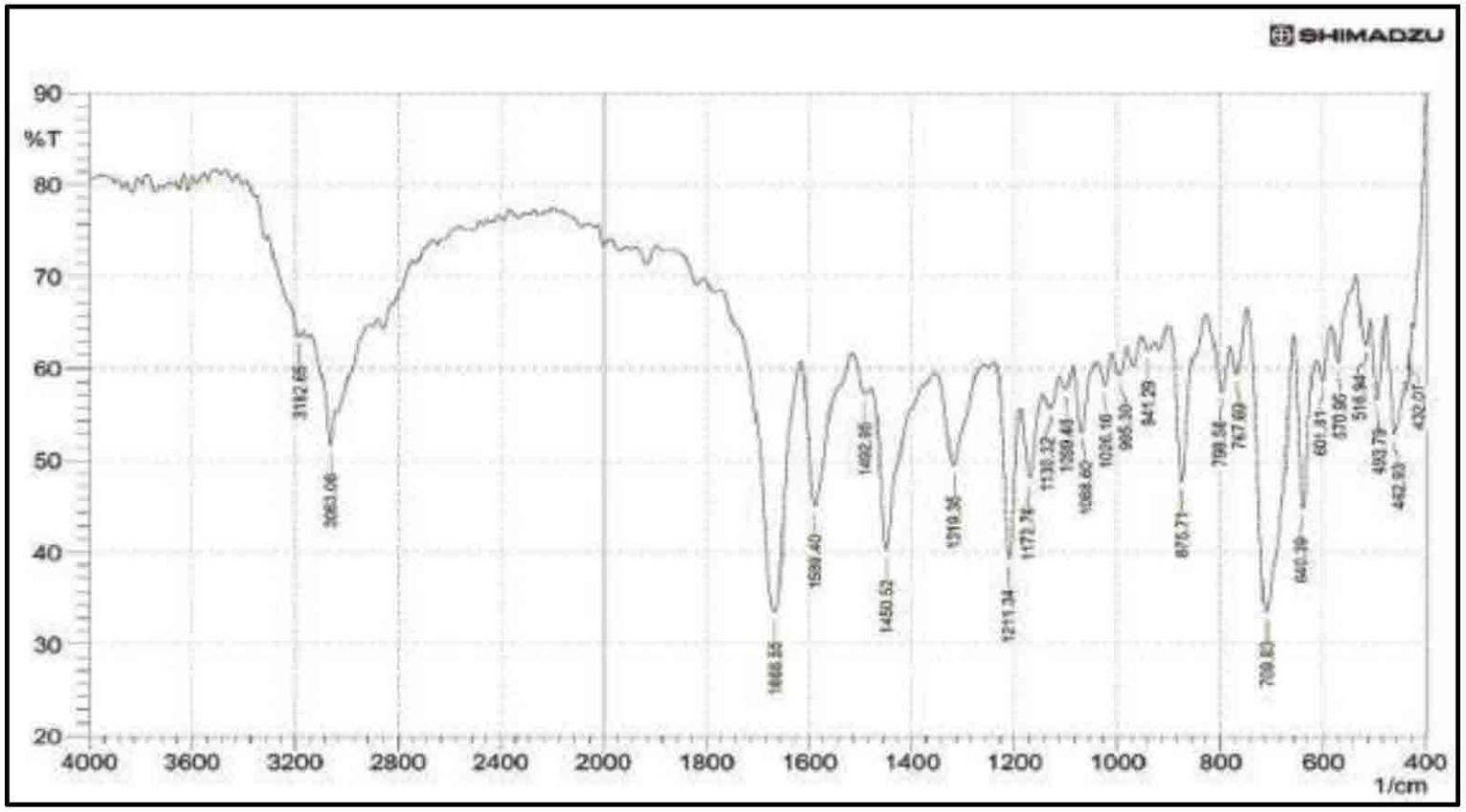

Fig. 32. ^{1}H NMR spectrum of 2-(4-chlorophenyl)-4,5-diphenyl-1*H*-imidazole (4k)

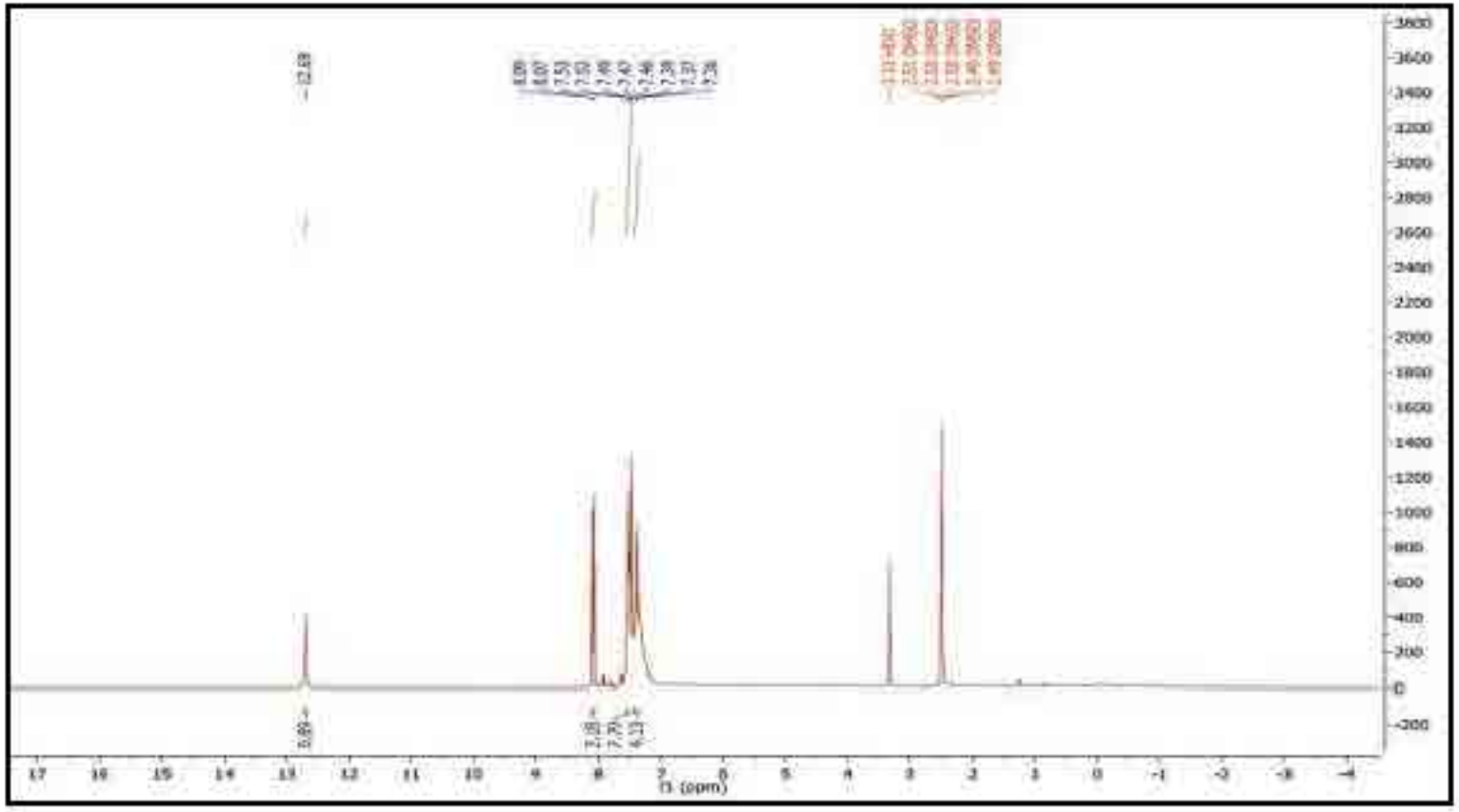

Fig. 33. MASS spectrum of 2-(4-chlorophenyl)-4,5-diphenyl-1*H*-imidazole (4k)